ORIGIN, WEATHERING AND PALEOCLIMATIC SIGNIFICANCE OF MIDDLE–LATE PLEISTOCENE SLOPE COVERS, MT. KENYA, KENYA

William C. Mahaney[1]*, Ronald G.V. Hancock[2]

[1] *Quaternary Surveys, 26 Thornhill Ave., Thornhill, Ontario, Canada, L4J1J4 and Department of Geography, York University, 4700 Keele St. N. York, Ontario, Canada, M3J 1P3; e-mail: arkose41@gmail.com*

[2] *Department of Anthropology, McMaster University, Hamilton, Ontario, Canada, L8S 4K1; e-mail: rgvhancock@gmail.com*

* corresponding author

Abstract:

Stacks of the Pleistocene tills and associated airfall/slopewash/colluvial sediment abound on East African Mountains but few localities exist where thick deposits of middle to Late Pleistocene age can be studied to bedrock with topography the main soil-forming agent over <0.8 Ma. Two tills form the main structure of the catena, the oldest buried in the crest, backslope and footslope of the deposit, the youngest forming the crest and upper backslope, with massive colluvial infill forming a still younger sediment mass superposed on older sediment in the lower backslope, footslope and toeslope, the latter all radiocarbon dated to within the last glaciation (Liki on Mt. Kenya; Weichselian in Europe, Wisconsin in North America). The moraine stack, first identified by J.W. Gregory in the late 19th century, as belonging to the 'Older Glaciation' (Illinoian in North America; Teleki on Mt. Kenya), is much older than originally thought with tills and other paraglacial sediment extending to saprolitic bedrock, paleomagnetic assessment and relative weathering indices placing the mass in the Brunhes Chron. These results demonstrate that despite erosion and weathering, paleosols in toposequences near the margins of successive glaciations retain properties allowing reconstruction of environmental changes over long periods of time.

Key words: paleosol catena, long-weathering sequence, ^{14}C dating of MIS 2 and 3 sediment beds, test of Fe-Al extractions, weathering unconformities

INTRODUCTION

The sites

Mount Kenya, one of the principal mountains of East Africa (Fig. 1A), lying astride the Gregory Rift Valley (Dawson, 2008), has been glaciated several times since the very Late Pliocene/Early Pleistocene with records left in moraine and paleosol sections (Gregory, 1894; Nilsson, 1931; Baker, 1967; Mahaney, 1990, 2011; Mahaney *et al.*, 2011, 2014). Early exploration of glaciation on the mountain in the late 19th century by Gregory (1984) differentiated the 'older glaciation' (later Teleki on Mt. Kenya) from younger sediment belonging to the last glaciation (Würm in Europe, Pinedale in the Rocky Mountains; Liki on Mt. Kenya). Gregory clearly understood his older glaciation was further back in the glacial sequence equivalent to older glacial sediment recognized in Europe, and while he mapped the

left lateral moraine deposit on the south side of the Naro Moru River, he did not excavate sections, probably because transport in 1892 was on foot all the way to Mombasa on the coast, with exfiltration by raft on the Tana River. While his deposit (Fig. 1B for stratigraphy) is clearly glacial in morphology, the first excavation (site TV23-1976) in the moraine crest was opened to determine the lithology, origin and weathering characteristics of the deposit. This revealed a sedimentary complex comprising more than one till in the section. Later, the TV61 section (1983) in the lower backslope was opened for comparative purposes, and at a later date (1987) other sections were sampled to reveal the weathering and paleomagnetic record (Fig. 2). With records extending to *in situ* saprolite and phonolite bedrock, encompassing what appeared to be a near complete Brunhes (<0.8 Ma-present) sedimentary weathering record, it seemed reasonable to excavate sections that would allow analysis of the toposequence from the top member, through
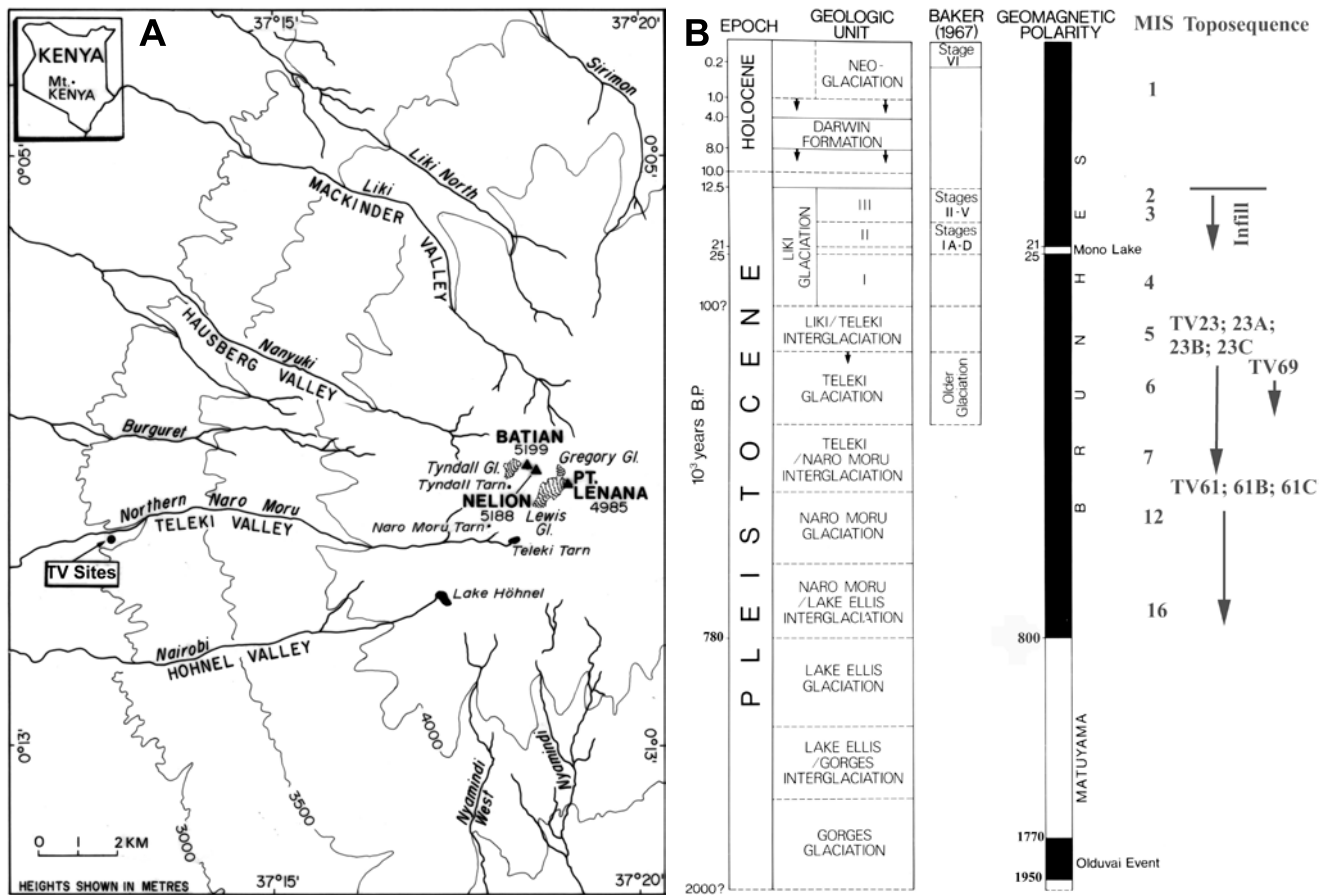
Fig. 1. A – location of sites (TV group) in Teleki Valley relative to the Central Peaks. The 5188 m asl mountain has been glaciated several times before and after the Olduvai subchron, the three most recent glaciations – Liki, Teleki and Naro Moru, from youngest to oldest – are represented by paleosols in colluvial, loess, slopewash, and till in a toposequence stretching across the Brunhes Chron (<0.8 Ma – present); B – glacial-interglacial stratigraphy, paleosol record and magnetostratigraphy, Mount Kenya Afroalpine Area (from Mahaney, 2011). MIS correlations older than stage 5 are estimates only without age controls. Correlations of glacial units with the toposequence in MIS 2–3 are based on ^{14}C and the adjusted Mono Lake time line.

the slope members, to the toeslope. It is the combined geomorphological, sedimentological, and weathering record of this toposequence, with its combined sequence of weathered bedrock, in situ tills and loess, all interlocked with reworked colluvial/slopewash sediment, that form the basis of this report.

Soil (Paleosol) Forming Equation

Taking soil-paleosol forming-factors into account (Jenny, 1941; Birkeland, 1999), soil/paleosol genesis relies upon the functional interrelationship of five soil-forming factors: $s = f(cl, o, r, p, t)$, where 's' = the soil system, 'f' = functional relationship, and cl (climate), o (biota), r (relief), p (parent material), and t (time) are considered independent and semi-dependent variables. To discuss $(\blacktriangle s/\blacktriangle r)$ $cl,o,p,t = (dr)$, the topographic factor 'r' considered a partial derivative of the ratio (ds/dr), and hence, one is forced to select sites where topography is variable from the upper member, across the backslope and footslope to toeslope members, with climate, biota, parent material and time

uniform or near uniform within selected lithic units. In this instance, the r independent variable is easy to calculate across the topographic sequence from the top member, through the backslope and footslope members to the toeslope. However, reconstructing the staggered record of episodic weathering, glaciation and mass wasting events is somewhat more difficult. While it is often possible to hold cl and o near constant, we did not measure microclimate or biotic variables at the measured sites. The p factor is uniform across the catena with sediment weathering sourced from phonolite produced from parasite flows younger than the country rock found in the central peaks area (Mahaney, 1990). Sediment within the toposequence, sourced from the Central Peak area by glaciation, includes syenite, phonolite, basalt and kenyte. An erratic syenite boulder, shown in Fig. 3A, is sourced from the Central Peaks ~7 km to the east. Within close space order of dozens of meters between sites (crest to toeslope = 100 m; Figs 1B, 2), the climatic (cl) and biotic (o) factors have changed over time and with different intensities in response to land surface evolution (e.g. weathering, erosion, plant distribution and variations in precipitation, temperature and evapotranspiration).
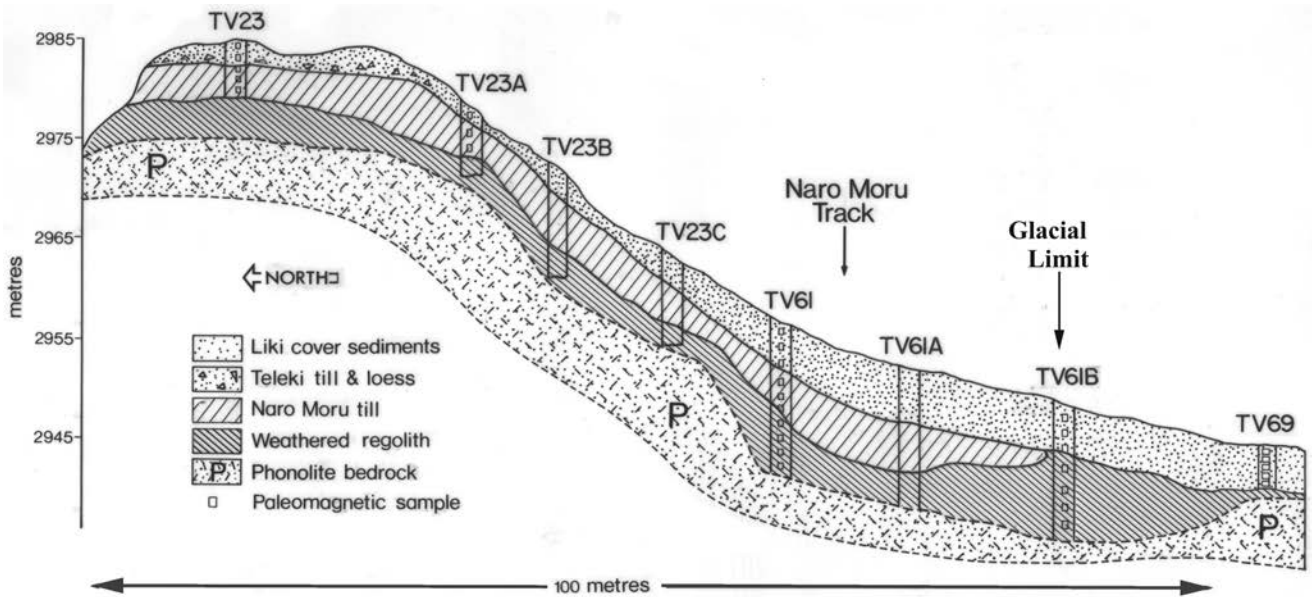
Fig. 2. Toposequence showing the location of eight sections selected from the topographic high member (TV23), through the upper backslope (TV23A, TV23B), lower backslope (TV23C, TV61) to the footslope (TV61A, TV61B) and toeslope (TV69).

According to the pollen record (Coetzee, 1964; Olago *et al.*, 1999), and thick peat beds in paleosols below the present timberline (~3150 m asl), shifts in the timberline during the last glaciation led to replacement of the Podocarpus/bamboo forest to Afroalpine meadow at the toposequence site.

Even though the biotic (o') factor is often considered unvarying in a macro sense once steady state is achieved, and as weathering progresses, mineral weathering may change the ecological kinetics affecting substrate/plant and microbial relationships (Mahaney *et al.*, 2016). Moreover, because the sites involved are within the present-day single biome of Podocarpus/bamboo forest, changes in the composition of groundcover vegetation from time zero to achievement of steady state for surface paleosols, at some indeterminate time following the Last Glacial Maximum (LGM), would have affected organic matter mass (carbon budgets), and thus, soil morphogenesis and horizon proliferation. To complicate matters, and previous to this, with the initial till and loess cover in place, time may at best be considered a semi-dependent variable from the onset of bedrock weathering that produced saprolite of total unknown depth at all sites (e.g., TV23). The saprolite measures 10–58 cm thickness in recovered sections, and represents weathering prior to the onset of the Naro Moru Glaciation (ca. 0.5 Ma), which means in this case that the oldest till and associated loess started weathering at the end of the Naro Moru Glaciation sometime after 0.5 Ma. This early-formed catena was later covered by till and loess from the Teleki Glaciation (~0.250–0.128 Ma). Within this sediment complex time may only be considered near uniform within the lower buried saprolite (lithic unit 5), lower combined buried till-loess units (lithic units 3 and 4), the upper exposed till-loess units (TV23, TV23A, TV23B, TV23C-lithic units 1–2) and inset mass wasting deposits of

Fig. 3. A – Lower backslope position showing site TV61 and erratic boulders of syenite and phonolite from the Central Peaks 8-km to the east. The site is located at ~2998 m below Met Station in Teleki Valley (3052 m asl; B – Site TV23B: author and Simon Murithi.
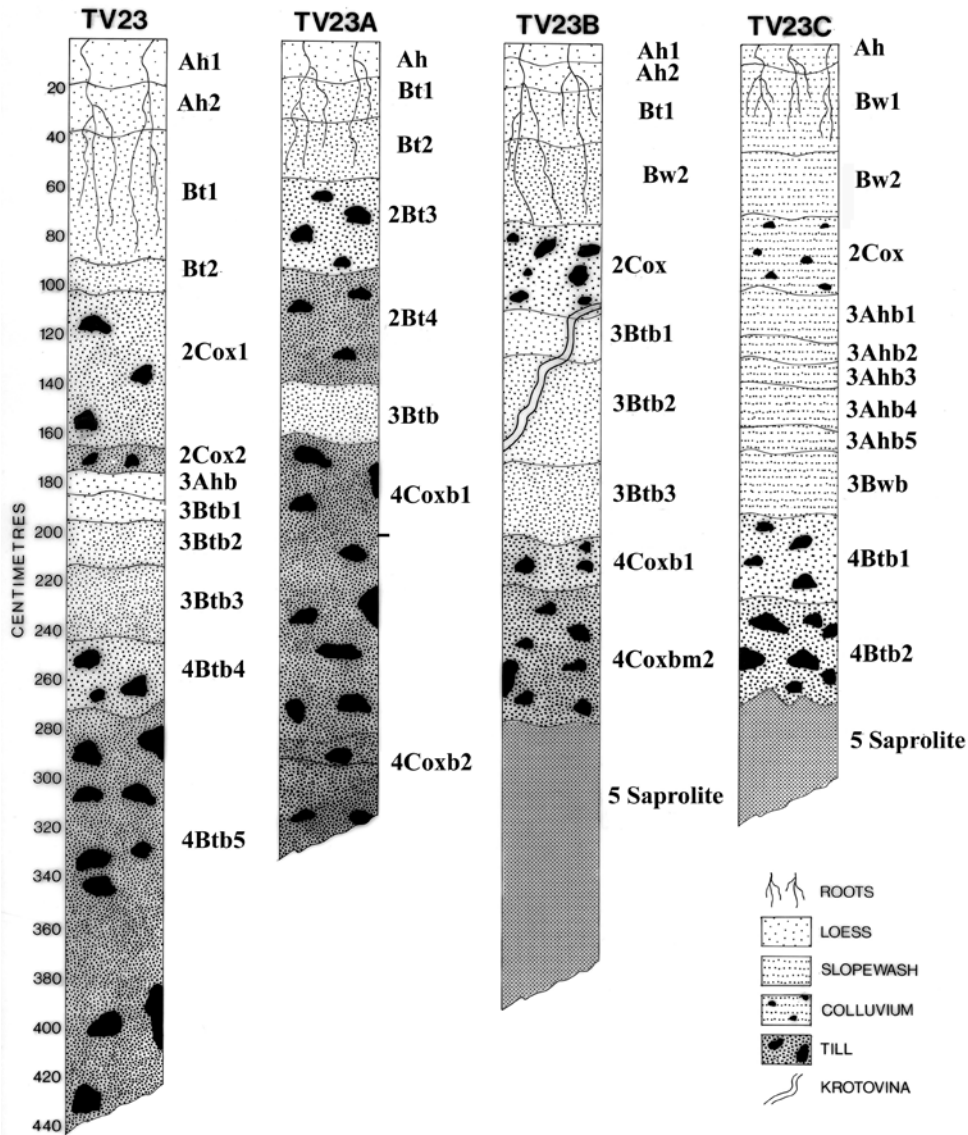
Fig. 4.   Stratigraphy of TV23, TV23A, TV23B and TV23C sections reaching to variable depths, sometimes into saprolite.

colluvium (TV23C, TV61A and TV61B). The lower lithic units in these paleosols have been subject to input of allochthonous sediment of indeterminate source but the presence of quartz within loess sheets is considered sourced mainly from the surrounding African craton, a small amount from volcanic quartz sources (Mahaney, 1990).

To strengthen the relative-age controls ('t' factor) of these sediments, we identified from marine isotope stages (MIS; Railsback *et al.*, 2015) the most prominent peaks within the weathering age brackets mentioned above. These peaks reveal that the Naro Moru Glaciation may correlate to the coldest peaks straddling 0.5 Ma which would be MIS 12 (~0.43 Ma and MIS 16 (~0.63 Ma), with MIS 14 somewhat warmer and possibly not cold enough to produce glaciation. While we assume the Teleki and Naro Moru deposits represent single glaciations, it is possible they represent more than one stage, so correlation to the coldest marine isotope stages is purely tentative. The overlying

Teleki Glaciation, considered to have occurred prior to the last interglaciation (MIS 5e) over a time span of ~0.25 Ma to 128 ka (MIS 6) (see Dahl-Jensen *et al.*, 2013 and Rovere *et al.*, 2016 for time lines for the last interglacial-stage 5). All paleomagnetic dating of these sections with the exception of the upper beds of TV61, show normal polarity (Barendregt, 1984; Mahaney, 1990). The TV61 section carries a near surface record close to the Mono Lake excursion bracketed 25–60 cm above ca 21–25 ka ^{14}C dated sediment (see Fig. 5) for the TV61 section and for magnetization profiles showing declination and inclination for samples see figs 5.17 and 5.20 (Mahaney, 1990).

Toposequence-Soil Weathering System

Soil/paleosol toposequences offer further challenges to understanding the soil/weathering system because paleosols
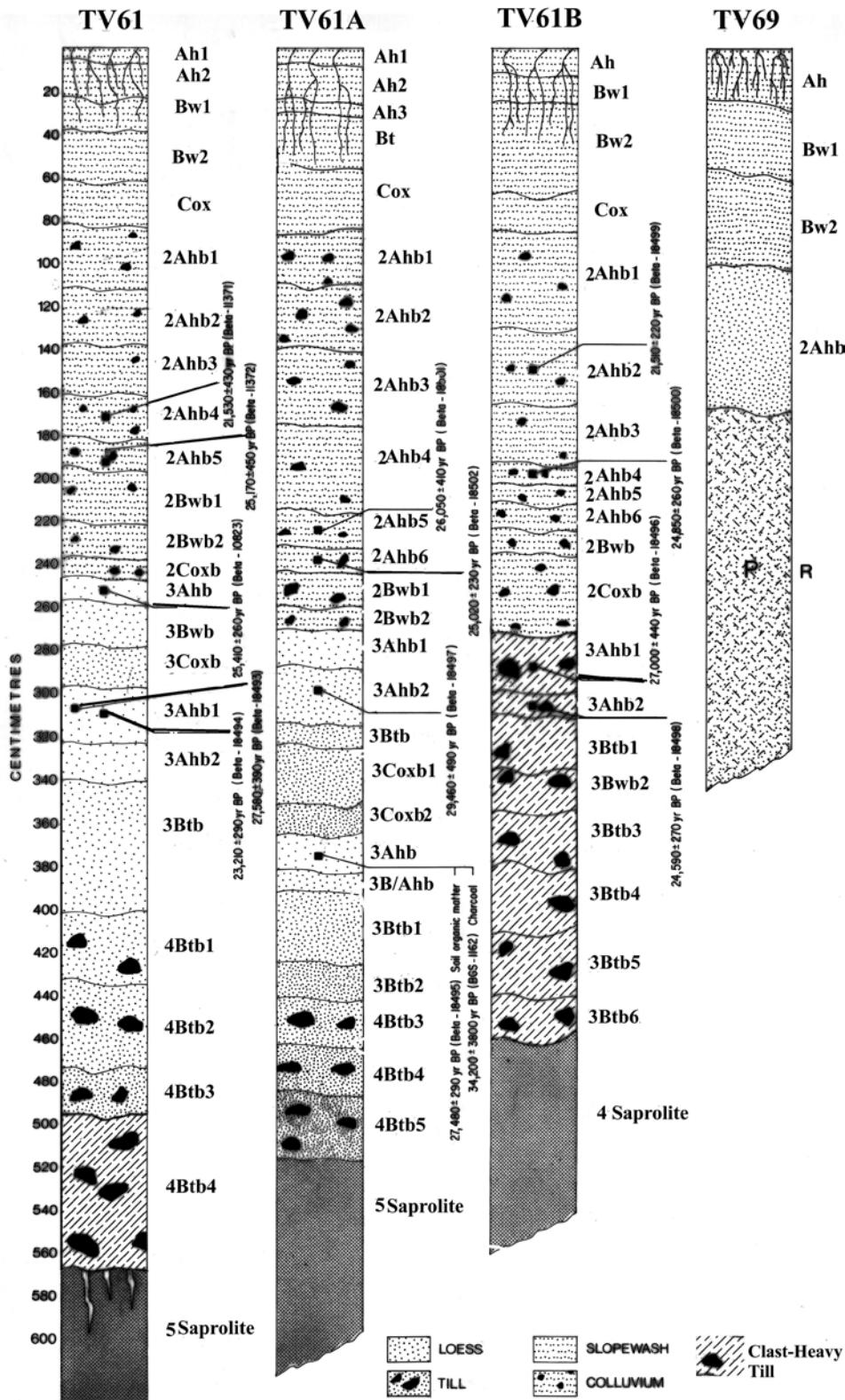
Fig. 5. Stratigraphy of TV61, TV61A, TV61B and TV69.

by definition are polyclimatic, that is, they are the product of weathering under more than one climate (Birkeland, 1999; Mahaney *et al.*, 2013, 2016), which should affect the character of the more advanced profiles in a soil/paleosol sequence, even over Late Pleistocene/Holocene and older time spans. Moreover, these profiles contain coupled till-loess components with their different clast divisions further complicating weathering trends. Thus, the microclimate factor

becomes semi-dependent and also exerts an influence on the biotic factor by either speeding up or slowing down biogeochemical processes during soil morphogenesis. Certainly, variations in both microclimate and biotic fluctuations will affect the chemical kinetics in a soil system by, for example, affecting redox potentials as well as plant and especially microbial nutrient availability for anaerobic respiration (i.e., electron acceptor release) (Mahaney *et al.*, 2016), which in turn have profound effects on chemical weathering (Young *et al.*, 2018). Alpine toposequences, among others, have received relatively little attention in the literature (Mahaney and Sanmugadas, 1983, 1989; Birkeland, 1999; Pevehouse *et al.*, 2020), and few studies (Mahaney and Boyer, 1987) have paid attention to microfloral components (fungi, eubacteria, and archaea). Bacteria (i.e., eubacteria and archaea) alone make up most of the biomass in a soil profile (Simpson *et al.*, 2007), with vegetation of secondary importance. It is important, therefore, to focus on mineral and chemical composition during the slow maturation of the soil/paleosol system from time zero to some distant time in the evolution of a catchment or stratigraphic window of importance. Here, we document a sequence of deposits in the distal reach of J.W. Gregory's 'older moraine' (Gregory, 1894), shedding new light on the complex array of weathered beds from <0.8 Ma to near the present, crossing the time lines of the Naro Moru and Teleki glaciations coupled with the re-energized slope mechanics during the last glaciation that radiocarbon date to MIS 2 and 3.

Soil toposequence (catena) research began with Milne (1937), his report in *Nature* drawing attention to the slow development of complex soils in topographic depressions (cumulative low catena member) from the cumulative lateral movement of particles from high to low members. Further work had to wait until after Jenny's (1941) treatise on soil-forming factors for Nettleton *et al.* (1968) to show how the movement of soil particles through a gravitational sequence led to changes in profile expression, the maximum effect seen in the topographic low member. Many early soil topographic studies were done on Late Pleistocene/Holocene granite and granodiorite substrates (Mahaney and Sanmugadas, 1983, 1989) with the intent to determine the effect of isolating the '*r*' soil-forming factor to determine differences in weathering and the effect of the throughput of moisture and sediment into the low soil member. In volcanic terrain of the Afroalpine zone on Mt. Kenya (Mahaney and Boyer, 1987) focused not only on weathering parameters but the effect of the '*r*' factor on soil depth, clay movement, Fe extracts and soil microbial compositions, including total fungi and bacteria. While erosion theoretically led to a thinner profile on a slope of ~30°, the Mt. Kenya catena crest, slope and depression member produced similar profile thicknesses, although a lack of P probably produced similar microbe numbers across the toposequence. Clay increased along with slightly enhanced Na-dithionite Fe in the low soil member. Similarly, other studies (Abtahi, 1980) showed the difficulty of separating topography and time in trying to understand soil morphogenesis. Later research, led by Birkeland (Birkeland

and Burke, 1988; Birkeland *et al.*, 1991) initiated attempts to study soil toposequence development through time by comparing catenas on different age deposits in the Sierra Nevada and on soil catenas in hot desert environments (Birkeland and Gerson, 1991).

Other slope cover studies are limited mainly to mountainous areas in the middle latitudes, as for example, Pawelec (2006) and Pawelec *et al.* (2015) who studied microstructure variations in slope sediment in the Tatra Mountains and Cracow Upland, Poland, and Karlstrom (1991) who interpreted paleoclimate from similar slope sites in southern Alberta.

Research Vector Over Time

Therefore, the research vector over time ranged from simple erosion studies to assess cumulative effects from high to low members in catenas, to more detailed studies of water and particle movement and structural stability over time, on to attempts to use catena-low-member soil/paleosol morphologies as more accurate indices of deposit relative age (Birkeland, 1999) than hitherto studies using moraine crest profiles (Mahaney, 1990). Moreover, not all toposequences are restricted to the Quaternary as evidenced by reconstruction of paleosols in granite-rhyolite of Precambrian age overlain with Cambrian-age sediment (Pevehouse *et al.*, 2020), the weathered unconformity the result of surficial weathering and interaction with basin fluids.

Thus, if we return to Jenny's (1941) equation, while total '*s*' remains elusive for the time being, understanding the combined role of changing climate and biotic community composition (*cl, o*), chemical weathering of normalized lithology (*p*), and with changing topography (*r*) in play during profile morphogenesis, comprehension of the total soil system may be closer at hand. To test the influence of trends in profile maturation we present here data from eight sections, all containing paleosols, nominally Inceptisols/ Alfisols/Andisols and possible Ultisols (National Soil Survey Center [NRCS] 2004). These profiles forming the toposequence were first affected by bedrock weathering and production of saprolite in different slope positions, followed by the onset of the Naro Moru Glaciation-loess-ash input, again followed by a long (~200 kyr) weathering episode (Naro Moru-Teleki Interglacial), lastly followed in turn by the onset of the Teleki Glaciation-loess-ash input and onset of weathering from MIS 6 to the present, accompanied by slope instability and emplacement of colluvium in lower backslope and footslope sections during MIS 2 and 3. While it is impossible to fully reconstruct somewhat variable warmer humid/cold (interglacial) to dry/cold (glacial) climate conditions, over the greater part of the middle to Late Pleistocene; here, we link the previously mentioned soil-forming analysis of Jenny with classical sedimentologic and stratigraphic databases.

The two oldest glaciations (Fig. 1B) on Mt. Kenya – Naro Moru and Teleki – are important stratigraphic markers of the middle Pleistocene (Fig. 1B), although with inexact

maximum and minimum time lines. The two main tills represent, with several weathering unconformities, the older and younger members of the superposed catenas, inset with younger deposits ^{14}C dated to the last interstadial (Liki) event. These younger sediments represent the latest infill of slope member materials in the history of this toposequence development. The key question is what this event-stratigraphic succession reveals about erosion-deposition on the lower slopes of Mt. Kenya following major glaciations and its relation to older stratigraphic-event histories studied in moraine stacks related to monsoon-affected terminal moraine sections on the east flank of the mountain (Mahaney, 1990; Mahaney et al., 2013, 2014). Specifically, these two younger moraine terminal elevations are out of elevation synchroneity on their respective flanks of the mountain – on the west (3150 m) and the east (3200 m), a difference of 50 m. While older deposits are missing below 2950 m on the west flank, they are spread out in echelon from 3200 m (older to younger – Gorges to Lake Ellis age, Fig. 1B) on the Nithi plateau to higher elevations on the east flank. The elevations alone from Plio/Pleistocene to the Late Pleistocene time suggest declining mass balances over time that may be related to variations in the monsoon (east flank) and thunderstorm activity (west flank).

Hence, this research seeks, not only to build upon similar research in the mountains of Poland (Pawelec, 2006; Pawelec et al., 2015) and Karlstrom (1991) in the Canadian Rocky Mountains, but to assess the 'r' (gravitation) factor in Jenny's soil-forming factor equation against climate, biota, parent material and time. Moreover, erosion over time, in the toposequence under study here, leaves weathering unconformities (Ahb horizons), all of which contain weathering archives of important paleoclimate importance, rarely assessed in other studies. Thus, as with many sedimentological studies, we are left with a minimal sediment complex to analyze and extrapolate from. The present catena presents with a stable vegetation-climate complex, that with future vegetation-climate changes leading to slope instability, one can only expect renewed erosion and reshaping of deposit thicknesses as in the past. Thus, the present middle paleosol complex (unit 3) of slopewash and colluvium will likely be replaced or buried by a new ensuite of similar sediment.

REGIONAL GEOLOGY

The description of the volcanic pile of Mt. Kenya, summarized by Baker (1967), expanded on earlier work by Gregory (1894, 1921) and Shackleton (1945), and included the first bedrock map of the massif and surrounding area. Later, Hastenrath (1984) included Mt. Kenya in his summary of glacial history in equatorial East Africa. Earlier surficial geological work by Nilsson (1931, 1935) summarized the landform record of the last glaciation, and suggested the pre-last glaciation record might be substantial, especially on the eastern flank of the mountain where a sequence of moraines existed as low as 2950 m in Gorges Valley. Later mapping and sedimentary analysis led to a slightly revised

age of 2.7 Ma for the mountain (Veldkamp et al., 2007), revision of 2.65 Ma (Everden and Curtis, 1965), and to the recognition (Mahaney, 1990; Mahaney et al., 2014) that a long sequence of glacial sediment lay, not only between the Gates (3200 m asl) and the upper Nithi River (2950 m asl) in Gorges Valley, but in adjoining valleys as well, including Hinde (Lake Ellis), Ruguti, and Hobley valleys (locations in: Barendregt and Mahaney, 1988; Mahaney, 1990; Mahaney et al., 1997, 2013) including sediment much older than what lay in the upper Teleki Valley where the Teleki Toposequence (Fig. 1A) is located. Age control for these deposits was established using relative-age controls, soil stratigraphy, and paleomagnetism. Out of all this work the terminal elevation of all glaciations on the eastern and western flanks of the mountain was established at ~2900 m asl.

The Mount Kenya Massif is encircled by Precambrian basement rock of the African craton, which surrounds the massif with eroded inliers that project above the oldest eruptive rocks of the Simbara series of basalt and agglomerate. Because these inliers project above the volcanic rocks in places, their distribution indicates that the Precambrian crust forms the structural underpinnings of the Late Neogene volcanic massif. Large metamorphic and igneous boulders of biotite gneiss, pegmatite and quartzofeldspathic granulite and muscovite schist, all ejected from the Ithanguni vent (northeast flank – 3894 m asl), are found sporadically in moraines and outwash fans on the eastern flanks of the mountain, thus validating Baker's earlier assumption about the composition of the local basement. Basalt, agglomerate and tuff of the Simbara Series and Nyeri Tuff of Miocene age are overlain by trachyandesite flows, which span the Miocene–Pliocene boundary (Mahaney et al., 2011). In places, these flows are exposed at the land surface, mantled with loess of the Pleistocene and the Pliocene age, and/or are otherwise buried by younger basalts and basaltic pyroclastic rocks. The Mount Kenya Volcanic Suite spans the Pliocene–Pleistocene boundary and is composed mainly of basalt, phonolite, trachyandesite and kenyte. The latter two lithologies form the bedrock beneath unconsolidated deposits in Gorges, Hobley and Teleki valleys. In the area of the Teleki Toposequence (Fig. 1A) on the western approach to the mountain, phonolite bedrock, with an undetermined age, considered to have been sourced from one of the numerous parasitic vents, forms a rock shoulder to the south of the Naro Moru River (Fig. 1B) that was molded and smoothed by glaciation prior to the weathering event that produced saprolitic beds at the base of sections in the toposequence. It is this erosional-depositional toposequence, built into its saprolite base of the middle Pleistocene age, with overlying successions of paleosols, that together provide a paleoclimate database linking glacial to interglacial cyclic episodes, up to the present.

MATERIALS AND METHODS

Field analysis. Eight sites in Gregory's lateral moraine (Fig. 1B) were selected based on field mapping and air-

photo interpretation (1 : 20,000 scale) of deposits. Sediment embedded in sections from the crest (TV23) along upper and lower backslope and footslope sites to the toeslope position (Fig. 2) were sampled, after excavating to variable depths of <~7 m. Paleosol profiles with polyclimatic characteristics revealed multiple buried and surface profiles grading from the crest (TV23) and upper backslope positions (TV23A, TV23B), the crest losing mass to sections lower down the slope. These sections, in turn, sourced lower backslope sections (TV23C and TV61), the throughput of sediment, while episodic after the Naro Moru Glaciation and between the Naro Moru and Teleki Glaciation, does not appear to have greatly affected the structure of individual profiles. Within the lower backslope (TV61), and footslope positions (TV61A, TV61B), the older and lower paleosols (lithic units 3 and 4) appear in place, but with unknown loss by erosion and emplacement of colluvial bodies of sediment sourced from above, and possibly also from allochthonous origins from up-valley or beyond. Amazingly, the toeslope positioned paleosol, while thin, shows a similar particle-size distribution to what exists in the lower backslope positions, but with somewhat lower pH and higher organic carbon and nitrogen inputs. The unusual low thickness of the toeslope paleosol (TV69) indicates it may have suffered from the throughput of soil water and removal of older sediment.

Soil descriptions follow guidelines established by the NSSC (2004), Soil Survey Staff (2010) and Birkeland (1999). The 'h' horizon designation (h = humus) follows the CSSC (1998) where color is darker than 10YR 3/1. Soil color determinations both moist (m) and dry (d) assessments are based on Oyama and Takehara's (1970) soil chips, which are essentially the same as the Munsell System (Macbeth, 1992), excepting the 1/1 (value chroma) is missing in the Munsell system. Otherwise the color chip notations are similar. Approximately 500 g samples were collected from horizons at each site, sufficient to allow for particle size, clay mineral, soil chemical, microscopic (light microscope-SEM/EDS), geochemical and amino acid analyses.

Laboratory sediment analysis. The air-dry equivalent of 50 g oven-dry material was weighed out for particle-size analysis and treated with 30% H_2O_2 to oxidize organic material. Particle grade sizes follow the Wentworth Scale with the exception of the clay/silt boundary (2 μm) which follows the U.S.D.A. After wet sieving the sands (2 mm – 63 μm), the <63 μm fraction (silt plus clay) was analyzed by hydrometer (Day, 1965). The materials were later dried and sieved to separate the sand fractions (2000–63 μm fractions). Organic carbon was determined by loss-on-ignition (Walkley and Black, 1934). Nitrogen was determined, partly by a Leco apparatus following Bremner (1965). Soluble salts were analyzed by electrical conductivity following procedures outlined by Bower and Wilcox (1965).

Elemental analysis of 61 sediment samples was performed on whole earth (<2 mm) and selected sands (63– 2000 μm) by instrumental neutron activation analysis (INAA) at the SLOWPOKE Reactor of the University of Toronto (Hancock, 1984). Appropriate standards were employed to calibrate the equipment (Harrison and Hancock, 2005).

Cation exchange capacity and extractable cations were obtained following the ammonium acetate method following Schollenberger and Simon (1945) and Peech *et al.* (1947).

The clay fraction was studied for mineral composition, by means of powder XRD, using a Toshiba ADG-301H and Norelco diffractometers with Ni-filtered CuK*ά* radiation. Scanning steps for oriented samples were 0.02° 2θ from 2 to 55° 2θ. A semi-quantitative mineral composition was determined from peak integral intensities of halloysite, metahalloysite, gibbsite, hematite, goethite, generic plagioclase, pyroxene, and magnetite (Whittig, 1965; Vortisch *et al.*, 1987).

Samples of very fine to medium grade size sand were selected for routine analysis by scanning electron microscope (SEM) and energy dispersive spectrometry (EDS) following procedures outlined by Mahaney (2002). The sands were pretreated for particle size analysis, subjected to light sonication to remove clay. Individual grains were selected for light microscopic examination.

The Fe_d and Al_d extractions, pioneered by Mehra and Jackson (1960) and Blume and Schwertmann (1969), were made from 1 g (< 2 mm fraction) subsamples, with Na-dithionite, releasing crystalline, amorphous, and organically-bound forms of Fe and Al, using sodium citrate buffers, following criteria set out by Coffin (1963), Dormaar and Lutwick (1983) and Mahaney *et al.* (2009). Processed in the dark, acid ammonium oxalate was used to extract Fe_o (×1.7 = ferrihydrite; Parfitt and Childs, 1988) following McKeague and Day (1966), and Al_o. Subsequently, concentrations of Fe and Al extracts were determined using a Perkin-Elmer 373 atomic absorption spectrophotometer (AAS); total Fe and Al by INAA. Iron and Al extracts were analyzed to determine if pyrophosphate (*p*), acid ammonium oxalate (*o*) and Na-dithionite (*d*) could provide raw concentrations for distinguishing strength of weathering for lithic groups within profiles. These raw data groups can then be converted using arithmetic functions to: test ratios of ferrihydrite (Fe_o) to total oxihydrites (Fe_o/Fe_d); adjusted raw concentration of Fe_o x 1.7 to approximate ferrihydrite; total Fe less Fe oxihydrites (Fe_t-Fe_d) to determine primary Fe; total oxihydroxides-ferrihydrite (Fe_d-Fe_o) to determine secondary goethite plus hematite; total oxihydrites/total Fe (Fe_d/Fe_t) as a proxy for relative age; pyrophosphate Al/total Al (Al_p/Al_t) as a proxy for organic carbon; and pyrophosphate extracts (Al_o-Al_p) to determine approximate concentrations of imogolite and allophane. These functional relationships follow procedures outlined by Parfitt and Childs (1988) and Mahaney *et al.* (1999).

Amino acid analysis was carried out on whole soil samples (<2mm fraction) and follows methods outlined in Mahaney *et al.* (1991). Samples were rinsed with distilled water to remove carbohydrates and salts and 10 ml rather than 5.5 ml of HCl for hydrolysis. Samples were equilibrated and twice sonicated during a 24-hr heating period; the resulting acidic solution separated by filtration rather than by centrifugation. As pointed out previously in other

publications (Mahaney, 1989; Mahaney *et al.*, 1991) these method changes result in purer amino acid results.

RESULTS

The Sites. Sites throughout the toposequence range: from the summit (TV23), to the upper backslope (TV23A, 23B), lower backslope (TV23C, TV61), footslope (TV61A, 61B), and the toeslope (TV69). The location for Met Station (3052 m asl; Fig. 1B) is 0°10'13.21"S, 37°12'48.32"E; site TV23 (3005 m asl) is at 0°10'10.16"S, 37°12'32.82" E; site TV61 (2998 m asl) is at 0°10'13.01"S, 37°12'31.44"E; and site TV69 (2988 m asl) is at 0°10'15.23"S, 37°12'31.91"E. These GPS elevation and coordinates were taken off Google Earth and are approximate only.

Summit site. The summit site (TV23: Fig. 4) has been the subject of previous publications (Vortisch *et al.*, 1987; Mahaney, 1990). Two paleosol bodies occupy the full ~4.4 m depth of section, lithic units differentiated by Arabic numbers, Unit 1 left undefined by convention. Unit 1, comprised of loess and ash with a thickness of ~1 m probably reflects its elevation and position relative to the Naro Moru Valley off to the north. Four horizons at the surface (A–B horizons) make up the epipedon (solum) of the upper paleosol profile overlying till in the 2Cox1 and 2Cox2 horizons comprising a thickness of ~77 cm representing a residuum left from glacial and aeolian erosion since the end of the Teleki Glaciation (circa 128 ka). The ridge crest site can be traced down-valley approximately 0.5 km to where loess and till grade into slopewash and colluvial beds intersecting the Naro Moru River (see Fig. 1B).

The lower paleosol in TV23 (Fig. 4) carries an upper and lower suite of sediment comprising loess, with a mix of weathered tephra forming the buried paleosol epipedon of 3Ahb, 3Btb1, 3Btb2 and 3Btb3 horizons. This mix of loess and tephra from unidentified sources comprises deposits emplaced during the interglacial weathering event of the Naro-Moru-Teleki glaciations (2nd to last interglacial on Mt. Kenya). Lithologic unit 4 comprises two horizons 4Btb4, 4Btb5), the upper horizon, based on clay development and mineral weathering, is more heavily weathered. Of the two paleosols, the upper unit contains less clay in the solum (A+B horizon group=epipedon) than the lower unit, which may be a function of time or different interglacial climates. The two lowest horizons (till) in unit 4 contain illuvial clay at ~90% which requires the 't' subscript and a B horizon designation.

Upper backslope paleosol complex. The upper paleosol in the upper backslope group of deposits (TV23A) consists of 4 lithic units (Fig. 4), including a loess body of ~60 cm depth with root networks at present extending to half the thickness, as in TV23, terminating just above the mid Bt2 horizon. Till in the upper paleosol (2Bt3 and 2Bt4 horizons) parallels the TV23 paleosol in that the upper till units contain an influx of silt (2Bt3), presumably loess, translocated from above. Thus, the 2Cox1 in TV23 and the 2Bt3

horizon in TV23A, even with different thicknesses, both in the two upper paleosols of TV23 and TV23A seem to have parallel leaching histories. While we cannot be certain of the silt input in both horizons it may be that the slightly higher silt content is the result of glacial grinding (Smalley, 1966). The lower paleosol in TV23A with fewer horizon subdivisions lacks the 3Ahb horizon prevalent in TV23. The lower units (3Btb, 4Coxb1, 4Coxb2) form what appears to be a truncated loess body comprised of loess-over-till weathered unit, representing a loess/till residuum lacking the organic accumulation (3Ahb), the loessic deposit that is thinly represented in TV23.

Descending the toposequence slope, the TV23B (Fig. 3B, site; Fig. 4, section), stratigraphy in the upper backslope comprises five lithic units, the upper paleosol epipedon with four horizons (A–B group), and with deeper penetration of present-day root systems to ~80 cm possibly reflect a more stable particle structure. Across a near horizontal contact, similar to horizon contacts of nearly all horizons in Fig. 4, a 40-cm thick 2Cox horizon comprises the lower till in the surface paleosol. Across a contact at ~120 cm, the thin body of till (2Cox) overlies a thick body of loess comprising three horizons (3Btb1, 3Btb2, 3Btb3), which extend to ~210-cm. Again, the missing 3Ahb horizon at the 2Cox-3Btb1 contact matches the missing Ahb in TV23A but with the upper truncated animal tunnel (krotovina) formed at some time after deposition of Teleki Till. This missing Ahb horizon was in all likelihood an organic-rich horizon eroded prior to burrowing by a hare or hyrax at some time in the past and its perfect preservation through the underlying 3Btb1 and 3Btb2 horizons speaks to profile structural integrity that seems to have prevailed through vast periods of time, i.e. following the Teleki advance. If the relative age-dating control estimated for this toposequence is correct, this preservation follows from the clay-rich particle-size distributions that will be discussed in a later section. TV23B is the first section in the descending transect with a bedrock weathered horizon (5Saprolite) below the ~280-cm level.

Lower backslope. The lower backslope in the toposequence comprises two profiles of which TV23C is the higher, located as shown in Fig. 2. The A–B horizon complex (paleosol epipedon, Fig. 4) exhibits a shallow present-day root system comprised of slopewash over colluvium at ~80 cm depth, the colluvial body of ~30 cm thickness overlies a buried paleosol with a five-part subdivision of Ahb horizon slope wash sediment (3Ahb1–3Ahb5 horizons), all differentiated primarily by color contrast indicating higher organic carbon above to lesser amounts below, the two lowermost horizons showing more intense oxidation (lower value, higher chroma, (Oyama and Takehara, 1970). Differentiation of the 3Ahb5/3Bwb is on the basis of color, the particle size distributions relatively similar in both horizons. Grading downward in section, the till body (4Btb1, 4Btb2) of some ~70-cm thickness more or less equates with TV23B, although somewhat thinner than in TV23 and TV23A and with evidence of clay translocation. The unit 5Saprolite begins at approximately the same depth as in TV23B.

The bottom section (TV61, site Fig. 3A, stratigraphy Fig. 5) of the lower backslope is a 6-m thick body of slopewash, colluvium, loess, and till with some additions and subtractions compared with sections higher up in the toposequence. The surface epipedon (Ah1, Ah2, Bw1, Bw2) formed in slopewash with horizons younger than ~21 ka given the ^{14}C ages of horizons in unit 2. Horizon differentiation is based on color changes reflecting mainly variations in organic carbon and mineral weathering. The Cox horizon marks the lowermost extent of the surface profile that formed presumably during the late stages of the last glaciation, and/or during the Holocene, or at least with additional moisture onset at the end of the LGM (~15 ka). Generating slopewash would in all likelihood accelerate during the LGM with Podocarpus and bamboo shifted to lower elevations approximately ~400 m down-valley, as estimated by Mahaney (1990). The onset of colluviation (Unit 2) after ~25 ka would certainly benefit from vegetation shifted to lower elevations with the onset of advancing Liki ice to terminal positions within ~200 m elevation above the toposequence in Teleki Valley. As with the surface profile, unit 2 paleosol horizon differentiations are based on color differentiation with only slight changes in silt and nil clay with depth from 2Ahb1 to 2Coxb. Interestingly enough paleomagnetic measurements in TV23, TV23A, TV61, TV61B and TV69 all register normal polarity with the exception of horizons 2Bw1 and 2Bw2, in TV61, both in slopewash sediment, which carry a paleomagnetic excursion matching the Mono Lake Excursion of ~21–25 ka (Barendregt and Mahaney, 1988; Mahaney, 1990). It could be that while this excursion matches the Mono Lake, its position matched with somewhat inconsistent ^{14}C dated beds may relate to an unidentified paleomagnetic event. Lithic unit 3 (3Ahb and 3Bwb) comprise loess younger than ~27,580 ± 390 (Beta-18493) contrasted with an age of 23,210 ± 290 yr BP (Beta-18494), the latter age possibly contaminated given the age of 25,410 ± 250 yr BP (Beta-10823). Judging by radiocarbon dating, the 3 unit falls within MIS 3 and possibly older given the clay increase in 3Btb. Crossing the contact between units 3 and 4, at 4 m depth, leads to till with similar silt distributions with depth against variable clay content. The three upper horizons comprising unit 4 are considered to be till with infills of loess or glacially-ground silt. The 4Btb4 horizon of ~90 cm thickness, with 20% clay and 40% silt, presents with leached tongues of clay infiltrating the underlying 5Saprolite bed. These leached tongues suggest that following erosion of the saprolite (unit 5) and deposition of Naro Moru Till, unit 4 till was heavily leached through the clast-heavy till into the saprolite.

Footslope units. Two sections make up the composite suite of sections in the footslope (Sections TV61A and TV61B) portion of the toposequence. The TV61A section is nearly a carbon copy of TV61 with a similar 6 m thickness and array of horizons that match closely, one section to another. The surface profile is strictly slopewash with cumulative Ah horizons depicting variations in organic carbon input, with a root network nearly twice as thick as in TV61, although

with similar B/C horizons, and the 'ox' subscript in the C horizons indicating appreciable oxidation. The colluvial body in unit 2 is similar and somewhat deeper than that in TV61, possessing inverted radiocarbon ages, both indicating an LGM age suggesting the sediment probably relates to erosion of the till sections from above. Crossing the contact between units 2 and 3, at 265 cm, leads to a loess segment dating between 25 and 34 ka indicating a link to MIS 3, showing a fully formed paleosol classified as an Alfisol, that is, with a fully formed B horizon with clay input, hence, the 't' = ton (German for clay). All this, combined with oxidized C horizons, indicates a reasonably wet interstadial time and with loessic sediment presumably sourced from a nearby MIS 3 glacial front. Unit 3 in the mid-upper paleosol grades across the 3Ahb1 horizon (270–290 cm) contact to a second and older loess body (lower unit 3 at 370 cm) that forms the epipedon of the lower paleosol with a clay content approximately half that in the lower paleosol of TV23, followed by a steadily increasing clay content into the till of unit 4. The 5Saprolite follows the distribution shown in TV61.

Depth of the TV61B section is somewhat less than in TV61 and TV61A, reaching the 520 cm level with fewer lithic divisions but with a similar range of slopewash, colluvium, loess and till to saprolite. The surface paleosol shows thinner A and thicker B horizons situated on a reduced slope less facilitative to movement of fine grade size material. The colluvial body reaches to the 270-cm level and dates to within MIS 2 (LGM), resting upon lithic unit 3 depicted as a till body with higher organic input in the 3Ahb1 and 3Ahb2 horizons through to the saprolite at the ~460-cm level. Radiocarbon dating of the upper epipedon in unit 3 contains inverted dates probably related to increased porosity and presence of younger material transported to lower horizons in the sequence. The presence of six horizons in the unit 3-till body most likely relate to a long weathering history with clay input overriding the genesis of C horizons. The clay content of the 4-Saprolite horizon is more or less the same as in overlying horizons suggesting a longer weathering event than in TV61 and TV61A.

Toeslope. The TV69 section in the toposequence toeslope presents a surface Ah/B horizon set overlying the 2Ahb horizon, that is, essentially slopewash over loess covering unweathered phonolite. There is nothing in textural or color parameters to suggest extreme weathering, which suggests the profile relates to the last glaciation either the LGM, or weathering through the Holocene. It may be that a warmer and wetter Holocene with heavy throughout of water may have removed older sediment, perhaps the latest of many episodic erosion events. The presence of unweathered bedrock lacking a saprolite cover strengthens this postulate.

THE PALEOSOLS

Sediment in all sections is weathered either directly from bedrock or from till and/or reworked sediment by aeolian or gravitational processes producing a stratigraphic

complex with section affinities tied together among various sites in the toposequence. All horizons, with the exception of the saprolite beds, are identified using standard pedologic identifiers: A(h) = organo-mineral complexes with colors in the 10-5YR hue, values ~2–4, chroma 1–4; B = 10-5YR hue, values 3–5, chroma 2–6; and C or Cox with 10-5YR hue, values 3–5, chroma 2–6. Commonly B horizons are the 'color B' variety with heightened secondary hematite or goethite, whereas others are clay rich (Bt), with the 't' added from 'ton' (German for clay). For a B horizon to qualify as Bt it must contain more than 1.4 x the clay concentration in the overlying horizon usually part of the A group. C horizons carrying the 'ox' subscript indicate oxidation effects, sometimes with a mottled character. Given the age of the *in situ* sediment and the reworked sediment almost all colors are designated from the 7.5 to 5YR (yellow red) pages of Oyama and Takehara (1970) equivalent to the Munsell soil color system.

Classifying these paleosols into the US Soil Taxonomy (Soil Survey Staff, 2010) is difficult since we do not have close-order data on temperature and precipitation at the sites in question. Classification at the order and suborder levels is based only on experience over several years operating in the field. Thus, the sites are considered to have mean temperatures of 7–10ºC with precipitation in the ~1000 mm amount, thus producing a udic moisture regime which means rainfall plus stored moisture regime exceeds evapotranspiration. During times of forest shift to lower elevations during ice advances, the moisture regime may have shifted to xeric, meaning soil moisture reductions might have produced dry conditions. Strictly, soil temperature regimes are based on the mean annual temperature at 50-cm depths, which are clearly not available in this case. While classification of these pedons is based more on climate averages than on pedogenic factors, the range of orders for the toposequence varies from Inceptisols to Alfisols, with some profiles wandering into the Andisol (formed largely in tephra) and Ultisol (low base saturation) orders. The only clear Andisols are in TV23 (lithic units 1–2 and 3). While some glass is found in other Ah and Ahb horizons it is not of sufficient weight to allow invoking the Andisol order. Ultisols are well developed soils with low base saturation that could fit the description of some older paleosols in unit 4 within the lower backslope and footslope. Inceptisols are immature or younger paleosols lying between still younger Entisols (A/C/Cu horizonation) and more fully developed weathering entities such as, in this case Alfisols (soils with argillic, clay-rich lower horizons). Within the Alfisols, the Udalf suborder largely predominates, the Ustept suborder within the Inceptisols (Soil Survey Staff, 2010). The paleo-prefix to suborders is only approximate.

Paleosols in the crest and upper backslope (TV23, TV23A, TV23B, Fig. 4) all carry the till couplet of Naro Moru (older) and Teleki (younger) deposits interbedded with loess with sharp, nearly horizontal contacts indicating structural stability for paleosols in these sections and rapid influx of loess, that is, less time for slow transition from glacial to interglacial conditions. Sections lower down in the lower backslope (TV23C (Fig. 4) and TV61 (Fig. 5) contain increasing slopewash with variable amounts of colluvium and loess, some lenses of which lend themselves to radiocarbon dating (see Fig. 5). Lower down in the toposequence within the footslope, both the TV61A and TV61B sections correlate closely with sections above, particularly TV61.

The surface profiles in TV23, 23A and 23B carry nearly 1-m thick loess beds, part of which appear to have released silt to the gravitational system allowing surface sediment throughput to slopewash beds in sections lower down in the toposequence. While we have no instrumental data on overland flow downslope, the lithic designations argue for slopewash transference from section to section. Lithic unit 2 (tills), in the three higher paleosols, exhibits progressive thinner bodies that may represent units that have lost sediment to gravitational movement into the lower backslope and footslope sections, culminating in or washed out of the toeslope unit.

While the toeslope section depicts part of a paleosol with internal clay movement, the overall thinness of the paleosol, unexpected as it is, seems to indicate a relative short time of sediment residence, the end product of a long episodic trend of erosion and deposition. Thus, we are left with a fresh bedrock surface overlain with a 2Ahb horizon of loess with an unknown, but young age, and covered with slopewash.

PARTICLE SIZE

TV23. The toposequence crest section presents with the highest silt content in the Ah1 horizon (Fig. 6) with ~80% recorded, dropping to 20–30% with depth throughout the surface paleosol (~175 cm). Clay content, steady at 10% in the Ah1, increases down section in stepwise fashion in the lower Ah group increasing from ~60% to ~80% in the Bt1and Bt2 horizons, decreasing slightly in the C horizon group of samples. The outstanding part of this pattern is the high silt in the Ah1, which presumably follows from the long exposure of the crest sample to wind moving off retreating Teleki ice and later terminal positions of Liki ice during various stades of the last glaciation, especially during the Last Glacial Maximum (LGM, ~25–15 ka). The increased clay in the Ah2 to 2Cox2 horizon is a product of weathering over the period 128 ka to present which seems to have been sufficient time to weather the silt content to its 20–30% values.

The lower paleosol profile depicts a stepwise increase of silt from the 3Ahb horizon through to the 3Btb2 horizon at 215-cm where concentrations reach ~80%, decreasing thereafter lower in the section, a trend that may indicate down-section transfer from ~180–380-cm depth. The stepwise increase in clay content from the 3Ahb through the B horizon group (including the till, unit 4), rather atypical of an Alfisol, is similar to or greater than in the surface paleosol reaching 90–95% in the 4Btb4 and 4Btb5 hori-
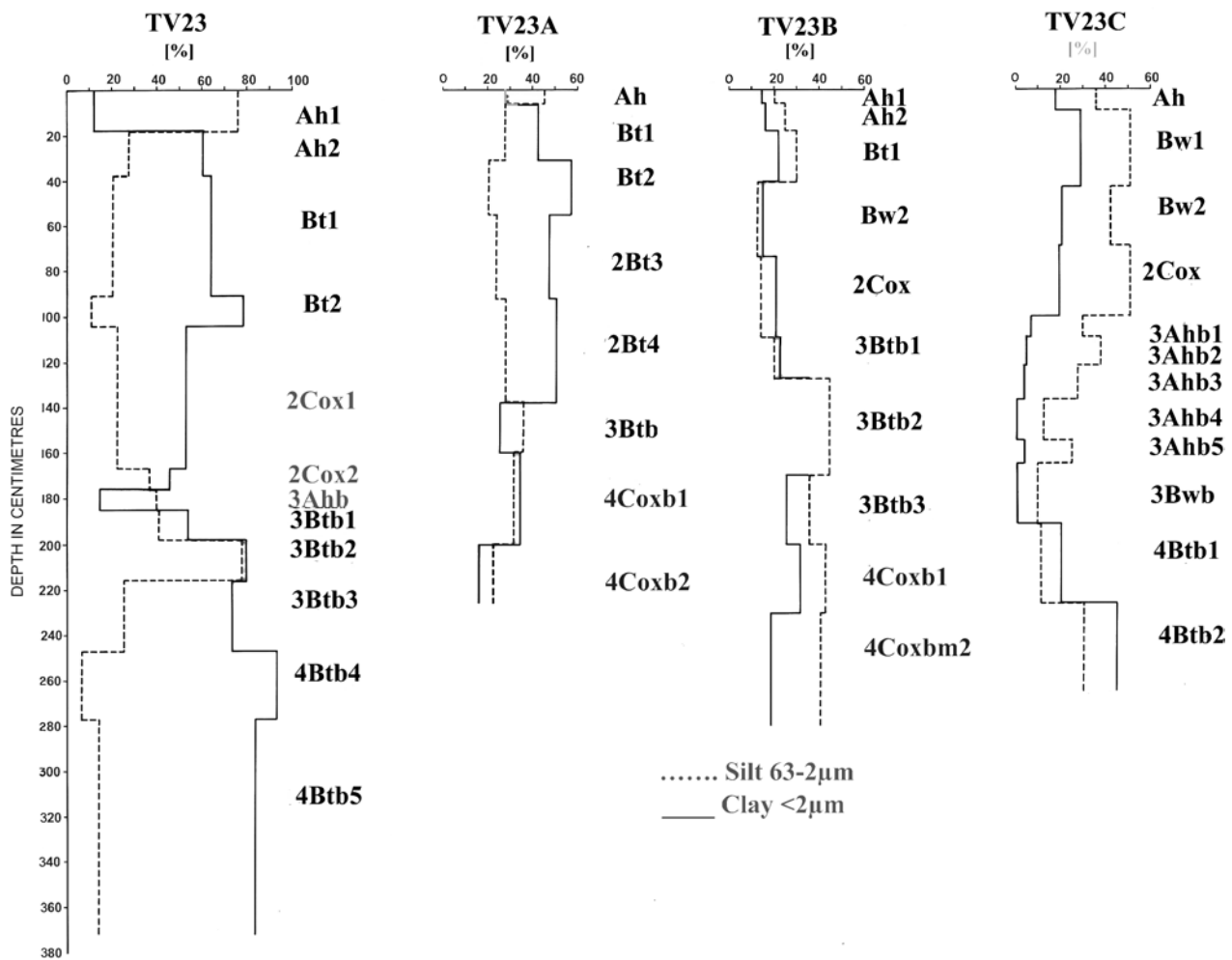
Fig. 6. Particle size distributions with depth in sections TV23, TV23A, TV23B, and TV23C.

zons. In most cases, clay percent increases in the lower paleosol horizons but in this case even with the increase in clay content, pebble content in the 4Bbtb4 horizon remains in place while the fewer sand clasts carry stronger weathering signatures. Sediment in units 3 and 4 takes on the textural character of clay-stone (without lithification), which in a weathering scenario requires either long time for both pedogenesis and diagenesis or extreme climate. Based on particle size distributions, stronger weathering in the lower paleosol indicates a longer weathering hiatus or stronger climate compared with the surface paleosol, a period more or less equivalent to ~0.3 Ma Naro Moru-Teleki Interglacial). The ratio of gibbsite to halloysite argues for time over climate as discussed later.

Both paleosols are considered to have provided source materials contributed to paleosol sections farther down slope with perhaps the surface paleosol providing a greater percentage, at least for the latest additions during MIS 3 and 2.

TV23A. Analysis of the particle size distribution in TV23A (Fig. 6), the broad shoulder-like site below TV23, yields

an interesting comparison to the crest site in that gravity action may have reduced silt content to about half of what is at the higher position. Slope is estimated at 10° with vegetation similar to TV23, predominately Podocarpus with minor bamboo. The Ah horizon, although thinner than in TV23 (<10 cm), the silt content is at ~45%, decreasing to 20% in the 2B group of horizons, rising slightly in the 3Btb transition zone, thereafter silt decreases to the base of the section. As in TV23, the two till units are present in both the upper (lithic unit 2) and lower (unit 4) paleosols, the clay content noticeably higher in the upper paleosol compared with the lower one. Broadly speaking the clay content in the upper paleosol is similar to its counterpart in TV23 suggesting a similar weathering history, if somewhat attenuated by gravitation movement of sediment downslope.

TV23B. The TV23B section, with stronger bamboo input and similar Podocarpus, rests on ~15° slope (Fig. 3B) leading to increased loess input as attested to by 20–25% silt in the Ah1 and Ah2 horizons, rising again in the Bt1 and decreasing in the Bw2 horizon. Even though clay rises slightly in the Bt1, it is barely sufficient to qualify for a 't'
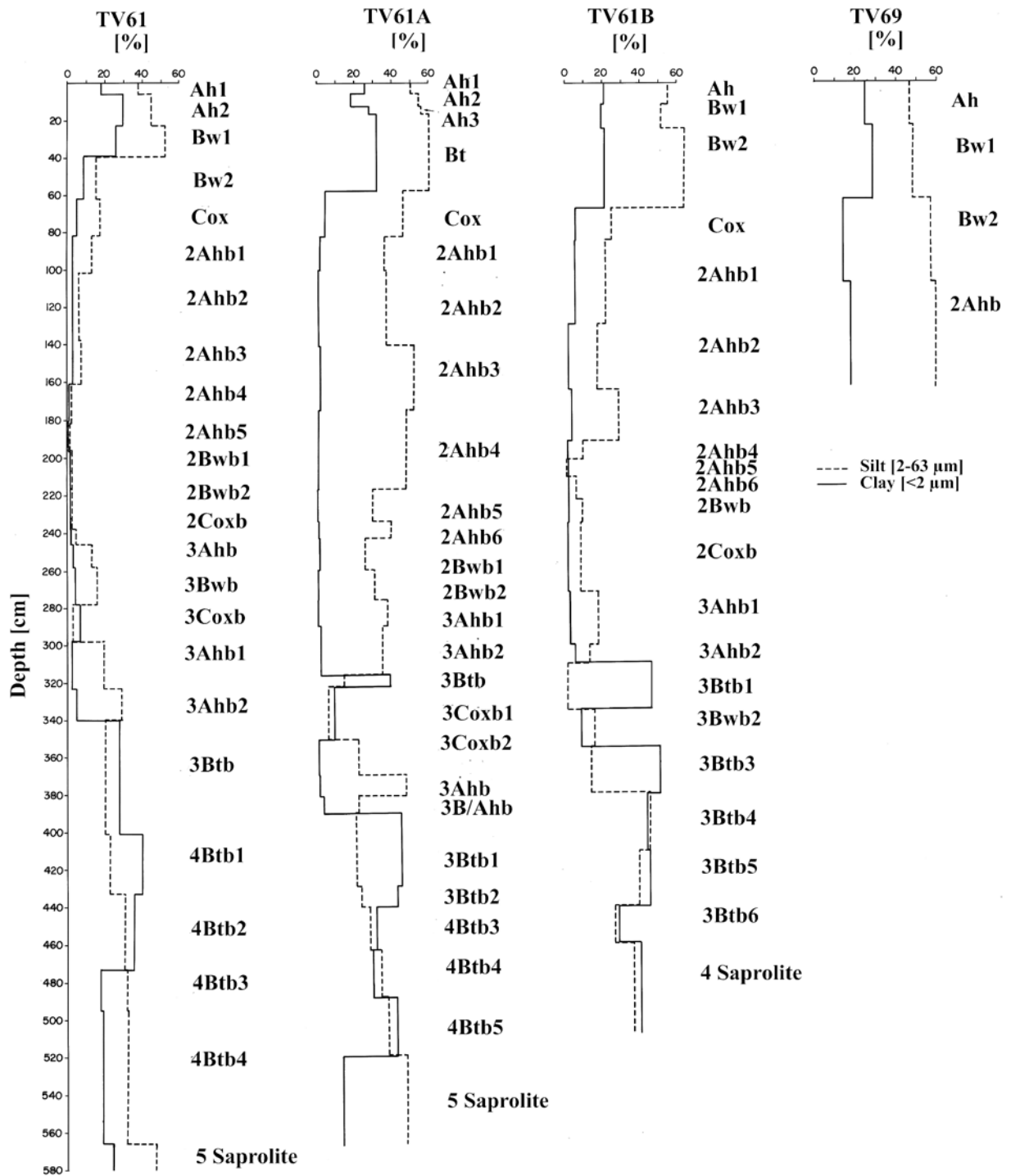
Fig. 7. Particle size distributions in sections TV61, TV61A, TV61B, and TV69.

designation (1.4 increase x the % clay in the overlying Ah2 horizon). The till in the upper paleosol (2Cox) rests on a truncated lower paleosol, with a missing organic horizon but with an upper krotovina (animal burrow), well preserved in the lower 2Cox, which is younger than the deposit. Compared with TV23 and TV23A, the two till units in TV23B are thinner by half, the loss probably reflecting gravitational stress and the increased slope angle.

TV23C. This site located lower down in the toposequence, crossing from the upper to lower backslopes, begins with an increase in slope to ~20º with increased bamboo and reduction in Podocarpus, the vegetation change offsetting the increased slope by lower root penetration but somewhat increased root networks acting with grass compared with forest root strength. Particle size exhibits a fully staggered descent of silt in units 1 and 2 shadowed almost perfectly

by clay, with sand taking up the difference. Below the surface paleosol into units 3 and 4, comprising the lower paleosol, silt decreases in step with decreasing clay into the 4Btb1 horizon where clay increases to near ~50% in the 4Btb2 horizon of the Naro Moru Till. The most remarkable aspect to the particle size changes with depth are the slight changes within the 3Ahb group of horizons making up the upper epipedon of the post-Naro Moru paleosol, horizon differentiation dependent upon variations in soil color reflecting changes in organic carbon content. Assuming this organic complex has been in situ for possibly ~0.4 Ma suffering throughput of soil water, although with isothermal conditions, it is astounding that the carbon input indicates longevity, all of which may reflect a high lignin input as indicated from research into much older sediments of Olduvai age on the far eastern flank of Mt. Kenya (Mahaney *et al.*, 2013).

TV61. Situated on a slope similar to TV23C, this site (Figs 3A and 7) is adjacent to the track leading to Met Station at ~3000 m (see Fig. 1A), the end of the road leading from Naro Moru township to the Teleki Valley trailhead (i.e. Met Station). Complete with a pronounced saprolite bed, this section reaches ~6 m thickness at the lower end of the backslope. Compared with sections higher up in the toposequence the two-till assemblage is missing, only the lower till-loess pedostratigraphic complex is present with an overburden of colluvium recognized from several ^{14}C dates as belonging to MIS 3, possibly partly from earlier episodic colluviation during the Liki I glacial stage (MIS 4). Younger unit 1 represents a surface paleosol of loess and slopewash to ~80-cm depth overlying colluvial beds (unit 2) to 220-cm depth, with horizons consisting largely of sand with minor variations of silt and clay, recognizable differences emanating from variable concentrations of organic carbon. What is more remarkable is that ^{14}C dates were obtained from sandy beds (to ~240-cm, once again highlighting the longevity of carbon in this environment. The upper section comprises loess and slopewash with till missing, overlying an older loess (245–300-cm), which in turn overlies another loess (300–400-cm), which may in whole or in part belong to the till in unit 4.

TV61A. Entering the footslope sections, TV61A is approximately 10 m south of TV61 (Fig. 1B) and about 3 m below the surface of TV61. Lithic units 1 and 2 extend downward to 280-cm depth, about 15–20-cm deeper than unit 2 in TV61. The staggered array of silt and clay with depth to unit 3, although similar to TV61 (Fig. 5 and Mahaney *et al.*, 1991), presents similar clay content but with considerably higher silt and less sand than in TV61. These differences in clay, silt and sand do not appear to have affected in situ carbon as ^{14}C ages are relatively consistent with depth and all ages have low standard deviations, although one charcoal date (BGS-1162 at 34,200 ± 3600 yr BP) at 360 cm depth is above ±10% of the age and therefore subject to caution. Lithic unit 3 from 280 to 440-cm depth progresses through two recognizable paleosols, with all horizons of variable

thickness, and with the lower profile (370–440-cm thickness) carrying somewhat thicker and stronger B horizons, signally longer time of formation or climate more conducive to weathering during MIS 3. Attesting to the overlying beds of colluvial sediment, the underlying loessic sediment was observed in place with no distorted beds. Unit 4, comprising the weathered beds of the Naro Moru till, shows a stepwise increase in clay from 20 to 40% from the 4Btb3 to the 4Btb5 horizon, presenting a different weathering history from TV61. While the lower paleosol in unit 3 could be part of the epipedon of unit 4, only a detailed sand analysis would confirm this assertion and could be tested from the mineral and chemical content as discussed later in this paper. The low clay content (10%) of the saprolite bed contrasts with the 20% content in TV61, the difference awaiting testing of the paired mineral and chemical properties discussed later. Relative section depth difference between TV61 and TV61A of ~45-cm is probably the result of relative erosion processes operating at the surface of the saprolite beds in the two sections.

TV61B. The surface paleosol in TV61B is a near copy of the A/B/C profile in TV61, and TV61A, with only minor differences in thicknesses of the B horizons. The colluvial unit in lithic 2 is similar to TV61A with less silt in place and clay close to 0%, but with greater sand content. Silt tends to increase upward from 2Ahb3 to 2Ahb1, possibly as loess was added during the onset of the Liki II glacial stage (LGM). Clay is <10% with a near uniform concentration through unit 2 to ~280-cm depth. Unit 3 presents with a complex buried Alfisol with two clay bulges in 3Btb1 and 3Btb3 which may represent two separate leaching events separated by truncation of the lower B horizon by erosion of a former A horizon between the two high clay segments. Crossing the boundary from units 2 to 3 (280-cm), presents with till in the lower unit considered, unlike the scenario in TV61A, to represent one weathered till sheet above the saprolite at ~460-cm depth where clay and silt are near 35%. The clast-heavy till at the base of the section may represent clast slippage at the terminus of ice during emplacement of the Naro Moru Till. This is the lowest elevational position (2998 m asl) of the Pleistocene ice on the west flank of the mountain, similar to terminal ice positions in Gorges Valley on the east flank (Mahaney, 1990).

TV69. The toeslope profile defeats all expectation with an Inceptisol (Ah/Bw1/Bw2) paleosol overlying a 2Ahb horizon at ~105-cm depth, contact with the underlying bedrock at ~165-cm leaving a 60-cm thick buried Ahb horizon. With substantial thicknesses of silt in slopewash beds in the surface paleosols of TV61–TV61B, the expected input of silt is seen to have been minimal in this depression site. The weathered state of the sediment complex in the Ah/Bw1/Bw2 horizons is suggestive of field colors and hence reworked material from the slopes above. Loess, underlying the slopewash in the surface beds, maintains a horizontal surface contact indicating little disturbance. Overlying horizon contacts present only a slight slope toward the
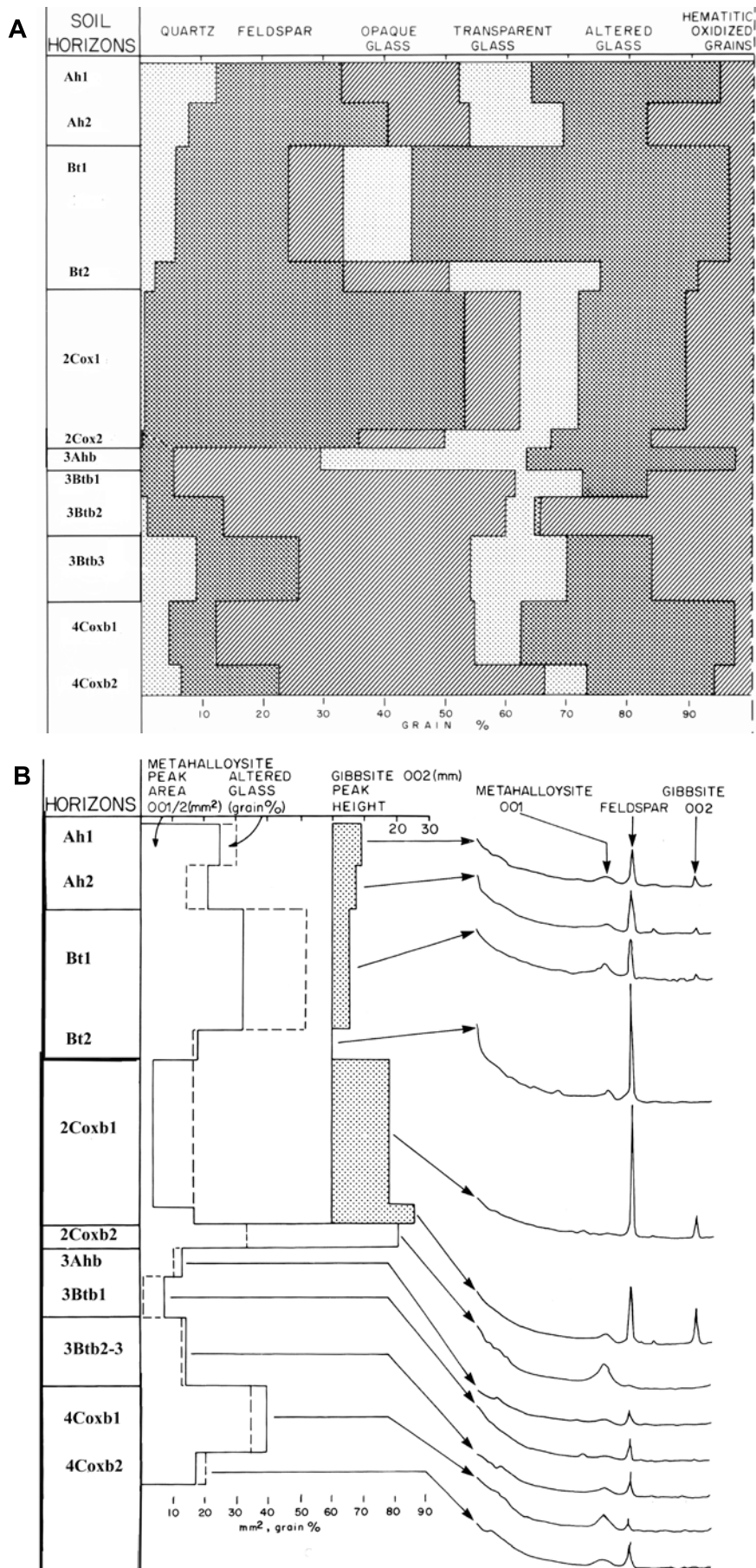
Fig. 8. A – Mineral composition in TV23; B – Oxides and clay minerals in TV23.

south suggestive of overland flow deposition with only slight erosive force. The phonolite bedrock presents as a fresh rock mass suggesting that emplacement of slopewash in the surface horizons (Ah/Bw1/Bw2) over the 2Ahb horizon occurred with little erosion. These data further suggest episodic emplacement of sediment with short residence times, insufficient time for bedrock weathering and development of saprolite, the present section representing only the most recent event.

MINERALOGY

TV23. Mineralogy of the sand and <2 μm fractions in TV23 centers on metahalloysite as the main clay mineral with lesser amounts of halloysite, concentrations matching leaching histories as outlined above (Fig. 8A). Metahalloysite, the dominant clay mineral, is highest in the B horizon group in the upper paleosol (units 1 and 2), whereas the pattern in the lower paleosol shows increases in the 3Ahb and 4Btb4–4Btb5 horizons, the latter distribution no doubt related to clay translocation following either a longer weathering episode or stronger interglacial climate. As a weathering index, gibbsite presents a pattern of present in the lower horizons of the upper paleosol, more or less absent in the lower and older post-Naro Moru paleosol, suggesting very different leaching histories, which may relate to the metahalloysite distributions. XRD patterns for feldspar (mainly sanidine, K-analbite (anorthoclase) series speak to stronger weathering in the lower and older paleosol compared with the upper and younger entity. The relationship between altered glass and metahalloysite is such that distributions down-section show the clay mineral-altered glass distance narrowing from the upper to lower paleosols, and in some horizons, volcanic glass is nearly consumed by clay genesis. Within the primary minerals, the ferromagnetic fraction clearly demonstrates that Fe mineral species dominate in the two tills nearly in opposition to quartz, with quartz more common in the Naro Moru till. Feldspar within the sand fractions follows from the XRD data for the fine fractions as shown in Fig. 8B. Various forms of glass – opaque, transparent and altered forms – present with stronger concentrations in the younger post-Teleki paleosol compared with the older post-Naro Moru profile, the trend presumably related to time vs. climate. Hematized oxidized grains are variably distributed down-section. The contrast between weathered states of common volcanic minerals vs. gibbsite in the two paleosols is a subject for further discussion later in the paper.

SEM/EDS analyses of samples in the TV23 surface and buried paleosols reveal differences between till and aeolian beds that relate to emplacement processes and mineral weathering. Imagery for till in the TV23-2Cox2 horizon shows a mix of quartz, feldspar and glass (Fig. 9A) as indicated above with higher magnification imagery down to micro scale revealing gibbsite in nodule form, verified by EDS (Figs 9B, C). Some grains in Fig. 9A are cracked, a microfeature that could result from applied vacuum during
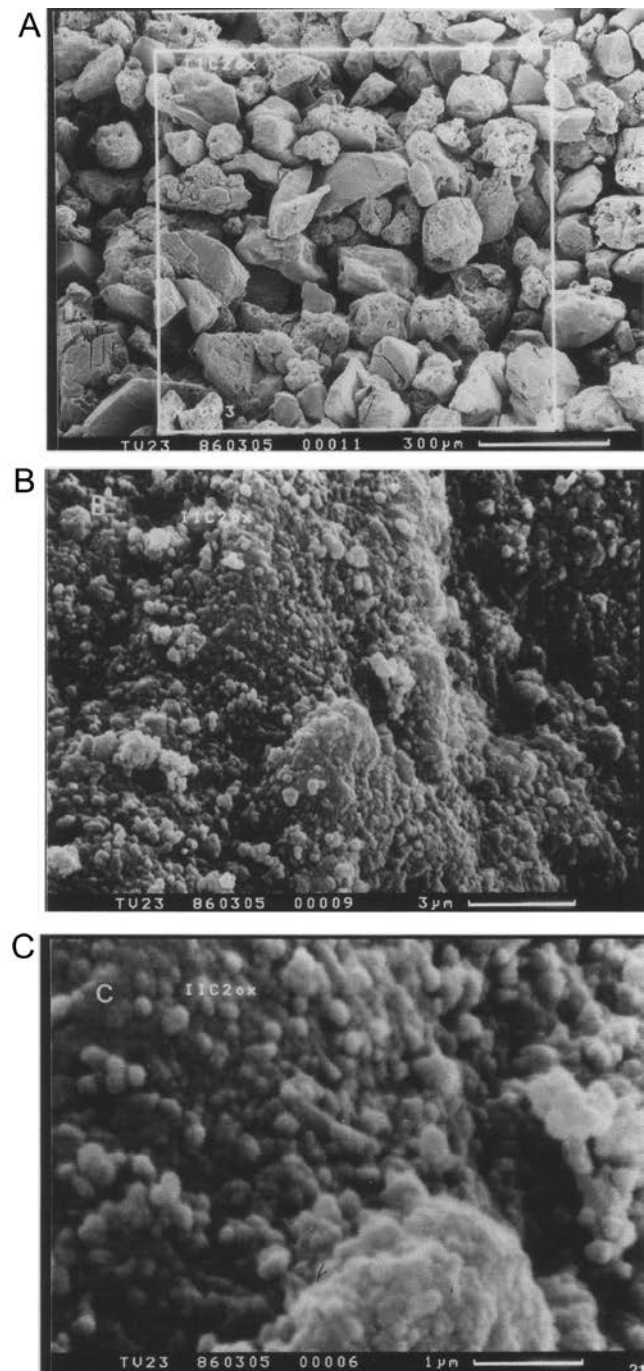
Fig. 9. A – grains in TV23, Teleki Till, 2Cox2 horizon; B – low magnification of gibbsite nodules; C – gibbsite nodules (avg dia. 500 nm).

analysis or from glacial grain traction or grain-to-grain contact during transport. A second imagery set (Fig. 10A–C), taken from the TV23-3Ahb horizon details a loessic sand sample, similar to the till in Fig. 9A, but composed of angular fragments heavier with glass than in the till, with quartz in upper left (arrow), all coated either with Si or Fe as in Fig. 9A. Some cracks are seen in a few grains but overall the angularity is little different from the till sample suggesting minor transport. The enlargement in Fig. 10B (×10) depicts a low magnification print with fibrous forms

of gibbsite present. The enlargement shown in Fig. 10C provides details of strands of gibbsite clustered center to left with metahalloysite dominating on a gibbsite-free grain in the upper right (reprinted from Vortisch *et al.*, 1987, and Mahaney, 2002: 164–165).

TV23A–TV23B. Mineralogical trends in the upper back-slope (TV23A and TV23B) differ only slightly from TV23 (Fig. 8B; Table 1, Supplement) with semi-quantitative concentrations within the two profiles varying in response to slope and possible leaching histories of the profiles. Within the Si:Al = 1:1 clay minerals, halloysite dominates over metahalloysite with trace to moderate quantities common in all horizons. Metahalloysite, sporadically distributed in trace quantities, but where present exists in the same quantity as halloysite; however, elsewhere the stand-alone halloysite is often in considerable concentration especially in the lower paleosol of TV23B. This trend follows with gibbsite, the highest quantities – in opposition to TV23 – located in the base of the TV23B lower paleosol. Staggered concentrations of secondary hematite and goethite dominate in both profiles in small to trace quantity, a relationship supported by oxihydrite extraction data discussed later. Quartz varies from nil to small quantities in the C group of horizons with large quantities present in surface and B horizons of both profiles. Undefined plagioclase is identified with trace to small quantities throughout both profiles almost in the same quantity as pyroxene. Magnetite is common in trace to small quantities in all horizons of both profiles. Illite, as expected is nil except as a trace mineral in the Ah horizon of TV23A.

TV23C–TV61. Metahalloysite and halloysite are virtually nil in all horizons of both profiles with the exception of the lower horizons of TV23C and TV61 (Tables 1 and 2, Supplement), with halloysite present continuously as small amounts in the lower horizons of lithic units 3 and 4 including the clay infill of grey saprolite and weathered bedrock. Gibbsite occurs with a staggered distribution of mostly trace concentrations in horizons of both profiles, but appears inversely with halloysite. Hematite and goethite exist throughout most horizons, the former stronger overall, with the latter in trace concentrations. Quartz is present in trace to large quantities dropping to trace quantity in the saprolite. Overall quartz, in large quantities, is found mainly in the aeolian-influxed horizons 1, 2 and 3 in TV23C and in unit 2 of TV61. Plagioclase is present mainly in small quantities, moderate amounts correlated to higher quantities of quartz, all considered sourced from the nearby African craton, suggesting that quartz is detrital rather than volcanic for the most part. Pyroxene pairs closely with magnetite, the former in small quantities, the latter in trace amounts.

TV61A–TV61B. As with TV61, the mineral distribution in TV61A (Table 2, Supplement) follows a similar pattern with metahalloysite virtually nil, while halloysite ranges from small to moderate amounts in lithic unit 4 and in the saprolite. Once again, as in TV61, gibbsite tends to form
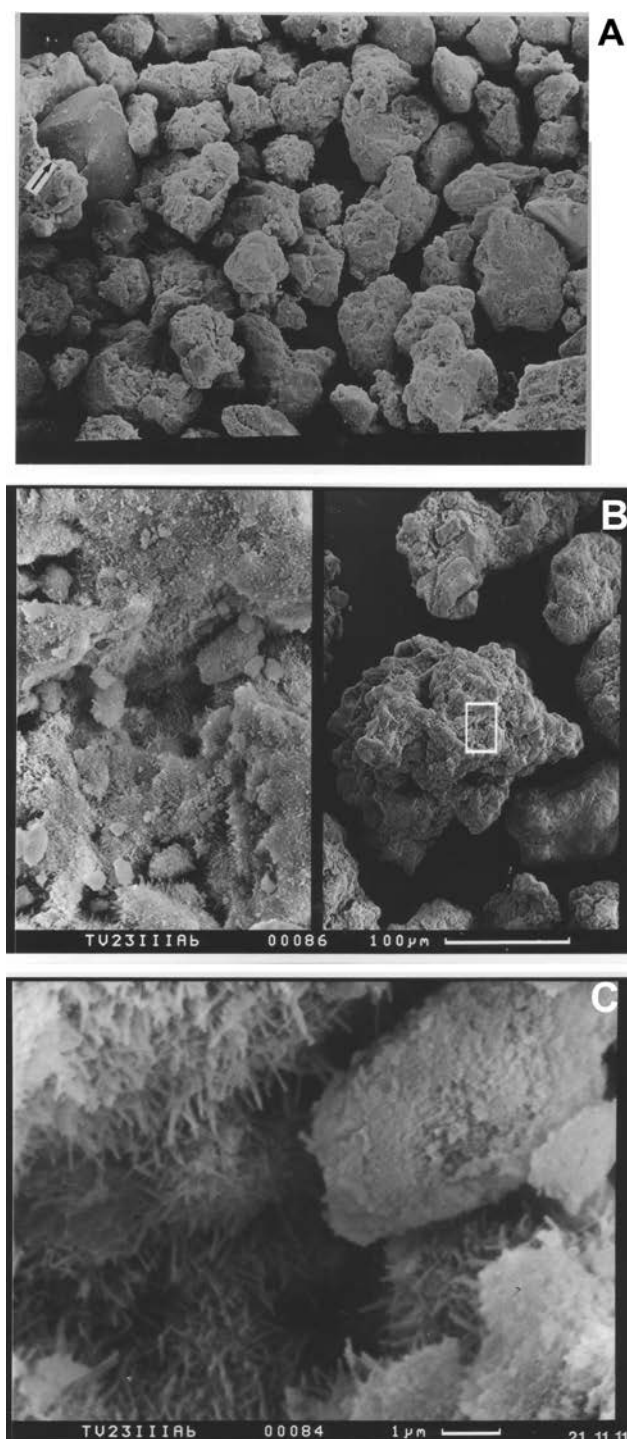
Fig. 10. A – variety of grains in the TV23-3Ahb horizon; B – low magnification image of grains (right inset), enlargement x10 (left inset); C – high magnification of fibrous gibbsite.

when halloysite or metahalloysite decline, the co-relationship attributed to extreme leaching of Si from both clay species (Vortisch *et al.*, 1987). Hematite and goethite follow the distribution in TV61 with hematite higher in small amounts than trace quantities of goethite. Quartz varies from nil to large quantities with the highest amounts in loessic horizons. Plagioclase trends are similar to what ex-

ists in TV61 with slightly higher amounts co-existing with higher amounts of quartz. Pyroxene and magnetite follow a similar trend to what is in TV61, this time with higher magnetite common.

Considering the mineral distributions in TV61 and TV61A sections, metahalloysite and halloysite are similarly distributed in TV61B (Table 3, Supplement), such that the highest concentrations are found in the lower horizons of the Naro Moru till. Gibbsite, mainly nil in units 1–2, tends to crop up as halloysite disappears, the appearance/disappearance a regular occurrence. Staggered distributions of hematite and goethite follow a similar trend in the profiles higher up in the toposequence. Quartz ranges, as in TV61 and TV61A, from nil to large quantities with higher amounts in the aeolian-derived horizons. Plagioclase ranges from nil to moderate with higher quantities co-related to higher quartz. Pyroxene and magnetite are co-aligned with TV61A, the former higher in amount, the latter lower, and all in trace to small amounts.

TV69. Unexpectedly, the depression member site is not a repository of well-weathered minerals (Table 3, Supplement). On the clay mineral side, metahalloysite exists only in trace quantity and halloysite, the fully expanded 1:1 mineral is nil, further reinforcing the young age assessment. Within the mineral suites, gibbsite, pyroxene and magnetite are nil, hematite and goethite present in small to trace quantity, quartz and plagioclase minerals vary from small to abundant quantities. The site is hardly an accumulation of minerals forming over a long period of time, but rather a way-station for minerals carried by throughput of soil water issuing out of the catena, as attested to by unweathered phonolite bedrock at just under 1 m thickness. The mineral distribution shown is presumably the last in a long record of episodic deposition and erosion.

CHEMISTRY

TV23. As indicated in Table 4 (Supplement), the crest paleosol presents with stronger acidity in the surface profile becoming less acid with depth as pH undergoes a slight increase. The leaching trend is attested to by low values for total salts, as indicated by the EC (electrical conductivity) values which fall from 2 S/cm^2 in the surface to detection limits below 15-cm depth. Organic carbon, registers ~8.5% in the surface, decreases steadily downward to the 3Ahb horizon, levelling off at ~0.07%, and increasing slightly in lower horizons. Colors useful as identifiers of oxidation or build-up of organic compounds, somewhat stronger, reaching 5YR hue in the C horizons of the upper paleosol (Teleki Till), and less strong at 10YR in the Naro Moru till beds, all in opposition to the clay trends elicited in the particle size data.

TV23A. Across the crest site and into the upper backslope site of TV23A (Table 4, Supplement), pH is slightly higher (>5) throughout with a trend showing a slight increase in the lower horizons. Following this trend, EC shows low but positive values with depth suggesting less leaching compared with the higher section (TV23), perhaps reflecting less water removal. Organic carbon, although lower in the upper profile compared with TV23, values stay near or above ~3%, to near 1 m depth suggesting less leaching than in the crest site. Correspondingly, N values are higher than in the crest site following organic matter trends. Colors, less staggered than in TV23, also show noticeable increases in oxidation with depth, partially opposite to colors in lower horizons of TV23.

TV23B. Lower down in the toposequence, TV23B, in the upper backslope, carries a stronger acidity (Table 4, Supplement) in the upper paleosol, with increasing acidity in the buried unit. Total salts show an inverted trend to pH with higher values in the surface profile and lower values below, followed by a sharp increase in the saprolite. Organic carbon, overall higher in the surface profile compared with sections above, is slightly higher again in the lower paleosol profile. Again, descending downslope, N is higher than in the two upslope sections. Colors are closer to the range of hues in the two upper sections, but with some variations indicating possible changes in the oxidation potential of various beds, i.e. B/A, and the upper three horizons in the buried suite of horizons.

TV23C. Within the lower backslope, TV23C (Table 4, Supplement) shows a near surface pH of close to 5 becoming slightly more acid near the contact with a complex series of Ahb horizons. These buried A's tend to become slightly less acid with depth to the 4Btb1 where pH rises to 5.6. EC decreases slightly in the surface profile, becoming higher below in the buried 3Ahb group, decreasing into the 4B horizon suite. Organic carbon rises again in the 3Ahb horizon nearly doubling compared with the crest site and more than doubling compared with the upper backslope sites. Nitrogen reaches ~1.5% following the rise in organic carbon and follows a slow descent through the surface and buried paleosols. The higher organic carbon content may relate to an increase in grass vegetation and thinning of forest, with bamboo more prevalent, or from translocation from above. The staggered array of 5-Ahb horizons in lithic unit 3 may relate to increasing grass vegetation at the site early after the end of the Naro Moru glaciation, with timberline depressed and Afroalpine vegetation covering the site, the resident high organic carbon (Table 4) a relic of what may have been a peat bed.

TV61. The pH at the lower end of the backslope (Table 5, Supplement) reveals little in the way of a trend except to show that the Ah group of horizons are markedly more acidic down section to the 2Ahb5 horizon, below where readings reach pH ~5 or slightly higher in lithic unit 4 (Naro Moru Till). The higher pH in unit 4 may result from organic deterioration or invasion of ground water. The electrical conductivity (E.C), as expected from the acid pH, represents low total salts, the upper slightly elevated values

in the Ah1 and Ah2 horizons probably represent leaf fall accumulations. Organic carbon concentrations represent a slow return of plant input at (~16%) at the surface to <1.5% in the Naro Moru Till and nil in saprolite at the base of the section. Nitrogen follows a similar trend with slight increases in the 3Ahb (loessic sediment). Color carries a uniform 5YR hue, variations in values and chroma reflecting the presence or absence of organic content (lower value and chroma). The only change in reddish colors comes within unit 4 with the exception of a stronger red-yellow hue in the saprolite. Alternative to the pedostratigraphy in TV23C above, the 2-Ahb group of horizons may represent peat buildup during MIS 3 and 2, given the ^{14}C dated sediment, that is, pre-and during the LGM.

TV61A. TV61A (Table 5, Supplement), in the upper part of the footslope, presents with a similar pH record to that in TV61, with the main difference represented by slightly less acidity in the Ah surface group of horizons which may reflect increasing bamboo and grass relative to Podocarpus. The E.C. trend down-section is similar also to TV61. Organic carbon, lower in the surface paleosol, steadies on at ~6–7% within lithic unit 2 as in TV61, and then declines lower down except where buried Ahb horizons occur. Within the Naro Moru Till (unit 4) organic carbon reaches its lowest degraded amount less than ~0.19%. Even with low organic carbon in the surface horizons, N levels are higher than in TV61. Otherwise N% declines as in the lower backslope. Color follows a trend similar to TV61 with stronger oxidation values down-section with the exception of the 3Ahb horizons where color lessens (darkens) somewhat in hue values staggered to 7.5 and 10YR hues with higher values and chroma lower in the section.

Amino acids, extracted from Ah and Ahb horizons down section, yielded D/L ratios for aspartic acid from 0.09 in the surface Ah horizon (Ah1 in Fig. 5) to 0.75 in the 3Ahb at 360 cm depth. No aspartic acid was detected in the lower horizons of lithic section 3 to 5, the saprolite, in particular, did not yield measurable results. The lowermost dated horizon, the 3Ahb, ^{14}C dated at 35 ka (date on charcoal) is considered at best a minimum age (Mahaney *et al.*, 1991). With a mean annual temperature taken during the IGY (1957–58), estimated at 7.4°C (Mahaney, 1990), these amino acid values are high, the 3Ahb approaching unity (0.75) at ~2990 m asl. Moreover, with depth and sediment compression, surface temperature heightens slightly, but most importantly, freezing temperatures are known to penetrate only ~5 cm in dry surface sediment, nil depth in wet sediment, all modeled on temperature fluctuations under lab conditions simulating ~4000 m asl (Mahaney, 1990, chapter 12).

Higher on the mountain, at 4200 m elevation, two profiles of vastly different age – TV65, an Inceptisol of ~12 ka, and TV66 (Entisol) of middle Neoglacial (~2 ka) – yielded aspartic acid quotients (Mahaney and Rutter, 1989), which provide an approximate estimate of slowed racemization at higher elevation with average winter (December to January 1957–58) temperature estimated at 1.7°C. Other short-term estimates of summer temperature range between -4.1°C

and 3.1°C (Mahaney, 1990). Assuming a mean annual temperature (MAT) of ~1.7°C at 4200 m asl and a MAT of 7.4°C (IGY data, Mahaney, 1990) at 3000 m (given the dry adiabatic lapse of 10°C/km), a difference of ~6°C between the toposequence and the high Afroalpine zone, is probably an underestimate). D/L values for the youngest soil (TV66) are 0.058 for the Ah horizon and 0.154 for the Cox horizon, no Cu horizon present. The older Late Pleistocene paleosol (TV65) yields D/L quotients for aspartic acid at: 0.15 for the Ah, 0.27 for the Bw, and 0.23 for the Cox horizon. Even considering the elevation and time discrepancies, the D/L in the Ah horizon of TV66 is, as expected, less than the D/L in the Ah of TV61A; the Ah D/L in the older TV65 is 0.09 higher than in TV66, the latter possibly a result of reworked organic matter.

With descent in the TV61A Section, organic-rich horizons in lithic subsections 2 and 3, range from aspartic acid D/L of 0.33 to 0.63 in unit 2 increasing to 0.75 at 370 cm, ^{14}C dated at 35 ka. Even considering the elevation/temperature/age discrepancy between sites, comparison between TV61A (3000 m) and TV65 (4200 m), shows an expected slowed racemization rate with altitude. More important, previously published (Mahaney, 1989) amino acid D/L ratios for aspartic acid in TV61, nearly match values reported here for lithic sections 2 and 3 in TV61A with a margin of plus or minus 10%.

TV61B. The low section (Table 6, Supplement) in the footslope presents a less acidic trend with depth remaining at pH ~5 or above from the surface paleosol to depth with only singular increases, reaching pH ~6 in the middle horizons of the Naro Moru Till. The surface paleosol is higher in total salts than in sections higher in the toposequence but otherwise shows a similar trend with depth to the base of the section. Organic carbon begins with similarly high values in the surface profile, decreasing with depth as in TV61 and TV61A. Nitrogen follows the trends reported for the two adjacent higher sections. Color trends differ from the two companion sections above, with the surface paleosol exhibiting 10YR hues, noticeably with less oxidizing effect than in TV61 and TV61A and noticeable decreasing oxidized effects from the 3Bwb2 horizon to the base of the section. Both TV61A and B carry relatively high carbon in unit 2, likely relics of an organic increase with the ingress of Afroalpine vegetation during a time of depressed timberline during MIS 3 and 2.

TV69. TV69, the lone section in the toeslope, presents with acid reactions to a depth of <~1 m, Electrical conductivity follows this trend, decreasing with depth to the paleosol/ bedrock contact where fresh, abraded phonolite presents with an absence of saprolite. The Ah horizon contains a higher concentration of organic carbon compared with the Ah1/Ah2 horizons in TV61B upslope, thereafter dropping by half through to the bedrock contact. Nitrogen mirrors the organic carbon trend. The colors with depth begin with stronger, that is, redder colors in the Ah/Bw1 horizons grading to 7.5YR hue below.
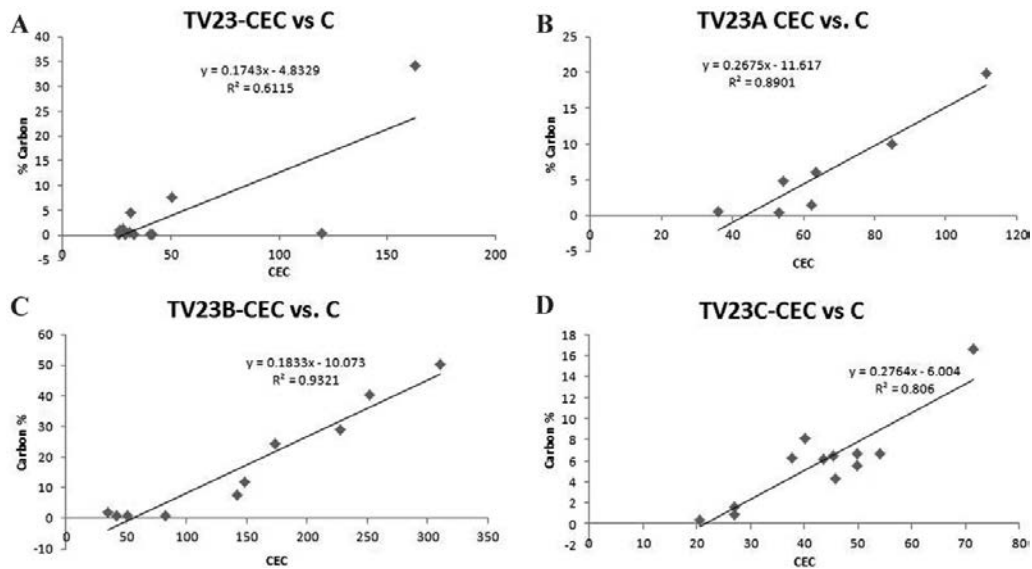
Fig. 11. CEC vs carbon regressions for: A, TV23; B, TV23A; C, TV23B; D, TV23C.
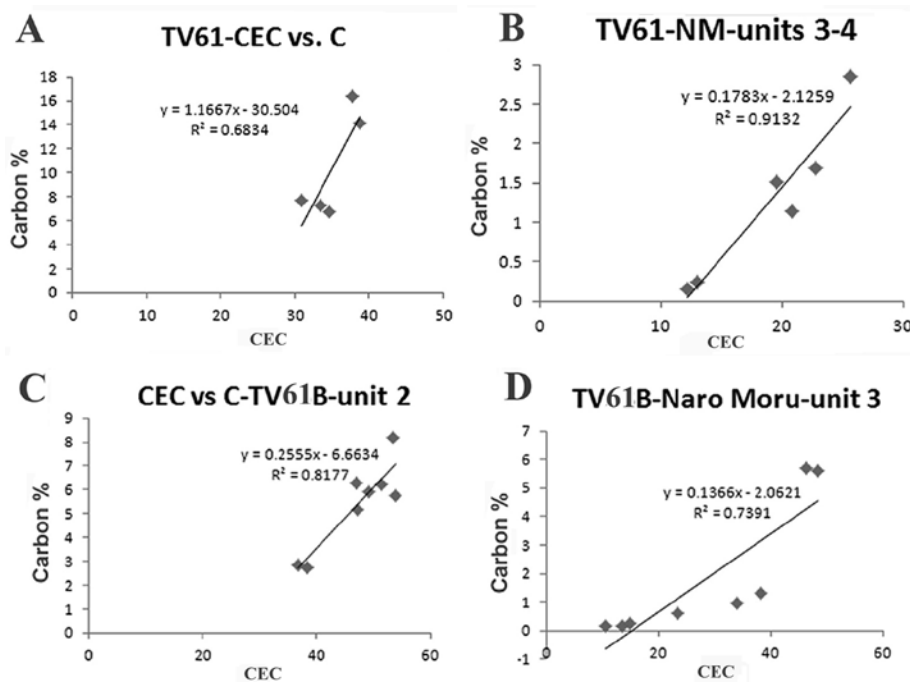
Fig. 12. CEC vs carbon regressions for: A – TV61 surface paleosol; B – TV61-Naro Moru units 3–4; C – TV61B unit 2; D, TV61B Naro Moru unit 3.

CEC vs. C. Because clay species have known CEC (cation exchange capacity) per 100 g/clay, and since organic matter is known to influence CEC, in order to estimate clay minerals present it is necessary to correlate CEC against organic carbon. Calculation is achieved by taking the trend in organic carbon per 100 g/clay, for example, a weathered sediment (soil) with 10% organic carbon and 20% clay, carbon (100/20 = 5 x 10% organic carbon = 50) approximates 50 g carbon per 100 g clay. Plotting CEC (x-axis) against % carbon (y-axis) down profile the regression trend line approaches 0% carbon, the recorded CEC providing an esti-

mation of clay minerals present. Testing this approximation against the known clay mineral composition yields the following: The full TV23 section (Fig. 11A) yields an adjusted CEC of 15 just outside the 5–10 approximate CEC (meq. 100 g dry weight-Birkeland, 1999, p. 93) for metahalloysite and halloysite within the XRD data in Fig. 8B. Similarly, the clay mineral approximation for TV23A (Fig. 11B) is estimated at 30 CEC which is between the range for hydrated halloysite and halloysite, correlating with the XRD data in Table 1 (Supplement). The CEC approximation for TV23B (Fig. 11C), estimated at 50 CEC is well within the

hydrated halloysite range and within the moderate amounts measured in Table 1. Finally, the data for TV23C (Fig. 11D) approximates at 20 CEC between metahalloysite and hydrated halloysite, which does not match the nearly nil XRD for this section (see Table 1, Supplement).

A further test of approximating the clay composition using CEC vs. C shows a CEC of ~30 for the surface profile in TV61 (Fig. 12A), a range within the halloysite group. The XRD data in Table 1 (Supplement) shows nil content for both metahalloysite and halloysite indicating that while the CEC is correct for Si:Al = 1:1 clay minerals, weathering has not produced the requisite crystalline material. Lower in the TV61 section, units 3 and 4 (Table 2, Supplement)) match the adjusted CEC value of ~10 shown in Fig. 12B. A test using XRD data in section TV61B (Table 3) shows a value of 20 CEC for lithic unit 2, which is, again, within the range for halloysite and hydrated halloysite (Fig. 12C). The lower profile of lithic unit 3 in TV61B, the Naro Moru Till – loess couplet, yields an adjusted value of ~10 well within the halloysite range which correlates well with the XRD in Table 1 (Supplement).

Of the eight tests attempted here, seven show a close correlation to what was approximated by CEC vs. carbon, and one failed possibly from leaching effects related to throughput of water.

FE/AL EXTRACTS

Key sections (crest to footslope) were selected to test Al as well as Fe oxihydroxides as relative weathering indices that provide relative-age controls. Among the sections discussed here – TV23, TV23B, TV61A – all were selected to give an overview assessment that might distinguish various lithic groups within each section and each paleosol.

TV23. A comparison of the upper and lower profiles in TV23 (Table 7, Supplement) depicts the Fe-extract raw data showing various trends with depth. The Fe_p reaches ~2% in the surface horizons decreasing with depth in the section, rising slightly in the Naro Moru Till. Fe_o follows with higher concentrations and shows little correlation with Fe_p. Raw values for Fe_d range from ~4–6% in the Teleki profile reaching to over 11% in the base of Teleki Till (2Cox2 horizon) where ferromagnesian minerals are highest (Fig. 8A). The down-section trend in the post-Naro Moru paleosol presents with a similar trend, although with slightly higher concentrations. Fe_t follows a similar pattern in both profiles, the slightly higher concentrations indicating that much of the primary Fe has been weathered to oxihydroxides. Al_p follows the Fe_p trend with higher values in the epipedon of the surface paleosol, declining with depth and increasing in the lower beds of the Naro Moru Till. The Al_o concentrations either slightly exceed Al_p, or in some cases equal values of Al_p, or present with lower values (see Ah2), which may mean the NH_4-oxalate extract was not fully performed. The Al_d trend with depth is similar with lower concentrations compared with Fe_d, rising slightly in the 2Cox2 horizon paralleling the pattern with Fe_d. Al_t is lower in the upper horizons of both profiles increasing with depth into both the Teleki and Naro Moru till beds.

Reviewing the functional relationships of the raw data discussed above, the Fe_o/Fe_d, formerly called the activity ratio (Dormaar and Lutwick, 1983), provides a measure of the near uniform concentration of ferrihydrite (Fe_o) calculated against the genesis of total Fe oxihydrites (hematite+goethite+ferrihydrite). Higher values in the epipedons of the post-Teleki and post-Naro Moru paleosols is offset somewhat by the slower weathering in the till bodies of both profiles (lithic units 2 and 4 in both profiles). This trend is paralleled by the adjusted ferrihydrite ($Fe_o \times 1.7$; Parfitt and Childs, 1988) in both profiles to depth in the section. Calculations of first-order hematite (Fe_t-Fe_d) reveals higher primary Fe mineral content in the epipedons of both profiles which follows from the Fe_t data in the section. A corollary to this is the trend of secondary hematite and goethite calculated by the relationship of Fe_d-Fe_o which is greater in the older post-Naro Moru paleosol. These data are strengthened by the ratio of dithionite-extractable Fe to total Fe (Fe_d/Fe_t) which yields quotients of 0.6 to 0.9, with only the 2Cox2 horizon in Teleki Till coming close to unity (1.0), complementing the particle size and mineral assessment of a strong leaching environment during the last interglacial. A proxy for organic matter content, the relationship Al_p/Al_t shows only minor variations from the surface Ah1 horizon downward, with only a tenuous correlation to organic carbon. A second proxy (Al_o-Al_p) for imogolite and allophane (semi-crystalline silicate clay minerals) highlights elevated concentrations in the Bt2 and 2Cox2 horizons of the post-Teleki paleosol, values spiking somewhat to 1.06% in the 3Ahb and the 3Btb1 and 2 horizons of the post-Naro Moru paleosol, matching other data indicating stronger weathering effects without aggressive leaching in the oldest of the two paleosols in the section.

TV23B. The Fe_p and Fe_o trends down section in TV23B (Table 7, Supplement) are similar to TV23 but with overall smaller concentrations of Fe_o, and somewhat higher values of Fe_p in TV23B, which may reflect increased slope. The distribution of Fe_d down-section, while similar to TV23, produces concentrations smaller than in the crest site, which again supports the hypothesis of movement downslope. The Fe_t follows a similar trend downslope, although with a wider spread in concentrations of Fe_d indicating less consumption of Fe primary minerals, again possibly illustrating the effect of increasing slope and throughput of water and mineral material. Al_p presents with a similar trend to TV23 although with strikingly lower concentrations in the lower, older Naro Moru beds. The Al_o trend with depth is similar again to TV23 with the exception that concentrations in the post-Naro Moru paleosol are lower. Al_d values are similar to TV23, although lower again in the post-Naro Moru paleosol. The Al_t with depth is similar to TV23, slightly lower with organic dilution in Ahb horizons.

Moving along into increasing slope positions, TV23B presents with the Fe_o/Fe_d function yielding similar quo-

tients through the epipedon of the post-Teleki paleosol, with the exception that values are twice as high in the Teleki Till, signaling higher production of ferrihydrite. Down-section into the post-Naro Moru paleosol, values are similar to the surface paleosol. Values for the adjusted ferrihydrite ($Fe_o \times 1.7$) are similar to TV23 (upper) and lower in the post-Naro Moru paleosol, the latter possibly the effect of soil water throughput (surface and ground) as ferrihydrite is partially soluble (Parfitt and Childs, 1988). Primary Fe minerals are similarly distributed in both paleosols in TV23B judging by Fe_t less Fe_d calculations in Table 7 (Supplement). Parallel calculations of secondary hematite + goethite, somewhat stronger in TV23, decline somewhat in TV23B, some horizons close to the 50% mark. Horizon-to-horizon in TV23B, values of Fe_d/Fe_t are lower by as much as 10%, possibly the product of less weathering in place and lower influx from above; the post-Naro Moru and post-Teleki paleosols are slightly lower when compared with TV23. The Al_p/Al_t proxy for organic carbon (Parfitt and Childs, 1988) shows slightly higher quotients in the epipedons of both paleosols as in TV23 but the correlation with organic carbon does not appear to follow the testing provided here. The test for imogolite and allophane shows a staggered distribution with slightly higher values in the post-Naro Moru paleosol, a possible product of time over climate.

TV61A. The raw data (Table 8, Supplement) for this pedostratigraphic complex, a couplet of older and younger deposits, respectively, in that order from bottom to top, comes complete with an unknown number of weathering unconformities. The contacts between Ahb horizons, and overlying sediment, probably represent a certain amount of time not represented by the sediment stack in place. As with all the sections analyzed no fresh, unweathered sediment was encountered during the course of field investigations. Thus, from bottom to top, all extracts are represented by strongly weathered beds (units 5 and 4), grading upward into a couplet of buried paleosols formed in loessic sediment (unit 3) weathered in interstadial time (~30 ka, MIS 3), overlain again by colluvium (MIS 2-LGM), ending with the surface paleosol (Unit 1). With ^{14}C ages in upper unit 2 indicating the surface paleosol is <20 ka), it must have formed partly in MIS 2 and 1, presumably up to the present.

The raw data for Fe_p (Table 8, Supplement), highest in unit 1, drops off precipitously in unit 2, rising again in unit 3 showing staggered movement down section in the 3Btb and 3Coxb2 horizons, and to a lesser extent in 3Btb2. After tapering off in unit 4, the saprolite registers a rise to 0.87%. Fe_o follows a similar trend with a high concentration in the saprolite, less in the Naro Moru Till, increasing upward into the loess of unit 3, dropping in sequence in unit 2, and increasing upward into the surface paleosol of unit 1. Within the raw data bank of Fe_d, the saprolite reaches nearly 7%, the Naro Moru Till variable from 3.6 to 6.2%, thereafter variable in the loess packages of unit 3 and the colluvium of unit 2, whereupon after crossing into unit 1, a slow decline continuous to the section surface. The staggered concentrations in units 2–3 may relate to reworking of sediment from sections higher in the toposequence so that preweathered (overprinted) sediment was transferred to younger deposits emplaced during MIS 2 and 3. The Fe_t is 1–2.5% greater than Fe_d and in some cases (3Btb2, 3Bwb2), the difference is ~1% indicating that weathering has nearly consumed all primary Fe minerals.

Concentrations of Al_p (Table 8, Supplement), higher than in sections upslope, are close to 0.9% in the 5Saprolite, drop to between 0.2–0.6% in the Naro Moru Till, rise to <0.7% in the lower loess of unit 3 and then rise to 1.3–2.7% in the upper beds of unit3, steadying down to 1–1.8% in units 1 and 2. The Al_o data yield a bivariate profile, from bottom to top, beginning with low concentrations in units 4 and 5, rising in mid-section, finally declining near the surface. Al_d outlines a similar pattern with 1–2% greater values up-section. The disparity between Al_o and Al_d is such that Al_o sometimes exceeds Al_d, which, given the method outlined by Dormaar and Lutwick (1983), Al_d should exceed Al_o. As argued by Mahaney *et al.*, 1994) it may be that Na-dithionite does not extract all Al present in some samples. Al_t, subject to organic dilution effects, is highest when organic carbon is low.

The activity ratio of Fe_o/Fe_d (Table 8, Supplement) is highest in unit 1, decreasing and steading up in unit 2, decreasing slightly in unit 3, decreasing yet again to <0.2 in unit 4, rising slightly in unit 5 Saprolite. Adjusted Fe_o (raw concentration x 1.7) shows values in unit 5 that nearly parallel unit 1 and follow a declining and staggered trend in unit 2, possibly with some horizons obtaining translocated weathered material from upslope. Considering that Fe_o represents ferrihydrite, and with this hydroxide being partially soluble, emplacement of colluvium likely comes with throughput of water. Primary Fe minerals represented by Fe_t-Fe_d are low in unit 5 (saprolite), rising to >2% in unit 4, increasing slightly to ~2% in most of unit 3, and then declining again in 3Ahb1 and 3Ahb2 horizons, possibly due to organic dilution. The colluvial body in unit 2, along with the surface paleosol of unit 1, shows an across-the-board decline of ~1% relative to the sediment below. Oxihydrites, represented by secondary hematite plus goethite (Fe_d-Fe_o), less ferrihydrite, are high in the 5Saprolite bed, thereafter low in 4Btb5 and rising to ~4% in 4Btb2 at the till/loess contact. Thereafter, a staggered decline continues upward to unit 1 where values drop to <2%. The Fe_d/Fe_t value of 0.85 in the saprolite bed is only matched or exceeded in 3Btb1, 3Bwb2, and 2Ahb2 horizons, these 3 samples probably represent, along with values in the 0.6–0.7 range the input of well-weathered sediment from higher in the toposequence in addition to weathering in place. The staggered pattern with depth in the section probably represents a fair degree of preweathering and translocation of sediment.

The Al functions, particularly Al_p/Al_t, higher in the paleosol of unit 1, declines in staggered array with depth reaching the lowest values in the Naro Moru Till. While these data parallel the Naro Moru Till in Table 7 (Supplement), the data defeat the proposed correlation with organic carbon proposed by Parfitt and Childs (1988). The calculations for imogolite and allophane (Al_o-Al_p), nil in

the saprolite, values increase in lower unit 3, increase upward in upper unit 3 and remain high in unit 2, decreasing in unit 1. These data suggest both minerals are time and climate dependent, the highest values in MIS 2 and 3, lower in units 4 and 5, further indicate they may be loess-dependent.

GEOCHEMISTRY

Four bedrock samples, and 57 sediment samples from discrete horizons, were chosen from TV23 (summit site – 12 samples), from TV23A (upper backslope paleosol – 2 samples of Naro Moru Till), TV23B (10 samples), from TV23C (lower backslope – 1 sample of Naro Moru Till), from TV61 (lower backslope – 2 samples Naro Moru Till), from TV61A (footslope unit – 26 samples), and from TV69 (toeslope unit – 4 samples). All of the samples were analyzed by INAA at the SLOWPOKE Reactor Facility of the University of Toronto. Selected elemental concentrations are presented in Table 9, Supplement (samples from TV23 and TV23B, in Table 10, Supplement (samples from TV61A), and in Table 11, Supplement (samples from TV69, Naro Moru Tills TV23A, TV23C, and TV61, and local bedrock). The very low Ca, K, and Na concentrations in all sediments, relative to the bedrock samples, indicate severe leaching over a long period of time.

The site-related chemical groupings presented in Tables 9–11 (Supplement) show two broadly different chemistries that are based primarily on the concentrations of the REEs (rare earth elements), especially La and Ce. One grouping has high La concentrations relative to Ce and other REE concentrations (e,g. grouping TV61A-1), and the other grouping has low La concentrations relative to the Ce and other REE concentrations (TV61A-2). The former group exhibits REE ratios that are similar to other sediments from around the world (Hancock et al., 2019). Samples in the second low-La grouping are shown in Tables 9–11 with an asterisk (*) following their Ce concentrations.

The complete analytical data set was sorted visually, and summary elemental concentration data are presented in Table 12 (Supplement). The ordering of elements in this table is alphabetically by major and minor element, followed alphabetically by trace elements, and then by atomic number for the REEs. Less than signs (<) in front of averages show where detection limit data were included in calculations.

The chemical groupings tend to be site-specific, but in some cases they are horizon specific. In Table 12 (Supplement), the TV23 chemical group contains all 12 analyzed samples from TV23 plus one deeply buried Naro Moru Till sample from section TV23A (4Coxb1) – see Fig. 4. The TV23B chemical group in Table 12 (Supplement) contains all 10 analyzed TV23B samples plus one deeply buried sample each from TV23A (Naro Moru Till 4Coxb2) and TV23C (Naro Moru Till 4Btb2 – see Fig. 4. The TV61A-1 chemical group in Table 12 (Supplement) contains 9 analyzed deeply buried samples (from 3Ahb2 to 4Btb5).The TV61A-2 chemical group in Table 12 (Supplement) con-

tains the samples from the 13 upper horizons at TV61A plus four deeply buried TV61A section samples (3Ahb1, and three adjacent horizons, 3Coxb2, 3Ahb, and 3B/Ahb) – see Fig. 5.

The bedrock samples in Table 11 (Supplement) include local porphyritic phonolite, syenite, kenyte, and basalt. These do not form a particularly coherent chemical grouping, with the porphyritic phonolite and kenyte being chemically similar, but distinct from the syenite and basalt, which are also similar (Table 11, Supplement). The porphyritic phonolite and kenyte pair is distinctly higher in Mn, Na, U, Cr, Cs, Hf, Sc, Ta, and Th, but lower in Ca, Ba, and Sr than are the syenite and basalt.

There are chemical similarities between the TV23, TV61A, and TV69 samples. As well, there are also chemical similarities between the TV23B samples; the two deeply buried TV61samples; the deeply buried basal beds in TV61A; and the bedrock samples. Selected chondrite-normalized REE concentrations from samples in TV61A are presented as Fig. 13. In this figure, sample (1)2 is Ah2; sample (1)3 is Ah3: sample 24(4) is 4Bbt4: sample 25(4) is 4Btb5, and sample 26 is saprolite, (5) is 5Saprolite.
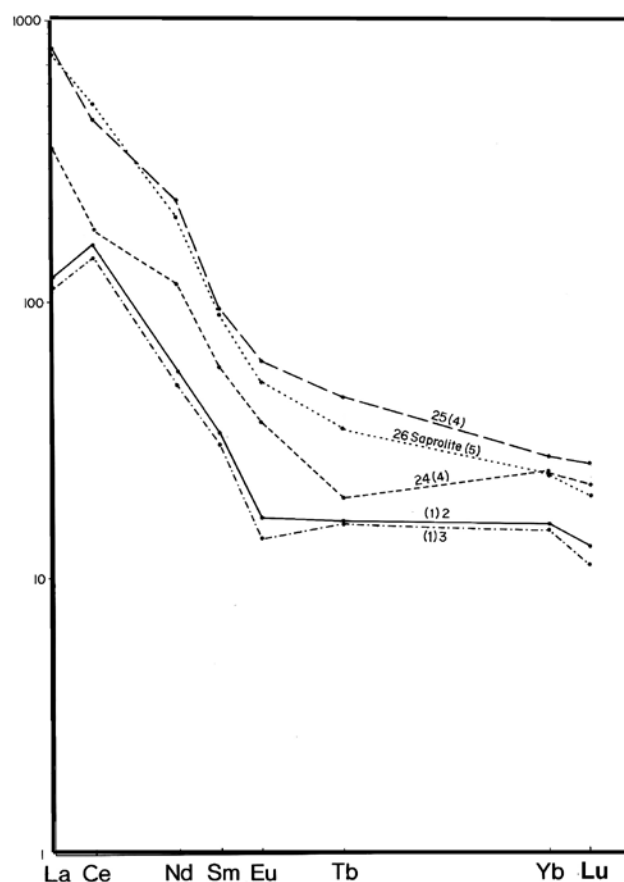
Fig. 13. Cross-section of REE concentration in the TV61A Section showing close correlation between 5Saprolite and the 4Btb5 (basal Naro Moru Till) and relation to other component horizons of the post-Naro Moru paleosol complex – 3Btb1–4Btb4 horizons – listed as 24(4). All additional samples from the middle of section 3 to the surface of section 1 fall within the boxed area of high to low REEs. This latter mix supports reworking of sediment that is the hall mark of most sections in the toposequence.

These plots (Fig. 13) show elevated L(light)REEs in both the 5Saprolite and the 4Btb5 horizon (basal Naro Moru Till) and slightly elevated H(heavy)REEs suggesting the basal till likely inherited its REE complex from the weathered bedrock. Because the clay content is different in the saprolite (5%) from the till (30%) (Fig. 7), it is clear the REEs in the saprolite were sourced not from clay but from other source minerals in the weathered bedrock. In the up-section area of TV61A–4Btb3–4Btb4 horizons – comprising the upper beds of the Naro Moru Till, and 3Btb1 and 3Btb2 (line 24 (4) comprising the Naro Moru loess, the LREEs decrease and the HREEs join the basal beds at Yb and Lu. Moving up-section again, from upper lithic unit 3 to 1, the REEs undergo a further decreased concentration with a Ce anomaly that may relate to undetected monzonite; however, Ce-monzonite is not recognized in the XRD data. In all, decreased REE concentrations up-section support previous interpretations of sediment reworking from the basal beds upward into the younger loess.

Table 9 (Supplement) shows three interesting TV23 samples with very high Mn concentrations. These are samples 3Ahb (1.41% Mn), 3Btb1 (0.99% Mn) and 3Btb2 (1.01% Mn), all within the buried loess of the post-Naro Moru paleosol in the TV23 chemical group. With these samples excluded, the average TV23 Mn concentration shown in Table 12 (Supplement) drops from 0.52±0.39% to 0.23±0.15%. This brings it into line with the other Mn concentrations in the other sections. These three samples are adjacent in the TV23 section (see Fig. 4), so the very high Mn concentrations may be significant and related to tephra input previously identified.

DISCUSSION

Stability-Instability in Pleistocene Sequences

Merging classical stratigraphy with a paleosol toposequence of extreme age allows analysis of combined *in situ* weathered beds with inset climatically-generated gravitational sediment, the latter stabilized after major glacial or loess-generated events. The initial early Brunhes event led to weathering of bedrock and production of saprolite over an unknown period but given the normal magnetism, the age is presumably less than 0.8 Ma. Because no saprolite is found below ~2900 m asl off the east end of Gregory's 'older moraine', the sites shown above represent the early to last vestige of weathering in subject weathering during the middle Pleistocene. The Naro Moru tills present in all sections, excepting TV69, represent the onset of the oldest known glaciation on the west side of the mountain. Where contact with saprolite is encountered till emplacement is seen to be less disruptive than expected, and in all such cases, this early event, no matter how much time was involved, ended with a till-loess couplet in place more or less at the terminal end of the first recorded the middle Pleistocene glaciation.

Because the lower Naro Moru-age till body varies in thickness from <1 m to ~2 m, the most stable positions are in the crest (TV23) and lower footslope (TV61B) sites, which indicate that erosional loss of sediment was, as expected, most pronounced on the slope segments, as predicted by Birkeland's catena model (Birkeland *et al.*, 1991). The loess bodies in contact with Naro Moru tills appear to be more or less intact, witness the horizontal contacts (Figs 4 and 5) representing stability without any convolutions present. Tills in tropical mountains are deposited near pressure melting temperatures, unlike middle latitude to near-polar positions where tills are emplaced under below freezing temperatures. It is for this reason that tropical tills are subject to paleomagnetic analysis with clear signals of inclination and declination obtained (see Barendregt, 1984; Barendregt and Mahaney, 1988). The upper lithic units (1–2) in the crest and upper backslope sections exhibit structural stability similar to the units (3–4) lower down in each section. Contacts between horizons, despite the limited section area shown, show no evidence of convolution outside of minor waviness indicating possible leaching/translocation effects. As with the lower lithic units the same occurs within the sections lower down, and in sections under somewhat steeper slopes, and nearer the surface where compression is less.

One of the outstanding features of sections recovered within the toposequence is the division of deposits with depth into individual paleosols with their own short and long weathering histories. Radiocarbon dating of the younger sediment – slopewash, loess and colluvium – provides a chronological succession of the latest erosional-depositional event in what is in all probability only one of several such events over time. Surely the initial emplacement of the oldest till (Naro Moru) and its couplet of loess and ash underwent a similar downslope gravitational movement of material, rapid at first with timberline well below the site, attenuated somewhat with the rise of timberline at some point during the Naro-Moru-Teleki Interglacial, sometime after 0.5 Ma. Assuming a period of semi-slope stability during this period, emplacement of Teleki Till and its loess-plus-ash component must have started renewed slope activity sometime after 0.2 Ma at the end of MIS 6, attenuated with the onset of the last interglacial climate during MIS 5. It is impossible to know how many slope episodes occurred during the onset of the last Pleistocene glaciation sometime after ~90 ka during the Liki I stage MIS 4), only starting during MIS 3 and into the LGM (MIS 2), slope instability led to movement from the backslope units to the lower backslope (TV23C–TV61 and onto the footslope units (TV61A and TV61B). What upset the weathering sequence is the reworking of sediment, already preweathered (overprinted) in upslope positions, to sections lower down in the toposequence. With minor adjustments in the interpretation of Fe and Al extracts, it is evident that the mix of material, even accounting for the input of allochthonous sediment by aeolian influx, makes distinct changes down-section through the buried paleosols to derive weathering effects for younger sediment during maximum and minimum ^{14}C dated beds doubly difficult.

Erosion-Depostiion Hypothesis

In support of the hypothesis of multiple periods of erosion and deposition, despite the presence of thinned-out beds (horizons), as likely evidence of missing sediment (undefined unconformities), it is improbable to consider the thinness of till beds (units 2 and 4 for the most part) to represent the full thickness of till deposited during these two middle Pleistocene glacial events. Moreover, tenuous as it may be, the link between unit 3 in the lower backslope and footslope positions with oscillations of Liki ice in the upper valley (Mahaney, 1990), the correlation based on ^{14}C dated beds in this toposequence and relative-age dated sediment in the upper valley (Mahaney, 1990), are about as strong as can be made at this time. Further support for the erosion-deposition oscillation hypothesis comes from the present surface paleosol (TV23) that while having lost some sediment into slope sections since the end of MIS 6 remains, and probably has remained structurally secure, during each episode of forest encroachment, first during the last interglacial (Olago et al., 1999), each interstadial of the Liki Glaciation, and during postglacial time when timberline was higher. Even sediment emplaced during late MIS 3, and with weathering beginning during MIS 2 in the TV61 section, left magnetic declinations/intact and readable when excavation of the section occurred in 1983. Thus, following the 21–25 ka ^{14}C dated beds at the ~200–240-cm level in TV61, a distinct paleomagnetic excursion is registered in the 40–60-cm levels, that appears similar to the Mono Lake event not previously seen in Africa (see Mahaney, 1990, figs 2.27 and 5.17). However, without precise renewed dating of these sediments it is impossible to determine if this is the Mono Lake or a hitherto unknown excursion in upper Brunhes sediment.

All sediment in lithic unit 1 of all paleosols, from the crest to toeslope, not only contains material weathered over various lengths of time, such beds also continue to produce weathered material today. Despite the thinking of some that buried profiles do not continue active in the weathering process, it is hard to believe that buried horizons are not affected by percolating soil water from throughput of moisture moving through the sections, or from groundwater effects. Surely, moist colors taken in the field show that some moisture is present in sediment at depth. This, together with root systems penetrating surface profiles, provide pathways for moisture moving downward into buried paleosols to assist in weathering processes.

Particle Size – Variant Relationships

Particle size data shown here suggest variable particle-size distributions in the two tills, despite weathering effects which tend to skew sand-silt-clay ratios from a near linear form on particle-size graphs (see fig. 5.7, Mahaney, 1990), to s-shaped or parabolic forms. The closest match to normal till particle-size distributions occurs in TV23 (Teleki Till) and in TV23A–TV23C (three Teleki till beds) and TV61–TV61B (3 Naro Moru till beds). The weathering effects in the Naro Moru till of TV23 with its high clay content skews the normal till particle size linear distribution.

Taking the silt-distributions-with-depth in the sections into account gives some indication of aeolian influx related to time and erosional effects. TV23-Ah is an illustration of a site positioned to receive airfall influx of sediment as indicated by the 76% silt value, dropping to <30% in lower horizons in the surface profile. Further downslope, silt in surface profiles drops to 45% in TV23A, 20% in TV23B, rising to ~35% in TV23C, the latter probably the result of input from sections above or from aeolian influx. The progressive increase of silt in surface horizons – ~40% in TV61, 50% in 61A and 70% in 61B – suggests a slow downward motion of silt reduced to 47% in TV69. If a hypothesis that silt is transitory in the surface beds of all sections, this flux of silt percentages seems to support that postulate. Moreover, if the hypothesis regarding older erosion-deposition episodes is correct, the distribution of silt within the loessic horizons of lithic units 3 and saprolite (unit 5) tends to further support it. In the oldest of the till sections (unit 4) the high silt content tends to support one of two hypotheses: that either the silt is glacially-ground (Smalley, 1966) and still in situ, or that it has moved downward from the overlying loess beds.

Differentiating loess from till relied on the presence of clasts with accordant or near-accordant magnetic azimuths and inclinations (dip), altered somewhat by slope, to represent till. No detailed fabrics were taken in the field, although weak to very weak stratification was observed in loess beds compared with the tills which had massive, clast-heavy to clast-light, non-sorted beds. Hence, loess identification was done mainly on the presence of silt with minor stratification and absence of clasts. SEM imagery of loess (Fig. 10A), at least within the fine sand fraction, shows little change in angularity after comparison with till (Fig. 9A).

Clay and Primary Mineralogy

Within the mineralogy assessed across the toposequence, the slow genesis of metahalloysite-halloysite postulated by Vortisch et al. (1987) and Mahaney (1990, 1991) seems to follow previous research outlined from other sites on the mountain. If metahalloysite-halloysite are found in weathered sediment (paleosols) <100 ka in age, the occurrence is considered to be the end-product of reworking of preweathered sediment from older sites. Commonly, in deposits older than Brunhes-age (Mahaney et al., 2014), that is older than the toposequence, metahalloysite carries on a presence-absence trend with halloysite appearing as metahalloysite disappears, judging from relative-age assessment of different horizons in paleosols. More importantly though the correlation of metahalloysite-halloysite with gibbsite postulates, that with increased leaching during

stronger interglacial paleoclimates, gibbsite tends to dominate as both halloysite and metahalloysite undergo Si leaching. The evidence reported within the toposequence only follows from some sites, not all, so that in TV23A and 23B both gibbsite and metahalloysite occur together; TV23C is deficient in both mineral species (leaching without production of gibbsite?); TV61, 61A, and 61B parallel the proposed leaching process; and TV69 contains only trace amounts of metahalloysite with nil gibbsite. Thus, from this mineral association, it seems gibbsite can be taken as a leached product following the degradation of halloysite-metahalloysite leaving only Si tetrahedra as detrital components. It may also be that degraded Si may combine with Al_2O_3 to recrystallize into halloysite or metahalloysite. What is interesting is the degree to which OH is taken up in the halloysite lattice with metahalloysite merging into full formed halloysite as evidenced by XRD traces indicating a slow buildup of a plateau from 7.2 → 10 Å, from an initial to fully formed halloysite lattice. Some of the change in clay genesis may relate to collection in the field and inadvertent exposure to sunlight despite precautions taken to shield samples from heat.

Oxihydrites and Age

As with the stratigraphic, mineralogic and chemical segments previously discussed, understanding the Al and Fe oxihydrites is best understood with respect to individual lithic units. Unit 1 in sections TV23, 23A, 23B and 23C represent weathering from MIS 5 to present, the profiles described presenting with minimal material given the episodic erosion postulated since deposition. Given the possibility of a hiatus between units 1 and 2, the 2-surface probably represents a minimum with some lost sediment. Lower down in the low backslope and footslope, unit 1 in these sections represents paleosols forming during MIS 1, or since late LGM time. Units 2 and 3 present weathered beds forming during the last glaciation, mostly during MIS 2–3. Lower down in these sections the loess in lithic unit 3 presents with a couplet of deposits, some upper beds of which can be radiocarbon dated, others beyond the range of C-14. Unit 3 in TV61B is all till overlain directly with colluvial sediment. Aside from the variations in Al and Fe oxihydrites noted throughout these various lithic units, the most outstanding result is the high concentration of Fe_d. Its relationship to Fe_t is such that in some cases the weathering of primary Fe minerals is nearly complete, the ratio near unity. While some material is postulated to have escaped the toposequence system through TV69, it is clear there is considerable reworking of sediment from older to younger beds, similar to the original rock cycle postulated by James Hutton (Hutton, 1795). Previous research (Mahaney *et al.*, 1994) has considered Al_d to sometimes represent an incomplete extraction. However, regression analyses of sample deposits (TV23, TV23B) in this set of sections show a reasonable correlation, such that while Al_d is less than Fe_d, the two extracts are shown to provide a reasonable proxy estimate of relative time.

Weathering Unconformities

Comparing the two paleosols (post-Teleki and post-Naro Moru), where present in single sections (TV23, 23A, 23B), and as singular occurrences (TV23C, 61, 61A and 61B), only with outcrops of Naro Moru Till, is it difficult to match the soil stratigraphy with pedological nomenclature. Moreover, combining till with loess as one conjoined unit is impossible to ascertain for certain, as with erosion dominating during interglacial and interstadial time, an unconformity is possible along contacts between both till and loess deposits. Other unconformities may well be present between various deposits making material-time connections and superposition uncertain at best. What is certain is that a multistory of sediments, a very complex pedostratigraphic sequence, attenuated by periods of stability and erosion, can be read by analysis of sections along a topographic gradient at the very limit of the Pleistocene glaciation in alpine tropical Africa.

Geochemistry-Link to Sediment Origin

From the geochemistry, the macroelements reveal a distant relationship to the four common lithologies on the mountain, as expected given the longevity of weathering and the open systems each lithic unit presented to the subaerial atmosphere following emplacement by episodic glaciation, airfall influx and gravitational movement downslope. An approximate estimate of bedrock to weathered sediment stack can be seen in Table 11 (Supplement) where fresh lithics can be measured against accumulated sediment in the toeslope position. Al and Ti, two stable elements, not subject to dissolution, closely match concentrations in both groups, minor differences accountable to organic dilution or to influx/loss by aeolian processes. Other less stable macroelements are subject to considerable dissolution by weathering over variable time brackets – ~10^3 to ~10^5 yr – with Ca and Na, in particular, reduced by nearly half an order of magnitude or more in the case of Na, down to detection limits for Ca. Iron increases from bedrock to variable horizons in TV69 (Table 11, Supplement), and greatly increases again upward in most sections, sometimes by x2. Often Fe increases in tandem with Ti suggesting the presence of ilmenite among other volcanic materials. However, ilmenite is rare but is occasionally present with magnetite in trace quantity in the clay fraction.

Within the microelements and REEs, Ta/Th presents a strong positive correlation. Tantalum and Th, often with Ni are accessory elements in ilmenite, a major Ti-rich mineral common on Mt. Kenya. Correlating Mn with Ti in TV23 (Table 9, Supplement) shows increases of Mn with Ti-Fe in 2Cox2 and 3Btb2 (3Ahb and 3Btb1 were not measured). Other strong correlations between La-Lu occur between the 5Saprolite in TV61A and the lower basal 4Btb5 horizon (Naro Moru Till), which indicates the Naro Moru ice sourced its REE concentration during transport. Tracing this REE signature upward in the higher till body (4Btb3–

4Btb4), and into its presumed loess component (3Btb1-2), shows, with lower concentrations, the loss of LREEs and retention of Yb and Lu within the HREE element component (Fig. 13). Higher in the TV61A Section, the lower concentrations of REE elements may be related to clay loss or to loss by aeolian out-flux and/or gravitational downslope action.

Using the REEs to trace phonolite weathering to bedrock, saprolite sourcing the Naro Moru Till in the TV61A section, and its relation to loess in TV61A, The Naro Moru Till in TV61→TV23C→TV23B→TV23A→TV23, provides a test of the chemical continuity from the lower footslope (TV61A) to the summit section (TV23). Using the ratios – Ce/La, Ce/Sm and Ce/Lu, bedrock to saprolite yields a close relationship of ±5%; saprolite to the 3 basal tills in TV61A – 4Btb5–4Btb3. All three ratios continue close to the loess samples (3Btb1–3Btb2 in TV61A), suggesting till ground up by the Naro Moru glacier contributed the bulk of the loess to the paleosol without much additional allochthonous sediment. Moving up slope to TV61, the Naro Moru Till within – samples 4Btb1 and 4Btb2 – Ce/La and Ce/Sm fall within the narrow ranges measured in the bedrock, the saprolite and the Naro Moru Till in TV61A. The Ce/Lu ratios are higher by factors of 2 to 3. Ascending still higher in the toposequence, to TV23C, the Naro Moru Till-4Btb2 – in the upper footslope remains remarkably close to sections lower down in the toposequence. In TV23B, the Naro Moru Till is lower in Ce/La and Ce/Sm, the Ce/Lu within the ranges measured below. In TV23A – 4Coxb1 and 4Coxb2 – the Ce/La and Ce/Sm increase overall while the Ce/Lu is split with the upper bed within the range seen below while the lower bed increased by up to half an order of magnitude. Rising still higher to the summit site (TV23), the Ce/La rises by times 2 (see Table 9) while the Ce/Sm and Ce/Lu remain similar to the lower sites. What this trend implies is that the strongest relationship between the bedrock, saprolite and lower Naro Moru till beds tend to widen out with strong similarities in Ce/La and Ce/Sm upward to TV23B and 23A and above to TV23 where Ce increases. The Ce/Lu remains static in the lower beds – bedrock, saprolite and TV61A – becoming more variable in TV61 to the crest, which most likely reflects on the variable chemistry of outcrops available to the Naro Moru ice up-valley and sediment reworking after emplacement.

Time vs. Climate

Taking all physical, mineral, chemical data and radiocarbon ages into account the evaluation of time vs. climate seems elusive, as in many other reported projects of a similar nature (Birkeland, 1999; Dahms, *et al*., 2012; Mahaney *et al*., 2014). The middle Pleistocene paleosols reported here – 5Saprolite, post-Naro Moru, middle subsection [3] loess in TV61 and TV61A, and the post-Teleki paleosol – all contain minimum weathered sediment records, most with timelines established by relative-age dating methods, and somewhat confounded by weathering unconformities.

Matching tills with loess assumes conformable relationships, but only in the sense that weathering in the till bodies seems of similar strength to the loess or, as previously seen, REE ratios closely match from till to loess. In TV61 and TV61A, a second loess body in lithic section 3 overlies the loess deemed part of the basal paleosol. At least full profiles of Ahb/Btb/Coxb stature are present with presumably minimal loss of sediment. In these two sections, at least, it may be that the upper loess in lithic section 3 represents a glacial resurgence that reached close to but did not overtop the toposequence, its presence marked by released aeolian sediment with no till deposition. Still more important the twin paleosols in TV23, 23A, and 23B present with varying textures, the highest clay content in the post-Naro Moru Till, less in the post Teleki paleosol, at least in TV23 (Fig. 4), which suggests either a time or climate argument to explain the difference. Results are mixed in TV23A-C with the post-Naro Moru Till either similar to the post-Teleki paleosol (TV23B) or less (TV23A, TV23C). Because TV23 is the most stable site given its position in the moraine crest it may be the other sites lost clay due to gravitational influences.

The estimated time allotment for saprolite weathering prior to onset of the Naro Moru Glaciation is approximate but could be ~300 kyr; Naro Moru-Teleki Interglacial is ~200–300 ka; the approximate time for the post-Teleki – present is ~130 kyr. If climate fluctuations between glacials and interglacials yielded dry glacials and humid interglacials, the two early periods are twice as long as the last event, and all assessment is based on the uncertainty of the time allotment for each glaciation and unknown effects of climatic shifts with timberline fluctuation across the toposequence sites. What confounds this scenario is the episodic mineral and chemical changes that have occurred in tandem across these time lines, all controlled by heat and moisture driving weathering processes to produce weathered products in quasi-equilibrium with prevailing climate. Higher in the toposequence, sites TV23, 23A and 23B all show variable responses to destruction of metahalloysite/halloysite to production of gibbsite, the latter with pH's greater than 4.0, a stable weathering end product. Using this model, TV23 carries gibbsite primarily in the post-Teleki paleosol suggesting its morphology is the product of stronger paleoclimate. In TV23A, abundant gibbsite in the post-Naro Moru paleosol supports just the opposite interpretation. In TV23C, although with a steeper slope, and near nil clay mineral content, lower concentrations of gibbsite are registered by XRD analysis. Lower down in the toposequence ratios of halloysite to gibbsite become variable, probably more subject to replacement by mass wasting, the only stable beds are in unit 4 and to some degree in the saprolite of TV61A.

About the only sure division between the relative importance of climate and time in paleosol morphogenesis comes with the pedostratigraphy of TV23. In all other segments of the toposequence the mineral-chemical database lends itself more to time than climate as shown with results in lithic unit 4. The original findings of Mahaney (1990)

that clay mineral genesis on Mt. Kenya requires, despite fluctuating climate, considerable time to the order of 100 kyr is approximately correct.

Moraine Time Synchroneity

One outstanding feature of this toposequence is the equivocal synchroneity of glacial terminal moraine elevations reached by the Naro Moru and Teleki glaciers in Teleki Valley (2950 m – west flank) with the eastern catchments (3200 m – east flank). When compared with terminal moraine elevations of Naro Moru and Teleki age in Gorges Valley (~3200 m – east flank), mass balances for both ice sheets seem to be offset by 250 m, which is all the more curious since the east side moisture is monsoon generated compared with the west flank which is thunderstorm driven. The ±250 m difference in terminal moraine elevation positions between the two major catchments further suggests that monsoon delivery of moisture may not have outpaced the west flank during cold periods of the middle Pleistocene. Added to this is the missing Plio/Early Pleistocene moraine record on the west flank compared with the east flank where pre-Olduvai ice (Fig. 1B) is considered to be of Late Pliocene age reaching to 2950 m asl, each successive moraine sequence staggered from oldest to youngest across the Nithi River plateau to near 3200 m asl (Mahaney, 1990; Mahaney et al., 2011, 2012, 2013).

CONCLUSIONS

Maintaining independent and non-changing soil-forming factors such as climate, biota, parent material and time in any toposequence is difficult to achieve. In normal Late Pleistocene catenas, researched over the last half century, distances between sites are often less than what is discussed here with elevational changes of much lower magnitude. Other catenas of greater age offer the prospect of better deposit differentiation using relative-age dating methods but require more robust analysis with a greater number of samples. In this case, clear microclimate variations undoubtedly occur from crest to toeslope, with macroclimate differences considered of little consequence affecting the databases obtained and discussed here. Deep changes in macroclimate between glacials and interglacials, with swings between marine-isotope stages, in more ancient times is another matter, with linkages between distinct MIS stages somewhat tenuous. According to Coetzee (1964) and Cooremans and Mahaney (1990), the temperature depression during the last glacial was ~8°C, possibly lower (Olago et al., 1999). While temperature is only known for Met Station ~50 m higher than TV23, and then only for the 1957–58 IGY period (Mahaney 1990), a mean of ~7.4°C, taking the depression into account yields a glacial temperature over the toposequence of approximately ~0°C.

The biota is clearly another matter again as any variation of bamboo and *Podocarpus* will bring differences in leaf intercept of precipitation and most certainly variations in microbes, the latter affecting oxidation potential, electron acceptors, and variations of anaerobes to aerobes with their offsetting weathering effects, and over longer time frames than normal. Just as vegetation change during the Miocene to Pliocene transition followed a climatic trend leading to wide scale glaciation in the tropical mountains (Cerling et al., 1997; Mahaney et al., 2011; Somelar et al., 2018), with punctuated, episodic glacial advances and withdrawals. During later times this oscillating effect of glacial advance punctuated with interglacials and associated paleosol genesis, shifted timberline across the Teleki Toposequence producing oscillations of section stability during interglacials (and interstadials) and instability with loss of forest during glacials. Such paleoenvironmental shifts can be read most clearly from the Late Pleistocene record, and accounting for sediment compression and erosion over longer periods of time, the middle Pleistocene record becomes less clear. Given the estimated timelines for the Naro Moru-Teleki Interglacial of 0.5 to ~0.2 Ma, it is interesting to factor in recent 'rediscovered' sediment samples from the base of a 1.3 km long ice core from Camp Century in Greenland (Voosens, 2019; J.-L. Tison, personal communication, 2019). As released in a news item from the Science column of the AAAS, preliminary estimates based on initial luminescence and ^{10}Be-^{26}Al dating of sediment from the ice-rock interface yield an age of ~400 ka, with the unexpected postulate that Greenland may have not only been ice free, but covered with flora from deep southern latitudes. If future research verifies these initial results, the postulated age of basal sediment in Greenland would support estimated timelines for a major interglacial time on Mt Kenya. Moreover, these recent findings follow from Schaefer et al. (2016) who show that Greenland was deglaciated in various degrees during the Pleistocene.

The parent material factor of the toposequence is difficult to pin down exactly since the sediment under question is a mix of syenite, phonolite, kenyte and basalt with syenite more common in the tills than in loess, slopewash and colluvium. The time factor varies from one lithic unit to another as represented from one deposit to another. Across the saprolite beds, the time factor could be held at <~0.8 Ma; across the Naro Moru Till-loess at <0.5–~0.2 Ma; the Teleki Till (<0.2 Ma to 128 ka); colluvium and slopewash (~50–~20 ka) and the surface profiles (<~20 ka).

Working out weathering times for various deposits in the toposequence depends upon when such entities come under subaerial weathering subject to polyclimatic effects or burial. Once buried, and covered with newly emplaced materials, such entities are still capable of diagenesis, if not partial pedogenesis, affected by the throughput of weathered sediment and groundwater. Most probably the whole of the toposequence can be considered to be responding to a full range of weathering processes, although somewhat attenuated after burial. Although we cannot identify unconformities in the usual sense, each weathering interval that generates a paleosol is a weathering unconformity, with deposition on hold and the relation between matter

and time subject to a hiatus. No matter how conformable sections might appear in this toposequence there are likely unconformities within and between lithic units. Thus, each Ahb/Cox contact can be considered unconformable representing weathering plus missing sediment following the morphogenesis of the older paleosol. Given thinness of the tills and some of the loessic sediment, it is most probable that erosion has removed some depositional evidence through episodic downslope movement leaving only the residuum representing a weathering interval for analysis and discussion. Thus, superposed deposits are hardly totally conformable with time.

Because other workers (Birkeland and Burke, 1988; Birkeland *et al.*, 1991; Birkeland, 1999) argue that catenas are better representatives of weathering differences over time using relative-age dating parameter differences between depression members in a chronosequence, this toposequence provides an exception with its cyclic weathering stages extending back several hundred thousand years and tied to several glacial/interglacial cycles. Its near quiescent present state, under interglacial climate (i.e. the Holocene), stabilized by the presence of forest without active sediment input, presents a window in time, valuable as it is, even with missing pieces of environmental evidence.

Acknowledgements

REFERENCES

Abtahi, A., 1980. Soil genesis as affected by topographic and time in highly calcareous parent materials under semiarid conditions in Iran. Soil Science Society of America Journal 44, 329–336.

Baker, B.H., 1967. Geology of the Mt. Kenya area. Geology Report 79, Kenya Geological Survey, Nairobi, 78 pp.

Barendregt, R.W., 1984. Using paleomagnetic remanence and magnetic susceptibility data for the differentiation, relative correlation and absolute dating of Quaternary sediments. In: Mahaney, W.C. (Ed.), Quaternary Dating Methods. Amsterdam. Elsevier, 101–122.

Barendregt, R.W., Mahaney, W.C., 1988. Paleomagnetism of selected Quaternary sediments on Mount Kenya, East Africa; a reconnaissance study. Journal of African Earth Sciences 7 (1), 219–225.

Birkeland, P.W., 1999. Soils and Gemorphology. Oxford University Press, Oxford, U.K., 430 pp.

Birkeland, P.W., Burke, R.M., 1988. Soil catena chronosequences on eastern Sierra Nevada moraines, California, U.S.A. Arctic and Alpine Research 20 (4), 473–484.

Birkeland, P.W., Gerson, R., 1991. Soil-catena development wtih time in a hot desert, southern Israel-field data and salt distribution. Journal of Arid Environments 21, 267–281.

Birkeland, P.W., Berry, M.E., Swanson, D.K., 1991. Use of catena field data for estimating relative ages of moraines. Geology 19, 281–283.

Blume, H.P., Schwertmann, U., 1969. Genetic evaluation of profile distribution of aluminum, iron and manganese oxides. Soil Science Society of America Proceedings 33, 438–444.

Bower, C.A., Wilcox, L.V., 1965. Soluble salts. In: Black, C.A. (Ed.), Methods of Soil Analysis, Part 2. American Society Agronomy, Madison, WI, 933–951.

Bremner, J.R., 1965. Total nitrogen. In: Black, C.A. (Ed.), Methods of Soil Analysis. American Society of Agronomy, Madison, WI, 149–176.

Canada Soil Survey Committee (CSSC), 1998. The Canadian System of Soil Classification. 1646. NRC Research Press, Ottawa, Canada (Publ.), 187 pp.

Cerling, T.E., Harris, J.M., MacFadden, B.J., Leakey, M.G., Quade, J., Eisenmann, V., Ehleringer, J.R. 1997. Global vegetation change through the Miocene/Pliocene boundary. Nature 389, 153–158.

Coetzee, J.A., 1964. Evidence for a considerable depression of the vegetation belts during the upper Pleistocene on the East African mountains. Nature 204 (4958), 564–566.

Coffin, D.E., 1963. A method for the determination of free iron in soils and clays. Canadian Journal of Soil Science 43, 7–17.

Cooremans, B., Mahaney, W.C., 1990. Palynology of the TV61 section on Mt. Kenya, East Africa. In Heine, K. (Ed.), Palaeoecology of Africa 20, 283–294.

Dahl-Jensen, D, Albert, M.R, Aldahan, A, Azuma, N, Balslev-Clausen, D., Baumgartner, M., Berggren, A.M., Bigler, M., Binder, T., Blunier, T., Bourgeois, J.C., Brook, E.J.,Buchardt, S.L., Buizert, C., Capron, E., Chappellaz, J., Chung, J., Clausen, H.B., Cvijanovic, I., Davies, S.M., Ditlevsen, P., Eicher, O., Fischer, H., Fisher, D.A., Fleet, L.G., Gfeller, G., Gkinis, V., Gogineni, S., Goto-Azuma, K., 2013. Nature 493 (7433), 489–494.

Dahms, D., Favilli, F., Krebs, R., Egli, M., 2012. Soil weathering and accumulation rates of oxalate-extractable phases derived from alpine chronosequences of up to 1 Ma in age. Geomorphology 151–152, 99–113.

Dawson, J.B., 2008. The Gregory Rift Valley and Neogene–Recent volcanoes of Northern Tanzania. Geological Society, London, Memoirs 33, 102 p.

Day, P.E., 1965. Particle fractionation and particle size analysis. In: Black, C.A. (Ed.), Methods of Soil Analysis. American Society of Agronomy, Madison, Wisconsin, 545–567.

Dormaar, J.F., Lutwick, L.E., 1983. Extractable Fe and Al as an indicator for buried soil horizons. Catena 10, 167–173.

Everden, J.F., Curtis, G.H., 1965. The potassium-argon dating of late Cenozoic rocks in East Africa and Italy. Current Anthropology 6, 343–385.

Gregory, J.W., 1894. The glacial geology of Mount Kenya. Quarterly Journal Geological Society 50, 515–530.

Gregory, J.W., 1921. The Rift Valleys and Geology of East Africa, Geological Society, London, 479 pp.

Hancock, R.G.V., 1984. On the source of clay used for Cologne Roman pottery. Archaeometry, 26, 210-217.

Hancock, R.G.V., Michelaki, K., Mahaney, W.C., Aufreiter, S., 2019. Justification for reassessing elemental analysis data of ceramics, sediments and lithics using rare earth element concentrations and ratios. Archaeometry 61(6), 1430–144.

Harrison, T.P., Hancock, R.G.V., 2005. Geochemical analysis and sociocultural complexity: a case study from early iron age Megiddo, (Israel). Archaeometry 47, 705–722.

Hastenrath, S., 1984. The Glaciers of Equatorial East Africa. Dordrecht, Reidel, 353 pp.

Hutton, J., 1795. Theory of the Earth. Vol. 1. Republished by The Perfect Library, 2019, 223 pp.

Jenny, H., 1941. Factors of soil formation. New York, McGraw-Hill, 281 pp.

Karlstrom, E., 1991. Paleoclimatic significance of Late Cenozoic paleosols of Waterton-Glacier Parks, Alberta and Montana. Palaeogeography, Palaeoclimatology, Palaeoecology 85, 71–100.

Macbeth Corp, 1992. Munsell Soil Color Charts (Munsell Color). Division of Kollmorgen Instruments Corporation, 29 pp.

Mahaney, W.C., 1989. Amino acids in buried soils on Mount Kenya. Journal of African Earth Sciences 9 (2), 327–334.

Mahaney, W.C., 1990. Ice on the Equator. Wm Caxton Press, Ellison Bay, Wisconsin, 386 p.

Mahaney, W.C., 1991. Distributions of halloysite-metahalloysite and gibbsite in tropical mountain paleosols: relation to Quaternary paleoclimate. Palaeogeography, Palaeoclimatology, Palaeoecology 88, 219–230.

Mahaney, W.C., 2002. Atlas of Sand Grain Surface Textures and Applications. Oxford University Press, Oxford, U.K., 237 pp.

Mahaney, W.C., 2011. Quaternary glacial chronology of Mount Kenya Massif. In: Ehlers, J., Gibbard, P., Hughes, P.D. (Eds), Quaternary Glaciations-Extent and Chronology Part IV-A Closer Look, Elsevier, Amsterdam, Chapter 77, 1075–1080.

Mahaney, W.C. Boyer, M.G., 1987. Late glacial soil catena in upper Teleki Valley, Mount Kenya Afroalpine area. Journal of African Earth Sciences 6 (5), 731–740.

Mahaney, W.C., Rutter, N., 1989. Amino acid ratio distributions in two late Quaternary soils in the Afroalpine zone of Mt. Kenya, East Africa. Catena 16, 205–214.

Mahaney, W.C., Sanmugadas, K., 1983. Early Holocene soil catena in Titcomb Basin, Wind River Mountains, Western Wyoming. Zeitschrift für Geomorphologie 27 (3), 265–281.

Mahaney, W.C., Sanmugadas, K., 1989. Mid-Holocene soil toposequence in Stroud Basin, Central Wind River Mountains, Wyoming. Geografisk Tidsskrift 89, 58–65.

Mahaney, W.C., Hancock, R.G.V., Rutter, N., Sanmugadas, K., 1991. Stratigraphy and geochemistry of a sequence of Quaternary palaeosols in the Lower Tekeki Valley, Mount Kenya, East Africa-implications for interregional correlations. Journal of Quaternary Science 6 (3), 245–256.

Mahaney, W.C., Hancock, R.G.V., Sanmugadas, K., 1994. Extractable Fe, Al, and Mn in paleosols of Late Quaternary age in the Virunga Mountains, northwestern Rwanda. Catena 20, 27–36.

Mahaney, W.C., Vortisch, W., Barendregt, R.W., 1997. Relative age of loess and till in two Quaternary paleosols in Gorges Valley, Mount Kenya, East Africa. Journal of Quaternary Science 12, 61–72.

Mahaney, W.C., Sanmugadas, K., Hancock, R.G.V., 1999. Extractable Fe and Al soils in the middle Teton chronosequence, western Wyoming, U.S.A. Zeitschrift für Geomorphologie 43, (3) 393–407.

Mahaney, W.C., Dohm, J.M., Kapran, B., Hancock, R.G.V., Milner, M.W., 2009. Secondary Fe and Al in Antarctic paleosols: correlation to Mars with prospect for the presence of life. Icarus 203, 320–330.

Mahaney, W.C., Barendregt, R.W., Villeneuve, M., Dostal, J., Hamilton, T.S., Milner, M.W., 2011. Late Neogene volcanics and interbedded palaeosols near Mount Kenya. In: Van Hinsbergen, D.J.J., Buiter, S.J.H., Torsvik, T.H., Gaina, C., Webb, S.J. (Eds), The Formation and Evolution of Africa: A Synopsis of 3.8 Ga of Earth History. Geological Society, London, 301–318.

Mahaney, W.C., Barendregt, R.W., Hamilton, T.S., Hancock, R.G.V., Tessler, D., Costa, P.J.M., 2013. Stratigraphy of the Gorges Moraine System, Mount Kenya: paleosol record and paleoclimate. Journal Geological Society, 170, 497–511.

Mahaney, W.C., Barendregt, R.W., Hamilton, T.S., Hancock, R.G.V., Costa, P.J.M., 2014. Soil mineralogy and chemistry of Late Pliocene–Early Pleistocene paleosols on Mount Kenya: age and paleoclimate reconstruction. Geomorphology 204, 217–228.

Mahaney, W.C., Somelar, P., Dirszowsky, R.W., Kelleher, B., Pentlavalli, P., McLaughlin, S., Kulakova, A., Jordan, S., Pulleyblank, C., West, A., Allen, C.C.R., 2016. A microbial link to weathering of postglacial rocks and sediments, Mt. Viso area, Western Alps, demonstrated through analysis of a soil/paleosol bio/chronosequence. Journal of Geology 124 (2), 149–169.

McKeague, A., Day, J., 1966. Dithionite and oxalate extractable Fe and Al as aids in differentiating various classes of soils. Canadian Journal of Soil Science 46, 13–22.

Mehra, O.P., Jackson, M.L., 1960. Iron oxide removal from soils and clays by a dithionite-citrate system buffered with sodium bicarbonate. National Conference on Clays and Clay Minerals, 1958. Pergamon, London, 317–327.

Milne, G., 1937. Normal erosion as a factor in soil profile development. Nature 138, 548–549.

National Soil Survey Center (NRCS), 2004. Soil Survey Laboratory Methods Manual. In: Burt, R. (Ed.), Soil Survey Investigations Report no. 42, version 4.0, U.S.D.A., 700 pp.

Nettleton, W.C., Flach, K.W., Nelson, R.E., 1968. A toposequence of soils in tonalite grus in the southern California Peninsular Range. USDA-SCS Soil Survey Investigations Report No. 21. U.S Goverment Printing Office, Washington, D.C.

Nilsson, E., 1931. Quaternary glaciation and pluvial lakes in British East Africa and Abyssinia. Geografiska Annaler 13, 241–248.

Nilsson, E., 1935. Traces of ancient changes of climate in East Africa. Geografiska Annaler 17, 1–21.

Olago, D.O., Street-Perrott, F.A., Perrott, R.A., Ivanovich, M., Harkness, D.D., 1999. Late Quaternary glacial-interglacial cycle of climatic and environmental change on Mount Kenya, Kenya. Journal of African Earth Sciences 29, 593–618.

Oyama, M., Takehara, H., 1970. Standard Soil Color Charts, Japan Research Council for Agriculture, Forestry and Fisheries.

Parfitt, R.L,. Childs, C.W., 1988. Estimation of forms of Fe and Al: a review and analysis of contrasting soils by dissolution and Moessbauer methods. Australian Journal Soil Research 26, 121–144.

Pawelec, H., 2006. Origin and palaeoclimatic significance of the Pleistocene slope covers in the Cracow Upland, southern Poland. Geomorphology 74, 50–69.

Pawelec, H., Drewnik, M., Żyła, M., 2015. Paleoenvironmental interpretation based on macro- and microstructure analysis of Pleistocene slope covers: A case study from the Miechów Upland, Poland. Geomorphology 232, 145–163.

Peech, M.L., Alexander, T., Dean, L.A., Reed, J.F., 1947. Methods of soil analyses for soil fertility investigations. Washington, D.C., U.S. Dept. of Agriculture Circular 757, p. 25.

Pevehouse, K.J., Sweet, D.E., Segvic, B., Monson, C.C., Zanoni, G., Marshak, S., Barnesi, M., 2020. Paleotopography controls weathering of Cambrian-age profiles beneath the Great Unconformity, St., Francois Mountains, SE Missouri, U.S.A., Journal of Sedimentary Research 90, 629–650.

Railsback, L.B., Gibbard, P.L., Head, M.J., Voarintsoa, N.R.G., Toucanne, S., 2015. An optimized scheme of lettered marine isotope substages for the last 1.0 million years, and the climatostratigraphic nature of isotope stages and substages. Quaternary Science Reviews 111, 94–106.

Rovere, A., Raymo, M., Vacchi, M., Hearty, P., 2016. The analysis of Last Interglacial (MIS 5e) relative sea-level indicators: Reconstructing sea-level in a warmer world. Earth-Science Reviews 159, 404–427.

Schaefer, J.M., Finkel, R.C., Balco, G., Alley, R.B., Caffee, M.W., Briner, J.P., Young, N.E., Gow, A.J., Schwartz., R., 2016. Greenland was nearly ice-free for extended periods during the Pleistocene. Nature 540, 252–255.

Schollenberger, C.J., Simon, R.H., 1945. Determination of exchange capacity and exchangeable bases in soils – ammonium acetate method. Soil Science 59, 13–24.

Shackelton, R.M., 1945. Geology of the Nyeri Area, Report No. 12 Ministry Of Environment And Natural Resources Mines And Geological Department Geology Of The Nyeri Area, Geological Survey of Kenya, 1–33.

Simpson, A.J., Simpson, M.J., Smith, E., Kelleher, B.P., 2007. Microbially derived inputs to soil organic matter: are current estimates too low? Environmental Science & Technology 41, 8070–8076.

Smalley, I.J., 1966. The properties of glacial loess and the formation of loess deposits. Journal Sedimentary Petrology 36, 669–676.

Soil Survey Staff, 2010. Keys to Soil Taxonomy, 11th ed. U.S. Gov. Printing Office, Washington, D.C.

Somelar, P., Vahur, S., Hamilton, T., Mahaney, W.C., Barendregt, R.W., Costa, P., 2018. Sand coatings in paleosols: Evidence of weathering across the Plio-Pleistocene boundary to modern times. Geomorphology 317, 91–106.

Veldkamp, A., Buis, E., Wijbrans, J.R., Olago, D.O., Boshoven, E.H., Marée, M., Van den Berg van Saparoea, R.M., 2007. Late Cenozoic fluvial dynamics of the River Tana, Kenya, an uplift dominated record. Quaternary Science Reviews 26, 2897–2912.

Voosens, P., 2019. Ancient soil from secret Greenland base suggests Earth could lose a lot of ice. Science, AAAS, October 2019, doi: 10.1126/Science.aba0351.

Vortisch, W., Mahaney, W.C., Fecher, K., 1987. Lithology and weathering in a paleosol sequence on Mt. Kenya, East Africa. Geologica et Paleontologica 21, 245–255.

Walkley, A., Black, I.A., 1934. An examination of the Degtjareff method for determining soil organic matter, and a proposed modification of the chromic acid titration method. Soil Science 37, 29–38.

Whittig, L.D., 1965. X-ray diffraction techniques for numerical identification and mineralogical composition. In: Black, C.A. (Ed.), Methods of Soil Analysis. American Society of Agronomy, Madison, Wisconsin, 671–696.

Young, J.M., Skvortsov, T., Kelleher, B.P., Mahaney, W.C., Somelar, P., Allen, C.C.R., 2018. Effect of soil horizon stratigraphy on the microbial ecology of alpine paleosols. Journal of the Total Environment 657, 1183–1193.

SUPPLEMENTARY TABLES

Table 1. Mineralogy of sections TV23A–TV23C, Teleki Catena, Mt Kenya. Mineral identification: MH = metahalloysite; H = halloysite; Gi = gibbsite; He = hematite; Go = goethite; Q = quartz; Pl = plagioclase; Py = pyroxene; Mag = magnetite; Ill = illite.

Site	Horizon	Depth (cm)	MH	H	Gi	He	Go	Q	Pl	Py	Mag	Ill
TV23A	Ah	0–8	–	–	–	tr	tr	xxx	xx	x	tr	tr
	Bt1	8–30	tr	tr	tr	tr	x	xxx	x	x	tr	–
	Bt2	30–58	tr	tr	–	x	tr	xx	tr	–	x	–
	2Bt3	58–90	tr	tr	–	–	tr	x	x	tr	tr	–
	2Bt4	90–145	x	x	x	–	tr	x	–	–	tr	–
	3Btb	145–160	–	tr	–	–	–	–	–	–	tr	–
	4Coxb1	160–205	–	x	–	–	–	x	tr	–	–	–
	4Coxb2	205–330	–	x	x	–	tr	tr	–	–	tr	–
	5Saprolite	330+	–	x	–	x	tr	x	x	tr	tr	–
TV23B	Ah1	0–10	–	tr	tr	–	–	xx	x	x	x	–
	Ah2	10–20	–	tr	tr	–	tr	xx	x	tr	tr	–
	Bt1	20–45	–	tr	tr	–	–	xxx	x	x	tr	–
	Bw2	45–85	–	x	tr	–	x	xx	x	x	tr	–
	2Cox	85–120	–	xx	x	–	–	xx	x	tr	tr	–
	3Btb1	120–135	–	tr	x	x	x	xx	x	x	x	–
	3Btb2	135–178	x	x	x	x	–	xxx	x	tr	tr	–
	3Btb3	178–215	–	xx	xx	tr	tr	x	tr	–	tr	–
	4Coxb1	215–230	–	xx	xx	tr	–	tr	tr	–	tr	–
	4Coxbm2	230–290	–	x	xxx	tr	tr	tr	tr	–	tr	–
	5Saprolite	290+										
TV23C	Ah	0–12	–	–	–	–	tr	xxx	x	x	x	–
	Bw1	12–35	–	–	–	x	x	xxx	xx	x	x	–
	Bw2	35–75	–	–	tr	x	tr	xx	x	tr	tr	–
	2Cox	75–112	–	–	tr	x	tr	xx	x	x	x	–
	3Ahb1	112–125	–	–	tr	x	tr	xxx	x	x	x	–
	3Ahb2	125–129	–	–	tr	x	tr	xx	x	x	x	–
	3Ahb3	129–135	–	–	–	tr	tr	x	x	tr	tr	–
	3Ahb4	135–150	–	–	x	x	x	xxx	x	x	x	–
	3Ahb5	150–175	–	–	x	x	x	xx	x	x	x	–
	3Bwb	175–196	–	–	tr	x	tr	xx	x	x	x	–
	4Btb1	196–235	–	–	tr	x	x	xxx	x	x	x	–
	4Btb2	235–270	tr	tr	x	tr	tr	x	tr	tr	tr	–
	5Saprolite											

Table 2. Mineralogy of the T61 and Tv61A sections, Teleki Catena, Mt. Kenya. Mineral identification: MH = metahalloysite; H = halloysite; Gi = gibbsite; He = hematite; Go = goethite; Q = quartz; Pl = plagioclase; Py = pyroxene; Mag = magnetite.

Site	Horizon	Depth (cm)	MH	H	Gi	He	Go	Q	Pl	Py	Mag
TV61	Ah1	0–5	–	–	–	x	tr	xx	x	x	tr
	Ah2	5–22	–	–	–	x	–	xx	x	x	tr
	Bw1	22–40	–	–	–	x	tr	xx	x	x	tr
	Bw2	40–62	–	–	–	x	tr	xx	x	x	tr
	Cox	62–82	–	–	–	x	tr	xx	x	x	x
	2Ahb1	82–102	–	–	–	xx	x	xxx	xx	x	x
	2Ahb2	102–138	–	–	–	**x**	tr	xx	x	x	tr
	2Ahb3	138–160	–	–	–	xx	x	xxx	xx	x	x
	2Ahb4	160–180	–	–	–	tr	x	xx	x	x	tr
	2Ahb5	180–195	–	–	–	x	tr	xx	x	x	tr
	2Bwb1	195–220	–	–	tr	x	tr	xxx	x	x	x
	2Bwb2	220–230	–	–	tr	x	tr	xx	x	x	tr
	2Coxb	230–246	–	–	tr	x	tr	xxx	x	x	tr
	3Ahb	246–255	–	–	–	x	tr	xx	x	x	tr
	3Bwb	255–277	–	–	x	x	tr	xx	x	x	tr
	3Coxb	277–297	–	–	–	tr	tr	x	x	x	Tr
	3Ahbl	297–320	–	–	–	x	tr	xx	x	x	tr
	3Ahb2	320–340	–	–	x	x	tr	xx	x	x	tr
	3Btb	340–400	–	–	xx	x	tr	xx	x	x	tr
	4Btb1	400–435	–	x	x	tr	tr	xx	x	x	–
	4Btb2	435–470	–	x	–	x	–	x	tr	tr	–
	4Btb3	470–490	tr	x	–	x	tr	xx	x	x	x
	4Btb4	490–565–	–	x	–	–	–	–	–	–	–
	5Saprolite	565+	–	x	–	–	tr	–	x	x	tr
TV61A	Ah1	0–8	–	–	–	x	tr	xx	x	x	tr
	Ah2	8–29	–	–	tr	x	tr	xxx	x	x	tr
	Ah3	29–33	–	–	–	tr	tr	xx	tr	tr	tr
	Bt	33–55	–	–	–	tr	–	x	tr	tr	tr
	Cox	55–88	–	–	–	x	tr	xx	x	x	x
	2Ahb1	88–110	–	–	–	x	tr	xx	x	x	x
	2Ahb2	110–140	–	–	–	x	x	xxx	x	x	x
	2Ahb3	140–176	–	–	–	x	–	xx	x	x	tr
	2Ahb4	176–215	–	–	–	x	tr	xx	x	x	tr
	2Ahb5	215–230	–	–	–	x	tr	xxx	x	x	tr
	2Ahb6	230–245	–	–	tr	x	tr	xx	x	x	x
	2Bwb1	245–260	tr	x	–	tr	–	xx	–	–	–
	2Bwb2	260–271	–	–	x	tr	tr	xx	x	x	tr
	3Ahb1	271–290	–	–	–	x	–	xx	x	x	tr
	3Ahb2	290–316	–	–	–	–	tr	x	tr	–	–
	3Btb	316–326	–	tr	tr	tr	tr	xx	–	–	= =
	3Coxb1	326–352	–	–	–	tr	x	xx	x	x	tr
	3Coxb2	352–367	–	tr	–	x	tr	xxx	x	x	tr
	3Ahb	367–380	–	–	x	tr	tr	x	tr	tr	tr
	3B/Ahb1	380–391	–	tr	xx	tr	tr	x	tr	tr	tr
	3Btb1	391–423	–	x	–	–	–	x	–	–	–
	3Btb2	423–440	–	xx	–	–	–	tr	tr	–	–
	4Btb3	440–463	–	xx	–	–	–	–	–	–	–
	4Btb4	463–488	–	xx	–	x	tr	xx	x	x	tr
	4Btb5	488–515	–	x	–	x	tr	xxx	x	–	–
	5Saprolite	515–600	–	x	–	tr	tr	tr	x	tr	–

Table 3. Mineralogy of the T61B and TV69 Sections, Teleki Catena, Mt. Kenya. Mineral identification: MH = metahalloysite; H = halloysite; Gi = gibbsite; He = hematite; Go = goethite; Q = quartz; Pl = plagioclase; Py = pyroxene; Mag = magnetite.

Site	Horizon	Depth (cm)	MH	H	Gi	He	Go	Q	Pl	Py	Mag
TV61B	Ah	0–12	–	–	–	x	x	xxx	x	x	tr
	Bw1	12–25	–	–	–	tr	x	xxx	x	x	x
	Bw2	25–68	–	–	–	x	tr	xx	x	x	tr
	Cox	68–85	–	–	–	tr	tr	x	x	x	–
	2Ahb1	85–130	–	–	–	tr	tr	xx	x	tr	tr
	2Ahb2	130–165	–	–	–	x	tr	xx	x	x	–
	2Ahb3	165–192	–	–	–	x	x	xxx	x	x	tr
	2Ahb4	192–202	–	–	–	tr	tr	xxx	x	x	tr
	2Ahb5	202–211	–	–	–	x	tr	xx	x	x	tr
	2Ahb6	211–223	–	–	–	x	tr	x	xx	x	tr
	2Bwb	223–235	–	–	–	–	tr	–	x	tr	–
	2Coxb	235–272	–	–	tr	x	tr	xxx	x	x	tr
	3Ahb1	272–300	–	–	–	x	tr	xx	x	x	tr
	3Ahb2	300–310	–	–	–	tr	–	–	x	x	tr
	3Btb1	310–335	tr	tr	–	x	tr	xx	x	x	tr
	3Bwb2	335–355	–	tr	x	tr	tr	–	tr	tr	tr
	3Btb3	355–380	–	x	tr	–	–	tr	–	–	–
	3Btb4	380–410	–	x	–	x	tr	xx	x	x	tr
	3Btb5	410–440	–	xx	–	x	tr	x	x	x	x
	3Btb6	440–460	–	xx	–	tr	–	tr	–	–	–
	4Saprolite	460+	–	x	–	x	tr	x	tr	tr	tr
TV69	Ah	0–23	–	–	–	x	tr	xxx	x	–	–
	Bw1	23–52	–	–	–	x	tr	xxx	x	–	–
	Bw2	52–78				x	tr	xx	x	–	–
	2Ahb	78–93				x	x	xx	x	–	–
	Bedrock93+										

Table 4. Selected chemical properties of profiles TV23–TV23C, Teleki catena, Mt. Kenya..

Site	Horizon	Depth (cm)	pH (1:5)	E.C. (S/cm^2)	Organic carbon (%)	Nitrogen (%)	Color
TV23	Ah1	0–18	4.65	2.00	8.52	0.878	10YR 2/3
	Ah2	18–38	4.90	0.25	5.05	0.503	10YR 3/2
	Bt1	38–90	4.55	<0.10	3.08	0.288	5YR 3/3
	Bt2	90–104	4.80	<0.10	0.98	0.101	7.5YR 4/4
	2Cox1	104–165	5.20	<0.10	0.66	0.040	5YR 4/6
	2Cox2	165–175	5.50	<0.10	0.40	0.028	5YR 4/4
	3Ahb	175–185	5.25	<0.10	0.07	0.010	10YR 5/6
	3Btb1	185–195	5.00	<0.10	0.07	0.009	10YR 5/4
	3Btb2	195–215	5.25	<0.10	0.17	0.011	10YR 4/4
	3Btb3	215–246	5.20	<0.10	0.10	0.010	7.5YR 4/4
	4Btb4	246–274	5.10	<0.10	0.20	0.003	10YR 4/6
	4Btb5	274–440	5.00	<0.10	0.07	0.003	10YR 4/4
TV23A	Ah	0–18	5.6	0.51	6.22	0.84	5YR 3/2
	Bt1	18–30	5.5	0.28	4.18	0.53	5YR 3/4
	Bt2	30–58	5.5	0.18	2.68	0.42	5YR 3/3
	2Bt3	58–90	5.2	0.14	2.91	0.35	5YR 4/3
	2Bt4	90–145	5.1	0.09	0.47	0.09	5YR 4/4
	3Btb	145–160	5.8	0.08	0.37	0.05	5YR 4/6
	4Coxb1	160–205	5.0	0.11	0.13	0.07	7.5YR 4/4
	4Coxb2	205–330	4.8	0.07	0.15	0.05	7.5YR5/4
TV23B	Ah1	0–10	4.5	0.60	7.40	0.95	7.5YR 2/3
	Ah2	10–20	4.5	0.51	6.39	0.78	7.5YR 3/4
	Bt1	20–45	4.3	0.23	5.27	0.62	5YR 4/6
	Bw2	45–85	4.5	0.17	4.25	0.39	7.5YR 4/4
	2Cox	85–120	4.7	0.12	2.42	0.29	7.5YR 5/4
	3Btb1	120–135	4.8	0.08	1.69	0.17	5YR 3/4
	3Btb2	135–178	5.1	0.08	0.62	0.02	5YR 4/4
	3Btb3	178–215	5.2	0.07	0.26	0.03	5YR 4/6
	4Coxb1	215–230	5.0	0.08	0.31	0.05	7.5YR 5/6
	4Coxbm2	230–290	5.0	0.08	0.17	<0.01	7.5YR 6/4
	5Saprolite	290+	5.4	0.35			7.5YR 6/1/6/6
TV23C	Ah	0–12	5.0	1.11	16.61	1.49	5YR 2/3
	Bw1	12–35	5.0	0.24	8.17	0.72	5YR 3/4
	Bw2	35–75	4.8	0.17	6.26	0.65	5YR 3/3
	2Cox	75–112	4.3	0.22	6.17	0.63	5YR 3/4
	3Ahb1	112–125	4.5	0.29	6.42	0.60	5YR 2/2
	3Ahb2	125–129	4.2	0.22	6.72	0.57	5YR 2/3
	3Ahb3	129–135	4.0	0.17	6.68	0.49	5YR 2/1
	3Ahb4	135–150	4.4	0.20	5.54	0.42	5YR 2/2
	3Ahb5	150–175	4.7	0.27	4.30	0.30	5YR 2/3
	3Bwb	175–196	5.0	0.14	1.58	0.18	5YR 4/4
	4Btb1	196–235	5.6	0.12	0.92	0.10	5YR 3/4
	4Btb2	235–275	5.6	0.12	0.34	0.07	5YR 4/6
	5Saprolite	275+					5YR 4/6

Table 5. Selected chemical properties of profiles TV61 and TV61A, Teleki Catena, Mt. Kenya.

Site	Horizon	Depth (cm)	pH (1:5)	E.C. (S/cm²)	Organic carbon (%)	Nitrogen (%)	Dry color
TV61	Ah1	0–5	4.2	1.11	16.37	0.899	5YR 2/3
	Ah2	5–22	4.1	1.25	14.12	0.691	5YR 2/2
	Bw1	22–40	4.8	0.24	7.69	0.591	5YR 3/3
	Bw2	40–62	4.6	0.17	7.20	0.419	5YR 3/4
	Cox	62–82	4.3	0.22	6.75	0.376	5YR 2/2
	2Ahb1	82–112	4.5	0.29	7.76	0.309	5YR 3/2
	2Ahb2	112–138	4.2	0.22	6.15	0.271	5YR 2/2
	2Ahb3	138–160	4.1	0.19	6.00	0.220	5YR 2/1
	2Ahb4	160–180	4.0	0.17	5.85	0.190	5YR 3/1
	2Ahb5	180–195	4.3	0.12	4.92	0.176	5YR 3/2
	2Bwb1	195–220	5.0	0.14	2.84	0.169	5YR 4/6
	2Bwb2	220–235	5.1	0.16	2.38	0.158	5YR 4/4
	2Coxb	235–246	4.9	0.12	3.30	0.219	5YR 5/4
	3Ahb	246–255	4.7	0.16	3.24	0.213	5YR 3/2
	3Bwb	255–277	4.6	0.10	3.01	0.201	5YR 3/1
	3Coxb	277–297	4.4	0.12	1.42	0.098	5YR 3/6
	3Ahb1	297–320	4.8	0.15	2.85	0.195	5YR 2/3
	3Ahb2	320–340	5.0	0.21	2.01	0.165	5YR 3/4
	3Btb	340–400	4.8	0.17	1.69	0.134	5YR 4/4
	4Btb1	400–435	4.6	0.10	1.15	0.102	5YR 4/6
	4Btb2	435–470	5.0	0.14	1.51	0.090	5YR 3/6
	4Btb3	470–490	5.4	0.08	0.25	0.007	7.5YR 4/6
	4Btb4	490–565	5.6	0.06	0.16	0.005	10YR 5/6
	5 Saprolite	565+	5.2	0.14	0.31	0.010	5YR 4/4
TV61A	Ah1	0–6	4.9	0.72	11.43	1.05	5YR 2/3
	Ah2	6–22	4.7	0.83	12.40	1.18	5YR 2/2
	Ah3	22–28	4.8	0.41	11.87	1.10	5YR 3/4
	Bt	28–55	4.5	0.30	8.61	0.85	5YR 4/4
	Cox	55–85	4.7	0.26	7,31	0.74	5YR 3/3
	2Ahb1	85–110	4.4	0.09	7.60	0.64	5YR 3/2
	2Ahb2	110–140	4.5	0.08	7.60	0.59	5YR 3/4
	2Ahb3	140–172	4.4	0.09	7.06	0.59	5YR 3/2
	2Ahb4	172–185	4.6	0.12	7.53	0.49	5YR 3/1
	2Ahb5	185–230	4.9	0.11	6.65	0.43	5YR 1/1
	2Ahb6	230–240	4.7	0.10	4.82	0.35	5YR 2/1
	2Bwb1	240–260	5.1	0.09	2.90	0.29	5YR 3/4
	2Bwb2	260–272	4.8	0,11	2.73	0.30	5YR 3/3
	3Ahb1	272–285	5.1	0.10	5.11	0.37	5YR 2/1
	3Ahb2	285–315	4.9	0,09	4.48	0.33	5YR 2/2
	3Btb	315–320	4.9	0.12	0.97	0.15	5YR 4/6
	3Coxb1	320–348	4.9	0.11	1.59	0.22	5YR 4/4
	3Coxb2	348–362	5.5	0.09	0.99	0.16	5YR 3/3
	3Ahb	362–380	4.8	0.10	2.44	0.26	7.5YR 2/3
	3B/Ahb	380–390	5.0	0.09	1.52	0.13	7.5YR 4/4
	3Btb1	390–425	5.2	0.15	0.34	0.03	5YR 4/6
	3Btb2	423–440	5.0	0.14	0.18	0.02	10YR 4/6
	4Btb3	440–462	5.2	0.10	0.10	<0.01	7.5YR 5/6
	4Btb4	462–490	5.3	0.11	0.12	<0.01	10YR 5/6
	4Btb5	490–519	4.8	0.09	0.19	0.01	7.5YR 5/4
	5Saprolite	519+	–	–	–	–	5YR 4/4

Table 6 Selected chemical and physical properties of paleosols, Teleki Catena, Mt. Kenya, East Africa.

Site	Horizon	Depth (cm)	pH (1:5)	E.C. (S/cm^2)	Organic carbon (%)	Nitrogen (%)	Color
TV61B	Ah	0–12	5.0	0.78	10.88	1.13	10YR 5/3
	Bw1	12–25	4.9	0.52	8.27	1.03	10YR 5/4
	Bw2	25–68	5.3	0.15	5.97	0.73	10YR 4/4
	Cox	68–85	5.1	0.08	6.50	0.70	7.5YR 3/4
	2Ahb1	85–130	5.2	0.07	6.25	0.61	5YR 2/2
	2Ahb2	130–165	5.2	0.06	5.93	0.52	5YR 2/3
	2Ahb3	165–192	5.0	0.07	6.28	0.45	5YR 2/2
	2Ahb4	192–202	5.3	0.07	8.16	0.46	5YR 2/2
	2Ahb5	202–211	5.4	0.08	5.77	0.43	5YR 3/1
	2Ahb6	211–223	5.4	0.07	5.15	0.37	5YR 2/1
	2Bwb	223–235	5.3	0.08	2.86	0.24	5YR 4/6
	2Coxb	235–272	5.3	0.07	2.72	0.29	5YR 3/3
	3Ahb1	272–300	5.2	0.07	5.71	0.31	5YR 3/2
	3Ahb2	300–310	5.2	0.07	5.63	0.38	5YR 3/3
	3Btb1	310–335	5.3	0.08	0.98	0.17	5YR 4/3
	3Bwb2	335–355	5.6	0.08	1.30	0.17	5YR 4/4
	3Btb3	355–380	5.9	0.13	0.61	0.08	7.5YR 5/6
	3Btb4	380–410	5.3	0.09	0.18	0.08	7.5YR 5/2
	3Btb5	410–440	5.2	0.11	0.18	0.07	10YR 6/2
	3Btb6	440–460	5.2	0.11	0.24	0.06	10YR 5/4
	4Saprolite	480+	5.6	0.13	0.04	0.04	10YR 6/3
TV69	Ah	0–23			13.93	1.32	5YR 2/3
	Bw1	23–52			6.95	0.70	5YR 3/3
	Bw2	52–78			6.41	0.65	7.5YR 3/4
	2Ahb	78–93			6.56	0.59	7.5YR 2/3
	Phonolite	83+					

Table 7. Iron and Al total concentrations and extraction functions in profilesTV23–TV23B Teleki Valley Catena, Mt. Kenya.

Site	Horizon	Depth (cm)	Fep %	Feo %	Fed %	Fet %	Alp %	Alo %	Ald %	Alt %
TV23	Ah1	0–20	1.44	1.66	3.75	5.21	0.67	0.70	0.71	9.0
	Ah2	20–38	2.16	2.32	5.29	6.51	1.17	1.10	1.22	11.1
	Bt1	38–90	2.17	2.26	5.75	7.50	1.20	1.20	1.61	12.9
	Bt2	90–103	0.20	1.60	4.66	7.06	0.50	0.95	1.10	15.5
	2Cox1	103–165	0.46	1.46	6.57	8.69	1.06	1.10	1.43	17.9
	2Cox2	165–178	0.20	1.92	11.59	13.10	0.34	0.79	1.78	17.9
	3Ahb	178–186	0.04	2.94	6.33	8.39	0.19	1.25	1.33	16.6
	3Btb1	186–195	0.16	3.02	7.49	12.70	0.48	1.13	1.17	10.8
	3Btb2	195–215	0.17	2.71	9.10	12.20	0.49	1.06	1.46	14.1
	3Btb3	215–245	0.20	2.52	8.55	11.15	0.55	0.91	1.29	15.3
	4Btb4	245–270	0.26	1.15	7.23	10.00	0.64	0.87	1.09	16.3
	4Btb5	270–440	0.32	1.88	6.89	9.30	0.89	1.09	1.12	15.8
TV23B	Ah1	0–10	1.24	1.50	3.60	5.31	0.70	0.81	0.90	10.2
	Ah2	10–20	1.30	2.03	3.80	4.47	0.76	1.04	0.98	11.0
	Bt1	20–45	1.54	2.15	4.19	5.92	1.01	1.01	1.25	12.4
	Bw2	45–73	1.75	1.85	4.19	6.40	1.40	1.44	1.54	12.9
	2Cox	73–109	1.82	1.84	4.45	6.41	1.60	1.46	1.55	14.1
	3Btb1	109–129	1.26	1.27	4.12	6.25	1.22	1.25	1.25	15.6
	3Btb2	129–170	0.18	0.66	4.69	6.84	0.19	0.65	1.33	16.5
	3Btb3	170–205	0.06	0.87	4.18	7.14	0.15	0.57	0.58	16.5
	4Coxb1	205–230	0.05	0.68	4.32	7.03	0.12	0.55	0.60	16.2
	4Coxbm2	230–275	0.04	0.58	3.27	6.70	0.19	0.50	0.51	16.8

Site	Horizon	Depth (cm)	Feo/Fed	Feox1.7 (%)	Fet–Fed (%)	Fed–Fe0 (%)	Fed/Fet	Alp/Alt	Alo–Alp (%)
TV23	Ah1	0–20	0.44	2.82	1.46	2.09	0.72	0.07	0.03
	Ah2	20–38	0.43	3.94	1.22	2.97	0.81	0.11	0.07
	Bt1	38–90	0.39	3.84	1.75	3.49	0.77	0.09	0.00
	Bt2	90–103	0.34	2.72	2.40	3.06	0.66	0.03	0.45
	2Cox1	103–165	0.22	2.48	2.12	5.11	0.76	0.06	0.04
	2Cox2	165–178	0.17	3.26	1.51	9.67	0.88	0.02	0.45
	3Ahb	178–186	0.46	4.99	2.06	3.39	0.75	0.01	1.06
	3Btb1	186–195	0.40	5.13	5.21	4.47	0.59	0.04	0.65
	3Btb2	195–215	0.30	4.61	3.10	6.39	0.75	0.03	0.57
	3Btb3	215–245	0.29	4.28	2.96	3.31	0.59	0.04	0.36
	4Btb4	245–270	0.16	1.96	2.77	6.08	0.72	0.04	0.06
	4Btb5	270–440	0.27	3.20	2.41	5.01	0.74	0.06	0.20
TV23B	Ah1	0–10	0.42	2.55	1.71	2.10	0.68	0.07	0.11
	Ah2	10–20	0.53	3.45	0.67	1.77	0.85	0.07	0.28
	Bt1	20–45	0.51	3.66	1.73	2.74	0.71	0.08	0.00
	Bw2	45–73	0.44	3.15	2.21	2.34	0.65	0.11	0.04
	2Cox	73–109	0.41	3.13	1.96	2.61	0.69	0.11	0.14
	3Btb1	109–129	0.31	2.16	2.13	2.85	0.66	0.08	0.03
	3Btb2	129–170	0.13	1.12	2.15	4.03	0.69	0.01	0.46
	3Btb3	170–205	0.21	1.48	2.96	3.31	0.59	0.01	0.42
	4Coxb1	205–230	0.16	1.16	2.71	3.64	0.61	0.01	0.43
	4Coxbm2	230–275	0.18	0.99	3.43	2.69	0.49	0.01	0.31

W.C. MAHANEY & R.G.V. HANCOCK

Table 8. Iron and Al extract, total concentrations and functios for Section TV61A, Teleki Catena, Mt. Kenya.

Site	Horizon	Depth (cm)	Fep %	Feo %	Fed %	Fet %	Alp %	Alo %	Ald %	Alt %
TV61A	Ah1	0–6	1.70	2.16	3.24	4.77	1.33	1.89	1.55	7.10
	Ah2	6–22	1.67	2.02	3.20	4.32	1.33	1.68	1.54	6.24
	Ah3	22–28	1.63	2.12	2.72	4.08	1.21	1.48	1.22	5.66
	Bt	28.55	2.47	2.67	3.58	4.95	1.89	2.08	1.71	6.97
	Cox	55–85	1.98	2.93	4.73	6.36	1.70	4.03	3.37	9.74
	2Ahb1	85–110	1.03	2.38	5.03	7.36	1.43	4.52	3.44	11.60
	2Ahb2	110–140	0.94	2.50	5.61	6.94	1.56	4.44	3.82	11.1
	2Ahb3	140–172	1.11	2.50	4.99	6.32	1.61	4.56	3.64	11.1
	2Ahb4	172–185	0.19	0.91	4.50	5.95	1.08	4.18	3.57	12.9
	2Ahb5	185–230	0.26	1.30	4.84	7.33	1.12	4.97	3.04	11.7
	2Ahb6	230–240	0.16	2.28	5.17	7.18	0.79	4.93	2.80	15.0
	2Bwb1	240–260	0.11	1.68	6.50	8.46	0.60	4.88	3.09	15.0
	2Bwb2	260–272	0.12	1.82	7.02	8.00	0.70	4.97	3.11	14.0
	3Ahb1	272–285	1.26	2.45	4.57	6.53	1.67	4.24	2.97	11.4
	3Ahb2	285–315	0.81	2.06	4.87	6.91	1.24	4.42	2.86	12.4
	3Btb	315–320	1.57	2.49	5.61	8.56	2.69	1.30	1.36	13.3
	3Coxb1	320–348	0.44	2.96	6.21	8.92	0.83	2.65	2.73	12.7
	3Coxb2	348–362	1.51	3.90	7.56	10.50	1.34	1.46	3.72	12.3
	3Ahb	362–380	0.18	2.89	5.56	8.04	0.70	3.77	2.56	13.1
	3B/Ahb	380–390	0.14	0.52	3.15	5.32	0.36	0.47	0.51	17.1
	3Btb1	390–423	0.11	2.54	5.64	7.31	0.53	2.90	2.54	16.5
	3Btb2	423–440	0.48	1.26	4.25	4.86	0.70	0.71	0.82	15.2
	4Btb3	440–462	0.27	1.24	4.88	7.44	0.60	0.62	0.92	16.2
	4Btb4	462–490	0.07	1.29	6.16	8.24	0.19	0.52	0.59	16.0
	4Btb5	490–519	0.05	0.88	3.62	5.79	0.16	0.41	0.43	16.8
	5Saprolite	519+	0.87	2.29	6.88	8.07	0.87	0.70	0.63	15.8

Site	Horizon	Depth (cm)	Fe_o/Fe_d	Fe_o x 1.7 (%)	$Fe_t–Fe_d$ (%)	$Fe_d–Fe_o$ (%)	Fe_d/Fe_t	Al_p/Al_t	$Al_0–Al_p$ (%)
TV61A	Ah1	0–6	0.66	3.67	1.53	1.01	0.68	0.19	0.56
	Ah2	6–22	0.63	3.43	1.12	1.88	0.74	0.21	0.35
	Ah3	22–28	0.78	3.60	1.36	0.60	0.67	0.21	0.27
	Bt	28.55	0.75	4.53	1.37	0.91	0.73	0.27	0.19
	Cox	55–85	0.62	4.98	1.63	1.80	0.74	0.17	2.33
	2Ahb1	85–110	0.47	4.05	2.33	2.65	0.68	0.12	3.09
	2Ahb2	110–140	0.45	4.25	1.33	3.11	0.81	0.14	2.88
	2Ahb3	140–172	0.50	4.25	1.33	2.49	0.79	0.15	2.95
	2Ahb4	172–185	0.20	1.55	1.45	3.59	0.76	0.08	3.10
	2Ahb5	185–230	0.27	2.21	2.49	3.54	0.66	0.10	3.85
	2Ahb6	230–240	0.44	3.88	2.01	2.89	0.73	0.05	4.14
	2Bwb1	240–260	0.26	2.86	1.96	1.57	0.77	0.04	4.28
	2Bwb2	260–272	0.26	3.09	0.98	5.20	0.88	0.05	4.27
	3Ahb1	272–285	0.54	4.17	1.96	2.12	0.70	0.15	2.57
	3Ahb2	285–315	0.42	3.50	2.04	2.81	0.70	0.10	3.18
	3Btb	315–320	0.44	4.23	2.95	3.12	0.66	0.20	nil
	3Coxb1	320–348	0.48	5.03	2.71	3.25	0.70	0.07	3.19
	3Coxb2	348–362	0.52	6.63	2.94	3.14	0.72	0.11	0.12
	3Ahb	362–380	0.52	4.91	2.48	2.67	0.69	0.05	3.07
	3B/Ahb	380–390	0.17	0.88	2.17	2.63	0.59	0.02	0.11
	3Btb1	390–423	0.30	2.14	0.61	2.99	0.87	0.05	0.01
	4Btb2	423–440	0.25	2.11	2.56	3.64	0.66	0.04	0.02
	4Btb3	440–462	0.21	2.19	2.08	4.87	0.75	0.01	0.33
	4Btb4	462–490	0.24	1.50	2.17	2.74	0.63	0.01	0.25
	4Btb5	490–519	0.17	0.88	2.17	2.63	0.59	0.02	0.11
	5Saprolite	519+	0.33	3.89	1.19	4.59	0.85	0.06	nil

Table 9. Major, minor and trace element chemistries for TV23 and TV23B.

Site	Horizons	Depth (cm)	Al %	Ca %	Mn (ppm)	Fe %	K %	Na %	Ti (ppm)	Sc (ppm)	Ta (ppm)	Th (ppm)	La (ppm)	Ce (ppm)	
TV23	Ah1	0–18	9.0	<0.40	5080	5.21	0.69	0.51	4900	4.93	16.4	22.3	33	180	*
	Ah2	18–38	11.1	<0.28	3650	6.51	0.85	0.58	4100	6.35	19.9	29.1	43	259	*
	Bt1	38–90	12.9	<0.26	3470	7.50	0.75	0.61	2800	9.24	26.0	38.3	42	455	*
	Bt2	90–104	15.5	<0.17	2690	7.06	0.74	0.45	6600	11.1	25.9	41.5	32	360	*
	2Cox1	104–165	–	–	1090	8.69	1.0	1.13	–	10.2	26.3	40.3	16	131	*
	2Cox2	165–175	17.9	<0.39	5570	13.1	0.68	0.75	4800	8.41	21.2	29.6	23	460	*
	3Ahb	175–185	16.6	<0.80	14100	8.39	0.13	0.22	–	5.56	35.4	52.6	47	397	*
	3Btb1	185–195	10.8	<0.6	9910	12.70	0.30	0.22	–	8.77	50.1	79.6	62	661	*
	3Btb2	195–215	14.1	<0.15	10100	12.2	0.17	0.12	5700	8.33	39.8	57.4	63	718	*
	3Btb3	215–246	15.8	<0.22	2420	9.51	0.08	0.045	2500	6.87	26.9	35.8	86	326	*
	4Btb4	246–274	15.8	<0.22	2420	9.51	0.08	0.05	2450	6.87	26.9	38.8	86	373	*
	4Btb5	274–440	15.8		3560	9.30	0.16	0.07	3650	6.86	26.1	34.8	117	498	*
TV23B	Ah1	0–10	10.2	<0.23	3760	5.31	0.12	0.28	3600	4.62	17.4	28.9	160	204	
	Ah2	10–20	11.0	<0.22	3230	4.47	0.59	0.34	4900	4.29	17.0	23.4	159	192	
	Bt1	20–45	12.4	<0.17	2260	5.92	0.42	0.28	4600	5.81	21.3	30.4	189	264	
	Bw2	45–85	12.9	<0.17	1620	6.41	0.48	0.36	5000	7.04	25.5	34.0	196	315	
	2Cox	85–120	14.1	<0.18	1730	6.41	0.51	0.47	5500	8.20	26.2	34.3	188	357	
	3Btb1	120–135	15.6	<0.09	1860	6.25	0.28	0.21	6000	6.68	27.8	34.8	176	330	
	3Btb2	135–178	16.5	<0.20	1430	6.84	0.10	0.033	5600	5.96	31.4	36.2	137	244	
	3Btb3	178–215	16.5	<0.15	2980	7.14	0.11	0.06	5200	6.11	33.8	38.7	279	362	
	4Coxb1	215–230	16.2	<0.11	1780	7.03	0.10	0.014	6000	6.25	33.9	38.1	109	360	
	4Coxbm2	230–290	16.8	<0.20	1360	6.70	0.10	0.056	5500	6.14	31.9	37.1	246	566	

– in sufficient sample; * sample with very low La/Ce ratios

Table 10. Selected major, minor and trace element chemistries for the TV61A section.

Site	Horizons	Depth (cm)	Al %	Ca %	Mn (ppm)	Fe %	K %	Na %	Ti (ppm)	Sc (ppm)	Ta (ppm)	Th (ppm)	La (ppm)	Ce (ppm)
TV61A	Ah1	0–6	7.1	<0.31	2390	4.77	0.66	0.45	3900	5.41	12.4	18.9	48	158
	Ah2	6–22	6.2	<0.17	2800	4.27	0.78	0.40	3700	4.80	11.0	16.2	40	133
	Ah3	22–28	5.7	<0.21	2050	4.08	0.59	0.34	3500	4.62	10.2	15.6	36	121
	Bt	28–55	7.0	<0.08	1520	4.95	0.74	0.51	3500	7.12	12.0	19.8	41	161
	Cox	55–85	9.7	<0.20	1720	6.36	0.87	0.57	5000	8.87	14.9	24.6	57	218
	2Ahb1	85–110	11.6	<0.09	1540	7.36	1.09	0.57	5100	10.7	17.2	30.3	72	304
	2Ahb2	110–140	11.1	<0.21	1630	6.94	1.00	0.63	4400	8.56	16.2	29.3	90	270
	2Ahb3	140–172	11.1	<0.17	1040	6.32	0.84	0.71	4700	9.43	12.5	21.8	92	243
	2Ahb4	172–185	12.9	<0.24	2340	5.95	0.55	0.29	2600	4.68	16.6	29.1	81	269
	2Ahb5	185–230	11.7	<0.13	3140	7.33	0.66	0.51	3400	5.95	20.6	33.9	116	282
	2Ahb6	230–240	15..0	<0.30	4230	7.18	1.07	0.75	3900	4.57	18.6	27.4	89	239
	2Bwb1	240–260	15.0	<0.30	3920	7.88	1.00	0.63	5200	5.4	21.7	30.1	41	228
	2Bwb2	260–272	14.0	<0.11	2410	7.79	0.90	0.54	5000	6.08	21.2	31.6	58	244
	3Ahb1	272–285	11.4	<0.11	878	6.52	1.00	0.58	5300	8.59	17.3	26.8	224	499
	3Ahb2	285–315	12.4	<0.11	611	6.42	0.90	0.59	5100	7.30	21.3	30.0	163	255
	3Btb	315–320	13.3	<0.11	1570	8.94	0.70	0.36	6700	8.50	21.7	24.5	144	204
	3Coxb1	320–348	12.3	<0.11	5900	10.8	0.70	0.31	7000	9.56	21.3	27.8	132	200
	3Coxb2	348–362	12.7	<0.26	4375	8.92	1.14	0.566	4100	10.7	21.5	31.2	82	368
	3Ahb	362–380	13.1	<0.11	2030	8.22	1.00	0.74	4500	7.23	20.5	29	80	330
	3B/Ahb	380–390	16.5	<0.11	3860	7.37	0.80	0.70	4200	4.05	21.1	28.4	73	210
	3Btb1	390–420	15.2	<0.11	1800	6.31	0.50	0.29	4900	5.61	25.7	32.1	213	326
	3Btb2	423–440	16.2	<0.11	3800	7.65	0.50	0.22	3700	5.14	27.8	35.0	201	390
	4Btb3	440–462	16.0	<0.38	5350	8.25	0.24	0.14	3800	5.92	26.3	32.9	249	416
	4Btb4	462–490	16.8	<0.14	1800	5.79	0.21	0.15	4600	5.93	29.2	36.6	256	372
	4Btb5	490–519	17.1	<0.10	702	5.32	0.30	0.21	5100	6.56	32.2	38.3	261	339
	5Saprolite	519–600	15.8	<0.27	2135	8.07	1.20	1.25	5200	6.55	19.6	23.1	111	146

W.C. MAHANEY & R.G.V. HANCOCK

Table 11. Selected major, minor and trace element chemistries for TV69 Section, NM tills, and bedrock on Mt. Kenya.

Site	Horizons	Depth (cm)	Al %	Ca %	Mn (ppm)	Fe %	K %	Na %	Ti (ppm)	Sc (ppm)	Ta (ppm)	Th (ppm)	La (ppm)	Ce (ppm)	
TV69	Ah	0–23	7.8	<0.23	1680	4.20	0.80	0.48	3600	5.09	12.1	18.3	52.5	128	*
	Bw1	23–52	8.2	<0.09	482	5.96	0.80	0.57	3300	7.24	17.1	26.7	68.2	178	*
	Bw2	52–78	12.3	<0.22	565	6.50	0.94	0.61	5400	9.13	18.8	30.7	77.1	230	*
	2Ahb	78–93	12.1	1.0	611	6.92	0.73	0.61	5500	10.1	19.3	34.4	85.4	286	*
TV23A	4Coxb1	165–210	12.7	<0.20	2770	8.67	0.70	0.43	6100	10.3	25.9	38.1	109	360	*
	4Coxb2	210–340	15.4	<0.20	2800	8.55	0.50	0.16	5000	10.1	31.6	42.0	317	477	
TV23C	4Btb2	230–270	16.0	<0.20	1870	6.53	0.14	0.31	460	6.85	27.7	34.7	300	491	
TV61	4Btb1	470–495	16.5	<0.20	2640	6.86	0.14	0.25	5500	6.58	31.2	39.4	340	466	
	4Btb2	495–568	17.7	<0.20	670	6.82	0.14	0.34	4200	4.71	25.0	31.1	289	338	
Phonolite			9.2	1.2	1970	4.66	2.7	7.3	5100	4.14	26.7	34.0	110	179	
Kenyte			9.1	1.3	1970	4.95	3.2	7.0	7100	4.74	19.4	27.1	111	173	
Syenite			9.2	1.7	1220	3.44	4.7	5.6	5600	3.50	10.8	15.2	73	118	
basalt			10.8	2.1	1120	4.79	2.6	4.1	7800	2.27	9.7	9.9	77	142	

* samples with very low La/Ce ratios.

Table 12. Summary of elemental concentration data.

	TV23	TV23B	TV61	TV61A1	TV61A2	TV69	rocks
	13 samples	12 samples	2 samples	9 samples	17 samples	4 samples	4 samples
Al %	14±3	15±2	17±1	15±2	11±3	10±2	10±1
Ca %	0.3±0.1	0.2±0.1	0.2±0.0	0.2±0.1	0.2±0.1	0.4±0.4	1.6±0.4
Fe %	9.1±2.4	6.5±1.0	6.8±0.1	7.5±1.7	6.6±1.4	5.9±1.2	4.5±0.7
K %	0.5±0.3	0.3±0.2	<0.1±0.1	0.6±0.3	0.9±0.2	0.8±0.1	3.3±1.0
Mn %	0.52±0.39	0.22±0.08	0.17±0.14	0.26±0.19	0.24±0.11	0.08±0.06	0.16±0.05
Na %	0.4±0.3	0.2±0.1	0.3±0.1	0.4±0.4	0.6±0.1	0.6±0.1	6.0±1.5
Ti %	<0.46±0.14	0.51±0.07	0.48±0.09	0.51±0.11	0.42±0.07	0.45±0.11	0.64±0.12
As ppm	<3.9±2.2	<2.9±1.8	<2.0±0.0	<6.3±4.9	6.2±1.5	5.6±1.5	<1.9±0.3
Ba ppm	530±100	1320±630	1030±80	900±420	460±120	520±70	1150±550
Co ppm	19±6	7±2	4±4	12±14	9±2	5±1	4±1
Cr ppm	26±13	21±8	13±3	36±31	51±18	63±14	7±4
Cs ppm	1.8±1.3	1.5±0.8	1.5±0.6	2.6±1.7	2.5±0.9	3.0±0.5	1.6±1.0
Hf ppm	35±11	26±5	27±4	24±4	18±4	19±5	15±7
Rb ppm	45±15	26±11	33±13	55±33	54±11	55±10	119±29
Sb ppm	0.6±0.3	0.5±0.5	<0.2±0.0	<0.4±0.2	<0.4±0.1	<0.3±0.1	<0.2±0.0
Sc ppm	8.0±1.9	6.5±1.5	5.6±1.3	6.8±1.4	6.9±2.2	7.9±2.2	3.7±1.1
Sr ppm	<90±30	<160±40	230±20	<180±90	110±40	<80±20	1040±450
Ta ppm	28±9	27±6	28±4	25±4	17±4	17±3	17±8
Th ppm	41±15	27±6	35±6	31±5	26±6	28±7	22±11
U ppm	<6±2	<5±1	<4±1	6±1	6±2	<5±1	<5±2
La ppm	58±32	217±60	315±36	192±57	78±44	71±14	93±21
Ce ppm	400±170	350±120	400±90	290±90	250±90	200±60	150±30
Nd ppm	69±34	111±46	155±8	105±34	66±33	71±21	62±11
Sm ppm	11±5	14±6	20±0	15±4	12±6	11±3	9±2
Eu ppm	1.7±1.8	3.1±1.8	4.4±0.3	3.2±1.0	2.0±1.0	2.2±0.6	3.2±0.2
Dy ppm	5.9±0.8	<4.5±2.0	7.5±0.6	<6.6±2.6	<7.1±4.2	<6.9±2.8	4.6±0.7
Tb ppm	1.3±0.5	1.2±0.5	1.9±0.1	1.7±0.7	1.7±0.9	1.1±0.5	1.2±0.3
Yb ppm	5.4±2.2	3.3±1.4	4.8±0.3	5.3±1.7	6.8±3.3	5.9±2.1	4.2±1.1
Lu ppm	0.8±0.3	0.4±0.2	0.6±0.1	0.7±0.3	0.9±0.5	0.8±0.3	0.6±0.3

All of the analyzed sediment samples have much lower Ca, K, and Na concentrations than do the local rocks (Tables 9–11). This implies either severe leaching over long periods of time and/or an influx of sediments made from different, non–local, parent materials.

Table 13. Selected REE ratios correlating Naro Moru tills in selected sections and the till/loess horizons of the post Naro Moru paleosol in section TV61A.

Site	Horizon	Depth (cm)	Ce/La	Ce/Sm	Ce/Lu
TV23	4Coxb1	246–274	3.8	25	308
	4Coxb2	274–440	4.3	31	380
TV23A	4Coxb1	160–205	3.3	23	360
	4Coxb2	205–330	1.5	35	1037
TV23B	4Coxb1	205–230	1.0	30	1274
	4Coxbm2	230–275	1.0	14	359
TV23C	4Btb2	235–270	1.6	16	622
TV61	4Btb3	470–490	1.4	24	832
	4Btb4	490–565	1.2	17	554
TV61A	3Btb1	390–423	1.5	22	543
	3Btb2	423–440	1.9	29	780
	4Btb3	440–462	1.7	24	671
	4Btb4	462–490	1.5	20	448
	4Btb5	490–519	1.3	16	290
	5Saprolite	519–600	1.3	13	206
	Phonolite	+600	1.6	17	221